1-1-2002

Thermochronology and geobarometry of the Granite Mountains, southeast California: Exhumation of a plutonic complex during collapse of the Sevier orogen

Joseph Louis Kula
University of Nevada, Las Vegas

THERMOCHRONOLOGY AND GEOBAROMETRY OF THE GRANITE MOUNTAINS, SOUTHEAST CALIFORNIA; EXHUMATION OF A PLUTONIC COMPLEX DURING COLLAPSE OF THE SEVIER OROGEN

by

Joseph L. Kula

Bachelor of Science
Montclair State University, Upper Montclair, NJ
2000

A thesis submitted in partial fulfillment
of the requirements for the

Masters of Science Degree
Geoscience Department
College of Sciences

Graduate College
University of Nevada, Las Vegas
December 2002

UNLV

Thesis Approval

The Graduate College
University of Nevada, Las Vegas

November 13, 20 02

The Thesis prepared by

Joseph Louis Kula

Entitled

Thermochronology and Geobarometry of the Granite Mountains, Southeast California: Exhumation of a Plutonic Complex During Collapse of the Sevier Orogen

is approved in partial fulfillment of the requirements for the degree of

Master of Science

Terry L. Spell
Examination Committee Chair

Dean of the Graduate College

Examination Committee Member

Examination Committee Member

Graduate College Faculty Representative

PR/1017-53/1-00

ABSTRACT

Thermochronology and Geobarometry of the Granite Mountains, southeast California; Exhumation of a plutonic complex during collapse of the Sevier Orogen

by

Joseph L. Kula

Dr. Terry L. Spell, Examination Committee Chair
Associate Professor of Geology
University of Nevada, Las Vegas

Thermochronologic data and geobarometry from the Granite Mountains indicate exhumation of mid-crustal plutons during Late Cretaceous extensional tectonics. U/Pb zircon and $^{40}Ar/^{39}Ar$ hornblende ages indicate intrusion, crystallization, and geologically instantaneous cooling through 500 °C at ~75 Ma. K-feldspar multi-diffusion domain modeling indicates a cooling rate gradient from SW to NE of 63, 32, and 16 °C/Ma for three samples spanning a transect across the range. NE K-feldspar cooled through ~252 °C by 73 Ma while other samples remained >375 °C suggesting a short lived down-to-the-east normal faulting event at ~75 to 74 Ma. Faster cooling rates with later initial K-feldspar recording (~71 Ma) suggest extension continued along a shallow down-to-the-southwest detachment active from ~73 to 69 Ma. U-Th/He apatite ages suggest the Late Cretaceous extensional event juxtaposed the deeper-seated Granite Mountains plutons with the shallow-level southern Providence Mountains plutons and the two cooled through 70 °C as a single block.

TABLE OF CONTENTS

LIST OF FIGURES

ACKNOWLEDGEMENTS

So many people unselfishly put time towards this project that it would be criminal for me to accept credit for its completion without acknowledging them and expressing my gratitude. On the reverse side of that coin, it would also be unfair for me to take all the blame without revealing all co-conspirators and guilty parties, so here it goes.

My advisor, Teespell, has been patient beyond the bounds of most human forms and I thank him graciously for it. For over two years he has been an incredible mentor and friend even after sitting through my psychotic ramblings and falling victim to my constant acts of immaturity.

I will never understand how one person can remember so much geology and come up with so many difficult questions, but I have to thank Michael Wells for doing it. I have benefited greatly from having him serve on my committee and I appreciate all of the conversations we have had. I would also like to thank Rod Metcalf for being on my committee and offering constructive criticism, a relaxed presence during consultation, and insight on barometry work, not to mention 'giving me shi, err...crap.' Barbara Luke is thanked for serving on my committee as well as for being easily approachable and genuinely professional and kind.

Keith A. Howard at the U.S.G.S. Menlo Park, CA is thanked for supplying unpublished K-Ar dates from the Granite Mountains and insight throughout this project. Ken A. Farley at California Institute of Technology is thanked for allowing me to visit his laboratory and for running U-Th/He apatite analyses. I would like to thank Oscar Lovera

at UCLA for his patience with my infinite number of questions regarding his computer programs.

I am very grateful for conversations about my thesis project with Andrew Hanson, Cathy Snelson, and Wanda Taylor. A gargantuan thank you is in order for Kathy Zanetti for letting me hang out in the lab all the time, helping me with my $^{40}Ar/^{39}Ar$ age determinations, putting up with my ridiculous antics, and getting me thrown out of "The Beach."

I thank my family for their long distance support, and advice in the kitchen. I am grateful to Pabst for offering a vegan beer at an inexpensive cost. Also, I need to thank my friends who have given me mental support even when they didn't realize they did it. I believe they know who they are (and do not need to see their name in a list here) and I thank these friends for being approachable, fun, and 'there' by choice and not obligation. An extra special 'thank you' goes to Melissa for just being. Of course, I also thank the Geoscience Department at UNLV for supporting me and allowing me to continue my graduate education here. I'm having a lot of fun.

This project was funded by UNLV SITE Grants, UNLV GSA Research Grants, UNLV Geoscience Department Research Grants, and Arizona-Nevada Academy of Science Research Grants.

CHAPTER 1

INTRODUCTION

In some areas of the North American Cordilleran interior evidence for rapid exhumation of mid-crustal rocks during the late Cretaceous extensional collapse of the Sevier Orogen is well documented (Foster et al., 1989; Wells et al., 1990; Hodges and Walker, 1992; Miller et al., 1996). However, in many areas this event is neither confirmed nor dated, partly because mid-Cenozoic extension (Basin and Range tectonics) also took place in the region (Foster et al., 1990). This results in a lack of evidence for north-south continuity of late Cretaceous extensional structures. This study focuses on the Granite Mountains, located in the eastern Mojave Desert of California. The Granite Mountains are situated at the southernmost extent of the Sevier Orogenic belt, an area in which details of the Sevier Orogeny are incompletely understood (Fig. 1).

Purpose

The Granite Mountains are a mid to deep-crustal plutonic complex consisting of Mesozoic granitoids that are also exposed to the northeast in the southern Providence Mountains (Howard et al., 1987; Young and Wooden, 1988; Fox and Miller, 1990). Previous geochronology in the Granite Mountains indicates preservation of Mesozoic isotopic signatures, suggesting the cooling histories of plutons may record Late Cretaceous exhumation and not Tertiary tectonic overprinting (Basin and Range

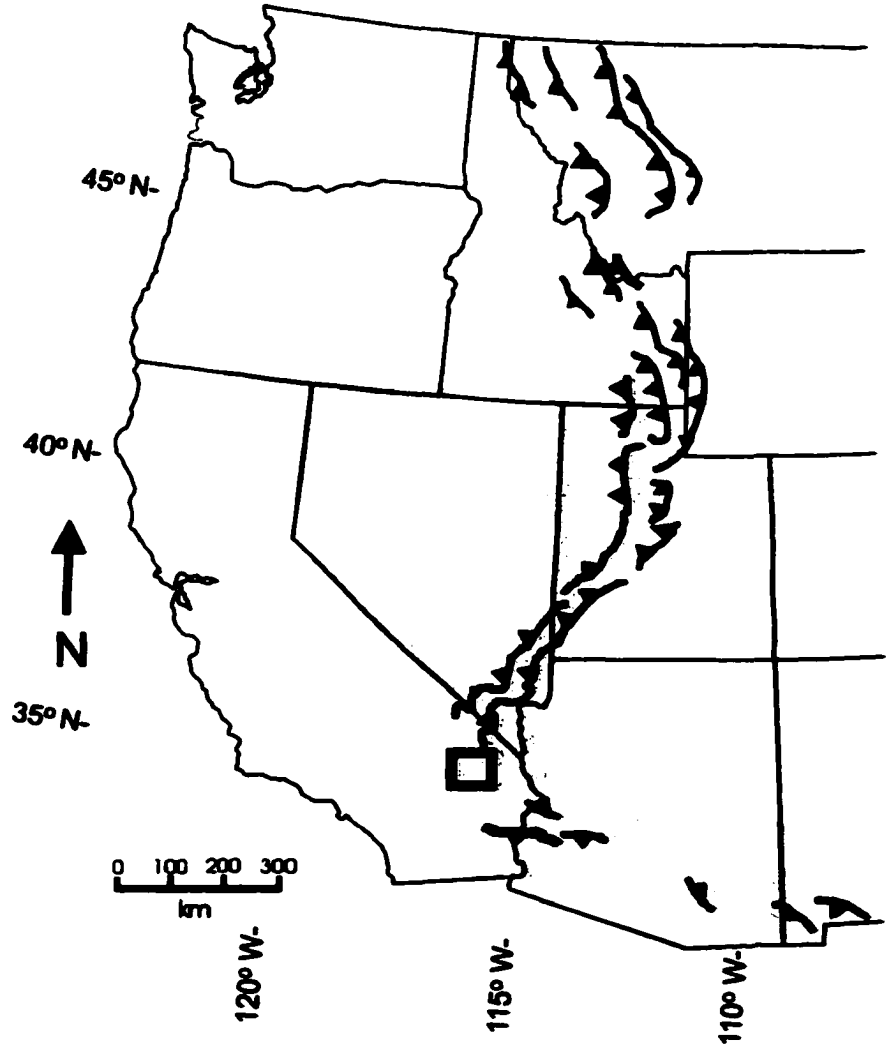

Figure 1. Mesozoic Sevier thrust belt and Cenozoic Basin and Range Province (gray). Modified from Lageson and Schmitt (1994) and Burchfiel et al. (1992). Square represents study area.

Extension). The purpose of this research project is to further document Late Cretaceous extensional tectonics at the southern extremity of the Sevier Orogen by using isotopic dating techniques and geobarometry to document the intrusion and exhumation history of Granite Mountains plutons. Timing of exhumation for these plutons may then be related to the known tectonic events that have affected the region, which include extensional collapse of the Sevier Orogen (Mesozoic) and Basin and Range Extension (Miocene).

Significance of Study

Contraction and subsequent extension in the Sevier Orogen were significant events in the geologic history of western North American. Although the Sevier Orogeny has been intensively studied for decades, its tectonic history remains incomplete. In Death Valley, the Mojave Desert, and adjacent terrains of the southern Sevier region, understanding of the tectonic history is limited due to both insufficient geochronological data and overprinting by Basin and Range extension. The results of this project provide information on the timing and rates of Late Cretaceous Sevier extensional tectonics. Information gained from this study not only adds to the growing body of knowledge of the geologic evolution of the North American continent, but also may be applicable to presently active orogens (e.g. Himalayan Mountains). A more complete understanding of the timing and regional extent of past orogenic events may allow for better interpretation and perhaps prediction of the tectonics of active orogenic terrains.

Research Questions / Hypothesis

The hypothesis for this study is that the exhumation of Granite Mountains plutons was a result of Late Cretaceous extensional collapse of the Sevier orogeny. Questions formulated to test the hypothesis and meet project goals include (1) What were the timing and rates of exhumation? and (2) What known tectonic event(s) led to the exhumation of plutons of the Granite Mountains?

The main goals of this project are (1) to determine the depth and timing of emplacement for plutons in the Granite Mountains, (2) construct the subsequent cooling histories for these plutons, and (3) relate these results to known tectonic events that have affected the region.

Field relations of rock units along with previous investigations in the Granite-Providence Mountains region suggests that these ranges may represent parts of a continuous crustal section. Exposures of shallow-to-mid-crustal rocks in the southern Providence Mountains have been described as similar to the mid-to-deep-crustal rocks found in the northern Granite Mountains (Miller et al., 1985; Young and Wooden, 1988; Young et al., 1992). This may be a preliminary indication that the Granite and southern Providence Mountains represent a tilted crustal section, or perhaps a crustal section with its deeper and shallower sections juxtaposed at the surface following extensional tectonics. This possibility may be resolved by answering several secondary research questions. These questions include (1) Is this an intact crustal section? If so (2) did tilting during exhumation expose deep plutons of the Granite Mountains adjacent to shallower plutons of the Southern Providence Mountains, or was some other process responsible?, and (3) What is the structural/ tectonic link between these two mountain ranges?

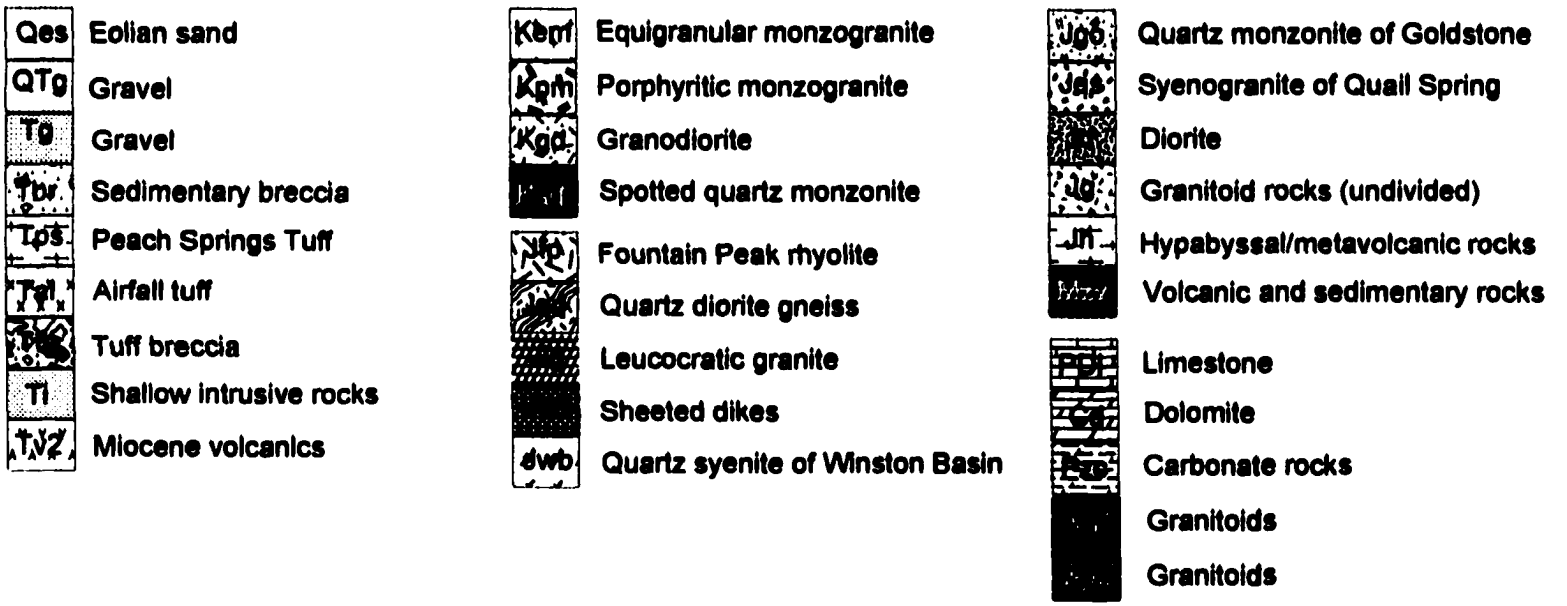

Figure 2. Geologic map of Granite Mountains and southern Providence Mountains in the east Mojave Desert, California (from Miller et al., 1985; Miller et al., 1991). Black circles indicate locations sampled. Arrows pointing to open circles indicate sample locations for Calvin from monzogranite pluton, Floyd from a central granodiorite pluton, Yoshi from a northeast quartz monzonite pluton, and Omar from the syenogranite of Quail Spring in the southern Providence Mountains. Along the northern base of the range is the Bull Canyon Fault. Fault lines in the eastern Providence Mountains represent the East Providence Fault Zone. Dotted line southwest of the Granite Mountains indicates inferred location of the Bristol-Granite Mountains fault zone. The fault through Granite Pass lies between Cretaceous rocks in the Granite Mountains and Jurassic rocks in the southern Providence Mountains.

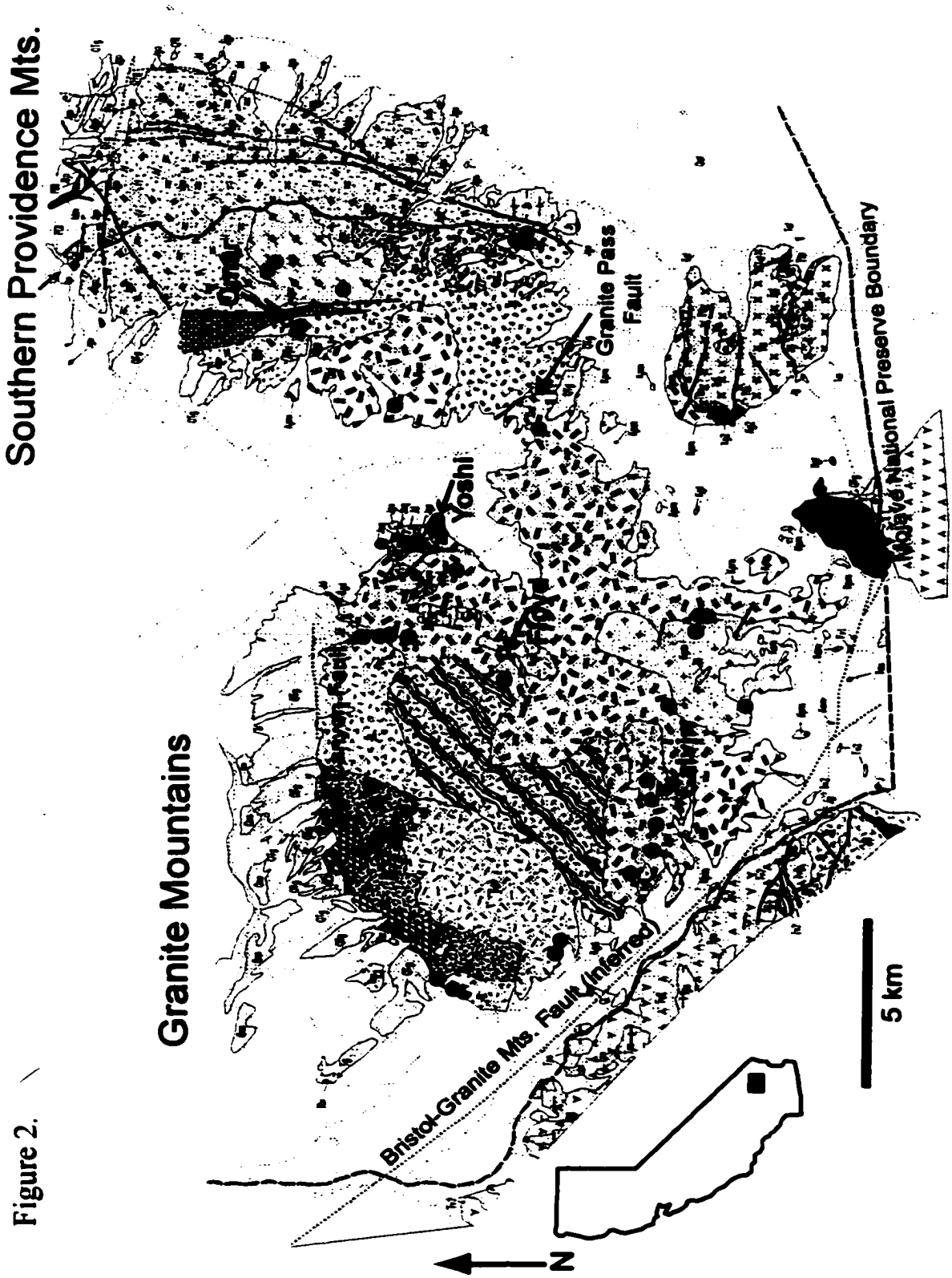

Figure 2.

CHAPTER 2

REGIONAL GEOLOGY

Sevier Orogeny

The Sevier Orogen is defined by a series of contractional structures extending north-south through western North America (Armstrong, 1968) (Fig. 1). Together, these structures are referred to as the Sevier fold-thrust belt. Deformation and plutonism of the Sevier Orogeny began in the Late Jurassic due to Farallon-North American plate convergence (Burchfiel et al., 1992). An increasing rate in Farallon plate subduction resulted in intensified arc magmatism, which heated and weakened overlying crust allowing fold-thrust deformation. By about early Cretaceous time a continuous belt of east-vergent thrust faults stretched from Canada to southeastern California (Livaccari, 1991; Burchfiel et al., 1992). To the west of this fold and thrust belt are associated Late Jurassic plutons (~165 to 140 Ma) that cut earlier Mesozoic deformational fabrics, folds, and thrust faults (Walker et al., 1995a; Burchfiel et al., 1992). The Sevier belt may be entirely younger than these plutons since the time of initial thrust faulting of the Sevier belt is unclear (Burchfiel et al., 1992). Evidence has been presented indicating development of east-vergent allochthons in the latest Jurassic to early Cretaceous (Armstrong and Oriel, 1965), whereas Heller et al. (1986) suggest the beginning of Sevier thrust faulting at about early Cretaceous time.

Overthickening of the continental crust resulting from convergent tectonics of the Sevier Orogen led to extensional collapse in the Late Cretaceous (Foster et al., 1989; Wells and Allmendinger, 1990; Wells, 1997). Extension in the Sevier hinterland has been well documented in Utah (Wells et al., 1990; Wells, 1997) and parts of California (Foster et al., 1989; Applegate et al., 1992; Miller et al., 1996). However, Mesozoic extensional structures and isotopic signatures related to the Sevier Orogeny are discontinuous due to subsequent overprinting by Cenozoic Basin and Range tectonics (Fig. 1).

Southeast California

Basement rocks of the eastern Mojave Desert are granitoids and high-grade gneisses and schists that were deformed and accreted to the North American craton in the Early Proterozoic (Bennett and Depaolo, 1987; Wooden et al., 1988). Middle Proterozoic anorogenic granitoids and diabases later intruded these rocks (Anderson, 1983; Fitzgibbon and Howard, 1987). During episodes of marine transgression and regression, the region was covered by 1-2 km of carbonate dominated sedimentary rocks during the Paleozoic and early Mesozoic (Stone et al., 1983). Deformation, plutonism and metamorphism during the Middle Jurassic occurred in the western and central Mojave Desert with tectonism also documented to the east in the Marble, Ship, Clipper, Piute, and Old Woman Mountains during the Late Jurassic to Cretaceous (Bishop, 1964; DeWitt et al., 1984; Burchfiel and Davis, 1981; Foster et al., 1990; Howard et al., 1995) (Fig. 3).

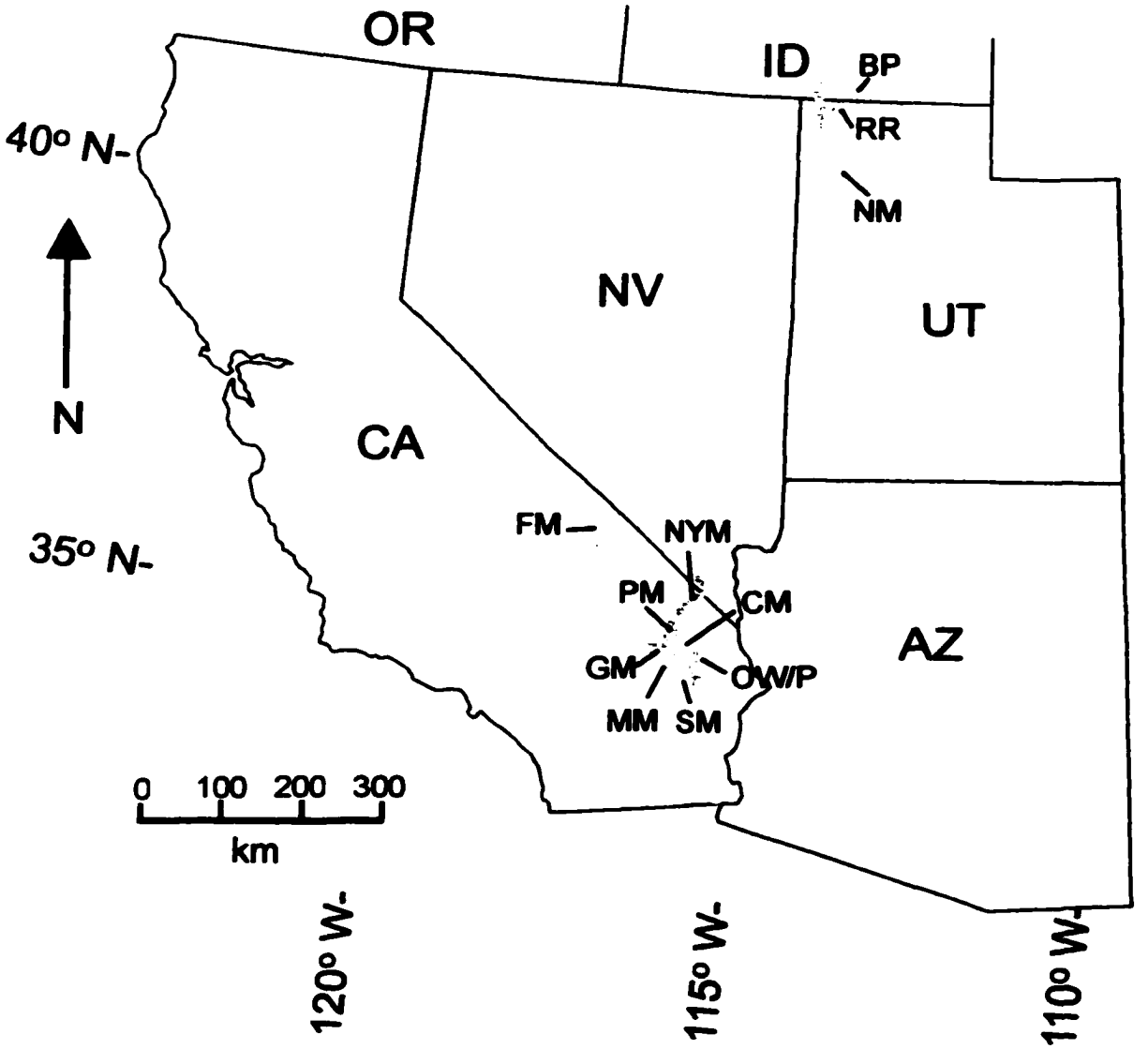

Figure 3. Map showing several locations in the Sevier hinterland that record extension during the Late Cretaceous gravitational collapse of the Sevier Orogen.FM=Funeral Mountains; RR=Raft River Mountains; NM=Newfoundland Mountains; BP=Black Pine Mountains; NYM=New York Mountains; PM=Providence Mountains; OW/P=Old Woman-Piute Mountains; GM=Granite Mountains (study area). Also shown are the Clipper Mountains (CM), Ship Mountains (SM), and Marble Mountains (MM). Adapted from Applegate et al. (1992), Allmendinger and Jordan (1984), Beyene et al., (2000), Miller et al., (1996), Foster et al., (1992), Wells et al. (1990), and Wells (1997).

Jurassic and Cretaceous age plutons in the Mojave Desert are part of larger magmatic arcs that extend throughout the U.S. Cordillera (Fox and Miller, 1992) (Fig. 4). In the Mojave region, Cretaceous plutonic rocks have compositions ranging from granodiorite to monzogranite, and are compositionally more homogeneous than Jurassic plutonic rocks (Fox and Miller, 1992). Jurassic intrusive rocks are more compositionally diverse and K_2O-rich and mainly yield K/Ar and U/Pb ages of 160 to 150 Ma and 165 to 160 Ma, respectively (Fox and Miller, 1992), although Latest Jurassic (~145 Ma) plutons have been dated north of the Granite Mountains in the Clark Mountains, Mescal Range, Striped Mountain, and Ivanpah Mountains. Cretaceous plutonic rocks are exposed as large composite batholiths throughout the region (Fox and Miller, 1990). These include the Teutonia batholith (Beckerman et al., 1982; Fox and Miller, 1990), the Cadiz valley batholith (John, 1981; Fox and Miller, 1990), and the Old Woman-Piute batholith (Foster et al., 1990). Cretaceous plutons were emplaced during two intervals based on U-Pb zircon geochronology; 99 to 95 Ma and 75 to 70 Ma (Wright et al., 1987; Fox and Miller, 1992).

Granite Mountains

The Granite Mountains expose rocks ranging in age from Paleozoic to Cenozoic, but are dominated by Mesozoic plutonic rocks described above (Howard et al., 1987) (Fig. 2). Metasedimentary rocks are exposed at higher elevations as small roof pendants (Howard et al., 1987). These metamorphosed strata are dominantly marble and siliceous marble, which may correlate lithologically with the Bird Spring Formation (Pennsylvanian and Permian) and the Monte Cristo Limestone (Mississippian) that are exposed in the northern Providence Mountains to the northeast (Howard et al., 1987).

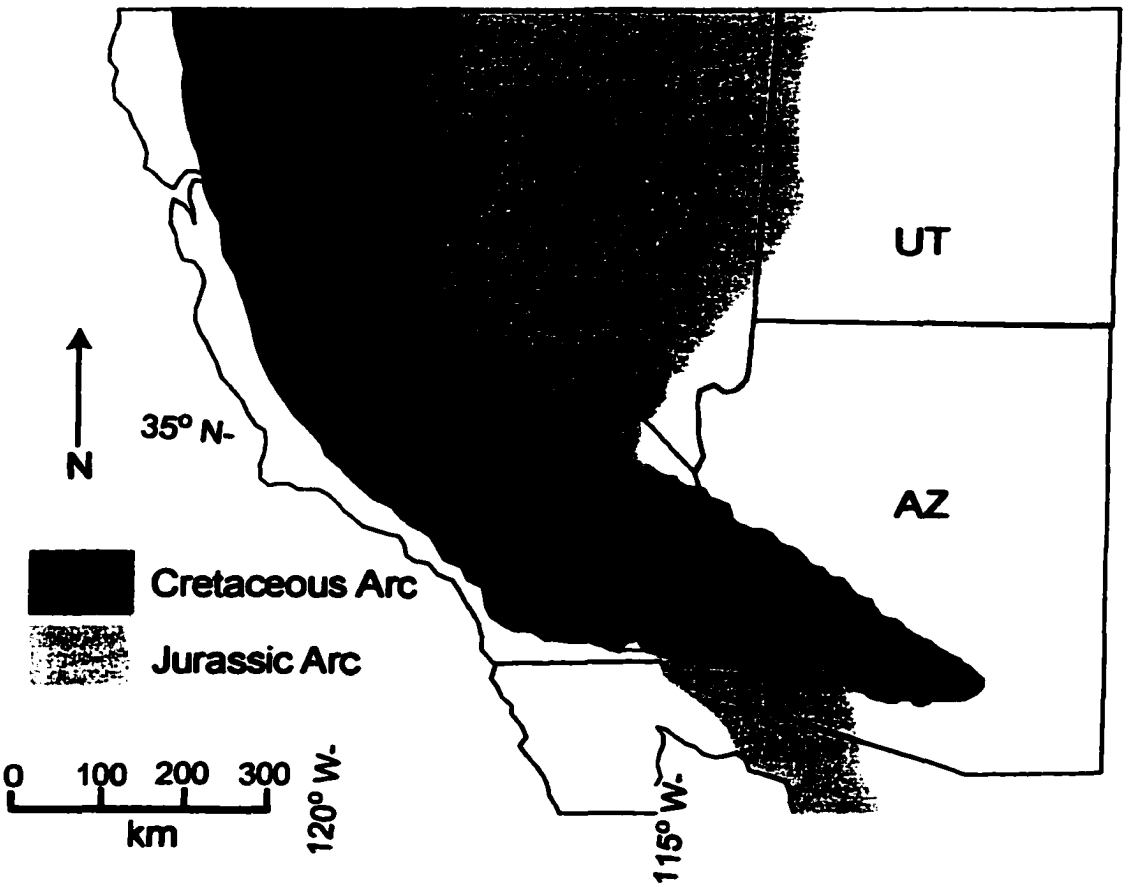

Figure 4. Map of Mesozoic magmatic arcs extending through the southern U.S. Cordillera (after Fox and Miller, 1990). Rectangle indicates area of study in the Mojave Desert.

Previous U/Pb and K/Ar ages from the Granite Mountains (Chapter 3) indicate preservation of original Mesozoic isotopic signatures and thus potential to provide information about Late Cretaceous tectonics. Previous geobarometry (Chapter 3) in the Granite Mountains region, indicating mid-to-deep crustal emplacement for Granite Mountains plutons and shallow crustal emplacement for southern Providence Mountains plutons, may have implications for a structural relationship between the Granite and southern Providence Mountains.

In contrast with the heavily faulted Old Dad Mountains to the west, there are few faults in the interior of the Granite Mountains; however, several faults are present on the perimeter (Howard et al., 1987) (Fig. 2). The Bull Canyon fault, a late Tertiary low-angle normal fault, traces around the northern margin of the Granite Mountains (Howard et al., 1987). The fault dips outward from the range at 20-40° north and northwest, and exposes a zone of red to tan breccia and gouge separating a chloritically altered footwall of Jurassic plutonic rocks from a hanging wall of chloritized and brecciated equivalents and Tertiary sedimentary breccia (Howard et al., 1987). Separating the Granite Mountains from the Old Dad Mountains is the northwest-striking Bristol-Granite Mountains fault zone (Gamble, 1959a,b; Howard et al., 1987; Howard and Miller, 1992) (Fig. 2). This fault dips northeast 70-80° and places Mesozoic plutonic rocks in the northeast over Tertiary supracrustal rocks in the southwest, indicating reverse motion (Howard et al., 1987). This fault has been described as a potential southern continuation of dextral-strike-slip faults in Death Valley, (Hamilton and Myers, 1966; Brady, 1988) and the eastern limit of the eastern California shear zone (Howard and Miller, 1992; Dokka and Travis, 1990) while Davis et al. (1974) suggest that the Bristol-Granite Mountains fault

zone is older than the southern Death Valley fault zone. In the northeast, a normal fault extends at least 3 km long striking northwest and dipping 45-50° to the northeast (Howard et al., 1987) (Fig. 2). A north-northwest striking fault to the east in Granite Pass places Cretaceous granite of the Granite Mountains against Jurassic syenogranite in the southern Providence Mountains (Howard and Miller, 1992) (Fig.2). This fault is interpreted as a down-to-the- east normal fault by Howard and Miller (1992), based on a greater abundance and coarser grain size of the Cretaceous granite west of the fault compared to that exposed to the east.

Providence Mountains

The Providence Mountains lie to the northeast of the Granite Mountains (Fig. 2). The southern region of these mountains consists of Mesozoic granitic plutons similar to those exposed in the Granite Mountains. Young and Wooden (1988) determined mid-to shallow crustal emplacement depths for these plutons using aluminum-in-hornblende geobarometry (Chapter 3). Along the east side of this range is the East Providence fault zone (Fig. 2), consisting of several steeply dipping (~65°-75°) down-to-the-west normal faults (Miller et al., 1996). The East Providence fault zone has been correlated as a segment of the East Mojave fault, which is a ~70 km long north-to northwest-striking Cretaceous extensional structure spanning across the eastern Mojave Desert (Miller et al., 1996).

CHAPTER 3

PREVIOUS WORK

Granite and southern Providence Mountains

Previous geochronology has yielded U/Pb zircon ages of ~174 Ma for a large Jurassic hornblende-quartz diorite (unit Jqd, Fig. 2) in the west-central region of the Granite Mountains (Howard, 2000) and 155 Ma for an adjacent diorite pluton (unit Jd, Fig. 2) (Young et al., 1992). A pluton described by Miller et al. (1991) as Cretaceous porphyritic monzogranite (unit Kpm, Fig. 2) gave a U/Pb zircon age of ~70 Ma and a K/Ar biotite age of 70.9 Ma (Howard, 2000). Other data include K/Ar ages for hornblendes and biotites ranging from 64 to 74 Ma (Miller et al., 1991; Howard, 2000). These ages indicate preservation of original Mesozoic isotopic signatures and thus potential to provide information about Late Cretaceous tectonics.

Aluminum-in-hornblende geobarometry indicates crystallization pressures of 6.0 to 7.5 kbar for Jurassic and Cretaceous granitoids in the northern Granite Mountains, corresponding to emplacement depths of 19 to 25 km (Young and Wooden, 1988). Lower crystallization pressures of ~3 kbar suggest mid to shallow crustal emplacement at 8-16 km depth for plutons exposed at the southern extent of the Providence Mountains (Fox and Miller, 1990; Young and Wooden, 1988) (Fig. 2). This may indicate exposure of deeper and shallower segments of a single crustal section.

Mojave Desert Region

The Granite Mountains belong to a region of the East Mojave Desert that records substantial contractional and extensional tectonics as well as plutonism in the Jurassic, Cretaceous and Miocene (Howard et al., 1995). Late Cretaceous extension is recorded in the East Providence fault zone along the east side of the Providence Mountains (Fig. 2) as well as in the Piute and Old Woman Mountains, ~65 km to the southeast (Foster et al. 1990), the Funeral Mountains in Death Valley (Applegate et al., 1992), and the New York Mountains, ~60 km northeast of the Granite Mountains (Beyene, 2000) (Fig. 3). The Old Woman Mountains underwent rapid unroofing and denudation at the end of the Cretaceous (~73-70 Ma), probably accommodated by a top-to-the-southwest shear zone (Foster et al., 1992; Carl et al., 1991; Gerber et al., 1995). Unroofing of the Funeral Mountains metamorphic core complex has been constrained by U/Pb zircon geochronology between 72 and 70 Ma (Applegate et al., 1992) (Fig. 3). Late Cretaceous extension (>70-65 Ma) was documented in the Pinto Shear Zone in the New York Mountains (Beyene, 2000) (Fig. 3). The Pinto shear zone is a top-to-the-southwest normal-sense shear zone active from ~71 to 65 Ma, based on $^{40}Ar/^{39}Ar$ thermochronology of K-feldspar, biotite, and muscovite (Beyene et al., 2000). Together, the Pinto, East Providence, and Cima (also a down to the southwest normal shear zone) fault zones make up the East Mojave fault, which shows evidence for widespread down to the southwest Late Cretaceous extension stretching from the Old Woman Mountains to the south, north to the Funeral Mountains in the Death Valley region.

Further north, extension in the hinterland of the Sevier belt is recorded in the Newfoundland Mountains, Utah, (Allmendinger and Jordan, 1984) the Black Pine

Mountains, Idaho, (Wells et al., 1990) and the Raft River Mountains, Utah (Wells et al., 1990; Wells, 1997; Wells et al., 1998) (Fig. 3). Mesozoic normal faults in the Newfoundland Mountains suggest extension following Sevier shortening (Allmendinger and Jordan, 1984). $^{40}Ar/^{39}Ar$ geochronology on synkinematically-metamorphosed rocks from the Raft River and Black Pine Mountains suggests east-west extension in the Sevier hinterland occurred during the Late Cretaceous (Wells et al., 1990). These data support the idea of widespread extensional collapse of the Sevier orogenic belt as a result of crustal overthickening during earlier (Jurassic-Cretaceous) contractional tectonics (Hodges and Walker, 1992; Livaccari, 1991).

CHAPTER 4

SAMPLING STRATEGY AND ANALYTICAL METHODS

Sample Collection

Approximately 40 samples were collected across the Granite Mountains into the southern Providence Mountains. Four samples; Omar, Yoshi, Calvin, and Floyd (appendix a), were selected for analyses based on the criteria that they (1) contain the appropriate mineral assemblages for isotopic dating techniques and geobarometry, (2) were representative of their host pluton, and (3) formed a transect across the Granite Mountains into the southern Providence Mountains. Calvin, Floyd, and Yoshi, from the Granite Mountains, represent mapped units of monzogranite (Kpm), granodiorite (Kgd), and quartz monzonite (Jsq/Ksq), respectively, of Miller et al. (1991) (Fig. 2). Omar was collected from syenogranite (Jgo) in the Providence Mountains (Fig. 2). Throughout this thesis, plutons will be referred to by the map unit names of Miller et al. (1991), whereas corresponding sample names are quoted in the appendices.

Mineral Separation/Preparation Techniques

Prior to mineral separation, rock samples were crushed and sieved. Separation of zircon, hornblende, and K-feldspar was done using heavy liquids. Methylene iodide (SG = 3.32) was diluted with acetone to SG = ~2.60 to separate K-feldspar from quartz and

plagioclase. Franz isodynamic magnetic separators, and hand picking were used in the final stages of purification. Zircon was extracted from the 50 – 150 μm fraction. Hornblende and K- feldspar separates, purity >99%, were taken from 150 – 250 μm fractions.

Apatite separations were done by Donelick Analytical, Inc. Samples were crushed and sieved below 300 μm mesh and separated using SG = 3.0 lithium metatungstate, SG = 3.3 diiodomethane, and a Franz magnetic separator. Apatites were divided into two size fractions, >106 μm and <106 μm of which the former was used for final selection of crystals for analysis.

Aluminum-in-hornblende Geobarometry

Hornblende is a common phase in hydrous calc-alkalic magmas crystallizing at depth. The composition of hornblende has been found to vary with rock composition, pressure, and temperature (Hammerstrom and Zen, 1986; Hollister et al., 1987). Using electron microprobe analyses on hornblende from rocks with independently known pressures of crystallization, Hammarstrom and Zen (1986) presented an initial empirical correlation between the total Al (Al_T: total number of cations of Al per formula unit based on 23 oxygens) in hornblende and the estimated pressure of crystallization for calc-alkaline granitoid rocks with the mineral assemblage plagioclase + K-feldspar + quartz + hornblende + biotite + sphene + magnetite. This is now referred to as the aluminum-in-hornblende geobarometer (Hammerstrom and Zen, 1986). Pressure estimates were made on plutons crystallizing at shallow and deep crustal levels (1.5-3 kbar and 7-10 kbar) resulting in a calibration with ±3 kbar uncertainties.

Hollister et al. (1987) subsequently confirmed and refined the correlation by independently determining pressures for plutons crystallizing at mid-crustal depths (4-6 kbar), thus filling the gap in the Hammarstrom and Zen (1986) data. The results of Hollister et al. (1987) included a reduction in error to ±1 kbar. A number of studies have subsequently refined the aluminum-in-hornblende geobarometer. These include Johnson and Rutherford (1989), Rutter et al. (1989), Schmidt (1992), Anderson and Smith (1995), and Ague (1997). All of these calibrations yield slightly different pressure estimates although they essentially overlap within uncertainties.

Analyses for aluminum-in-hornblende geobarometry were done at the Electron Microanalysis and Imaging Laboratory at UNLV using a JEOL 8900 Electron Probe Microanalyzer. Instrument parameters were a 1μm spot size with a 2×10^{-8} A beam intensity and an accelerating voltage of 15 kV. Kakanui hornblende (Harvard standard; USNM 143965) was the standard used during the analysis (five unknowns were analyzed between each standard analysis). The chemical composition for Kakanui hornblende along with the other standards used to calibrate for weight percent Al_2O_3, FeO, K_2O, Na_2O, SiO_2, CaO, MgO, MnO, and TiO_2 are listed in appendix B. Analyses were conducted as 5-point transects from rim to core to rim across single hornblende crystals to identify any heterogeneity in distribution of aluminum within the crystals. Five crystals were analyzed for each sample, however, only analyses from one crystal (5 data points) were used from Omar (appendix B; Omar-7a-e), as the other four crystals define compositions that are not typical hornblende due either to alteration, or accidental analysis on a phase other than hornblende.

Following electron microprobe analysis, weight percent data was converted into structural formulas by dividing the oxide values obtained for major elements by their atomic weight and then converting to a molar proportion. From the molar proportions, the oxygens are summed and divided by 23. This value is multiplied by the cations yielding the total aluminum per 23 oxygens, which is used in a calibrated barometry equation for estimating the pressure of emplacement. Errors at 1σ represent quadratic summation of microprobe and calibration uncertainties.

U/Pb Geochronology

Geochronology using the U/Pb isotopic system is probably the most accurate method of dating for rocks older than a few tens of millions of years (Moser and Scott, 2000; Ludwig, 1998). This is in part due to the availability of three isotopic ratios for use in age calculations: $^{238}U/^{206}Pb$, $^{235}U/^{207}Pb$, and $^{207}Pb/^{206}Pb$. For an ideal analysis, where the sample is concordant and undisturbed (i.e. closed system), all three systems will yield ages that are equal within analytical error (Ludwig, 1998).

Zircons have been widely used as a U/Pb geochronometer. Cherniak and Watson (2000) found extremely slow diffusion rates for Pb, indicating that zircons will remain closed systems under most crustal conditions. From this data the closure temperature for zircons of standard analytical size (~100 μm) are in excess of 900 °C, whereas a typical crystallization temperature for granitic magmas is lower at ~750 °C. Thus, for granitic magmas such as those in this study, zircons are immediately closed to U and Pb diffusion upon crystallization and are interpreted to record timing of crystallization for plutons. The closure temperature for zircon in this study is thus taken as 750 °C.

Two methods for determining U/Pb zircon ages are ion microprobe analysis and what is referred to as 'conventional' U/Pb dating. Conventional U/Pb dating is done using a thermal ionization mass spectrometer along with isotope dilution to determine isotopic ratios. Results from this method tend to be very precise, however accuracy may be compromised due to the presence of multiple U/Pb systems within single zircon crystals such as older inherited cores with younger overgrowths (Fig. 5). Analysis on a high-resolution secondary ion mass spectrometer has proven to be a more accurate method in obtaining U/Pb zircon ages in such cases (Williams, 1992). Accuracy is gained using this method because areas only tens of microns in diameter may be analyzed, which allows for direct analysis of distinct age domains within individual zircon crystals. Using the ion microprobe, accuracy is increased, although analyses tend to be less precise than the conventional method as a result of the small amount of sample being analyzed. Thus, for zircons with complex internal U/Pb systematics, relatively imprecise ion microprobe analyses could be more useful than high precision conventional analyses (e.g. Williams, 1992). The ion microprobe method was chosen for the U/Pb analyses conducted in this research.

Zircons were analyzed at the National Ion Probe facility at UCLA using a CAMECA ims 1270 high resolution, high sensitivity ion microprobe. The zircon standard used for these analyses was AS-3 which yields a conventional U/Pb age of 1099.1 ± 0.5 Ma (Paces and Miller, 1993). Twenty-six analyses of AS-3 gave a Pb-U calibration with slope = 0.34 ± 0.07 (1σ), y-intercept = 7.66 ± 0.49 (1σ), and an MSWD of 12.58. Because the samples in this study are Mesozoic in age, the data are presented using Tera-Wasserburg concordia U/Pb diagrams where the X-axis is $^{238}U/^{206}Pb$ and the

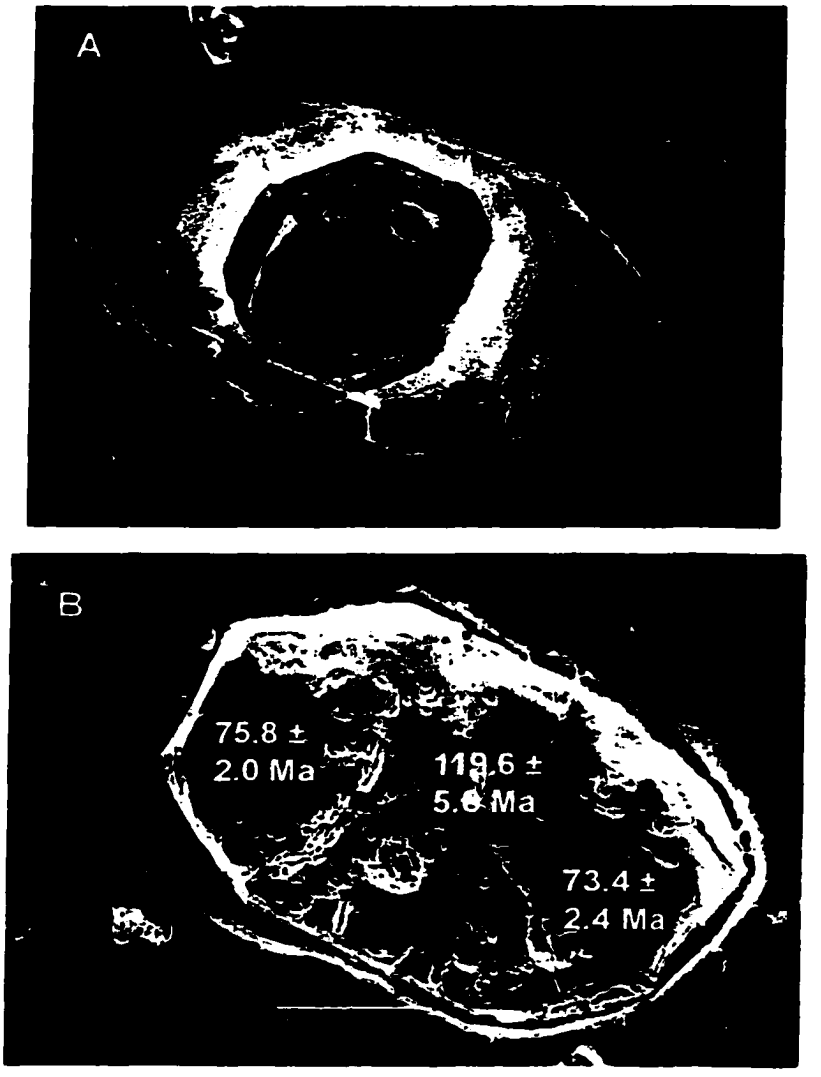

Figure 5. Example of inherited core with multiple U/Pb systems within a single zircon crystal. A. Cathodoluminesence image of zircon crystal from granodiorite prior to ion microprobe analysis. The crystal shows the presence of a distinct core within zoned overgrowths. B. Post-analysis SEM image of the same crystal. Analyses show an inherited core, yielding an age 50 Ma older than the rims.

Y-axis is $^{207}Pb/^{206}Pb$, allowing uncorrected $^{206}Pb/^{238}U$ points to define a linear array representing a mixing line between common Pb (y-axis) and age (x-axis) (Tera and Wasserburg, 1972). Tera-Wasserburg concordia diagrams have less correlated errors in the X- and Y-axis values making relative scatter of data points more evident (Ludwig, 2001). Also, for Mesozoic and Cenozoic samples, discordance is difficult to detect on conventional concordia plots due to the large uncertainties of $^{235}U/^{207}Pb$ ages and the relative linearity of concordia for young samples (few 100 Ma's). Linear regressions were done based on the MSWD criterion of Wendt and Carl (1991), where exclusion of analyses (inherited cores) was based on failure to obtain a statistically valid regression. The U/Pb zircon ages presented in this paper are uncorrected for common Pb and quoted at 1σ errors with decay constant errors included. Analytical data are presented in Appendix C.

$^{40}Ar/^{39}Ar$ Geochronology

$^{40}Ar/^{39}Ar$ dating was developed as a variation of the K/Ar method, which is based on the decay of ^{40}K to ^{40}Ar ($t_{1/2}$ = 1250 Ma), after it was found that during irradiation in a nuclear reactor, neutron interactions with ^{39}K produced ^{39}Ar (Merrihue, 1965; Merrihue and Turner, 1966). Through calibration of this conversion rate, both parent and daughter can be measured at the same time yielding more accurate and precise ages. Since this discovery, the $^{40}Ar/^{39}Ar$ method has become a widely applied technique for solving geologic problems (McDougall and Harrison, 1999).

There are numerous advantages in using the $^{40}Ar/^{39}Ar$ method over the K/Ar method. Among these is the ability to measure parent and daughter ratios accurately,

precisely, and simultaneously using a mass spectrometer. This is in contrast with K/Ar dating where these element abundances are measured on separate splits of the sample using different analytical techniques (McDougall and Harrison, 1999). $^{40}Ar/^{39}Ar$ dating thus allows for a smaller amount of sample for analysis. Another advantage is the incremental measurement of Ar released from the sample. Step heating yields several (usually 10 to 15) analyses for each sample, which allows for determining chemical information, argon distribution within the sample, and testing of the assumptions involved in K/Ar dating (McDougall and Harrison, 1999).

Principal assumptions applied to the K/Ar and $^{40}Ar/^{39}Ar$ methods include (1) the decay rate for ^{40}K is known accurately and precisely and is independent of temperature, pressure, and composition; (2) the isotopic composition of K ($^{40}K/K$) is constant in nature, since it is never measured directly; (3) the ^{40}Ar measured in the sample has been generated only by in situ ^{40}K decay since the time of crystallization; or (4) corrections for any nonradiogenic ^{40}Ar initially present in a sample can be made; and (5) the sample must have been a closed system with no loss or gain of K or radiogenic Ar (McDougall and Harrison, 1999). These assumptions may be tested and (for some) assessed more readily by the $^{40}Ar/^{39}Ar$ method than the K/Ar method, thus providing the basis for determining the reliability and meaning of measured ages (McDougall and Harrison, 1999).

The closure temperature for argon in hornblende is 500 ± 50 °C (McDougall and Harrison, 1999; Harrison, 1981). K-feldspar age spectra were modeled by the multi-diffusion domain model technique (when possible) (Lovera et al., 1989) to record a continuous cooling history from ~350 to ~150° C (Lovera et al.; 1991 Lovera, 1992).

Closure temperatures for any K-feldspar sample unsuitable for multidiffusion domain modeling were calculated using equations from Dodson (1973), and following Harrison and McDougall (1982).

Analyses were done at the Nevada Isotope Geochronology Laboratory at the University of Nevada, Las Vegas using a MAP 215-50 mass spectrometer. The atmospheric $^{40}Ar/^{36}Ar$ ratio and corresponding mass discrimination (4 AMU) factors are measured weekly and are recorded in data tables for individual samples (Appendix D). Samples were irradiated for 7 hours in the Oregon State University Radiation Center TRIGA type reactor. Analyses on K-glass and CaF_2 fragments were used to determine correction factors for interfering neutron reactions on K and Ca. $(^{40}Ar/^{39}Ar)_K$ values were 0.0132 ± 0.012. Correction factors for Ca were $(^{36}Ar/^{37}Ar)_{Ca} = 2.77 \times 10^{-4}$ ($\pm$ 2.28%) and $(^{39}Ar/^{37}Ar)_{Ca} = 7.44 \times 10^{-4}$ ($\pm$ 0.37%). J-factors (assigned 0.5% errors) were calculated using single crystal laser fusion of 3 to 5 Fish Canyon Tuff sanidines from each level of neutron flux throughout the irradiation package. Sample ages were calculated using an age of 27.9 Ma (Steven et al., 1967; Cebula et al., 1986) for the Fish Canyon Tuff sanidine. Plateaus are defined as three or more consecutive steps totaling at least 50% of the ^{39}Ar released with ages that overlap at 2σ analytical errors (excluding J error). Isochrons are defined by greater than three consecutive steps corresponding to at least 50% of the ^{39}Ar released, and follow the MSWD criterion of Wendt and Carl (1991).

K-feldspar Modeling

Heating schedules of 49 to 50 steps were used for step heating of K-feldspars. This allows for determination of argon diffusion parameters (frequency factor and activation energy) intrinsic to each sample (Lovera et al., 1989; Lovera et al., 1991).

Arrhenius plots of these data show a linear array for the low temperature steps of the heating schedule followed by a departure from linearity, which can be explained by multiple diffusion domain sizes within the sample (Lovera et al., 1989; Richter et al., 1991). The linear portion of the plots is produced by the smaller diffusion domain sizes, which are outgassed at low temperatures (Lovera et al., 1989). Multiple diffusion domain theory assumes that argon loss follows an Arrhenius Law, that the ^{39}Ar loss measured during step heating is by the same mechanism responsible for diffusive loss in nature, and implies that all domains have the same frequency factor (D_o, which is expressed as a combined parameter with the diffusion domain size, D_o/r^2) and activation energy (E) (Lovera et al., 1989; Lovera, 1992; Lovera et al., 1993). Experiments performed by Lovera et al. (1993) have supported the assumption of the same activation energy in multiple domains and Lovera et al. (2002) and Richter et al., (1991) showed that samples with highly correlated age and diffusion properties exhibit laboratory argon release that replicates natural diffusion mechanisms.

Computer programs were used to model Arrhenius data, log r/r_o, age spectra, thermal histories, and correlations between the laboratory results and modeled results (Lovera et al., 1989; Lovera et al., 2002). Acceptability of models was based on statistical criteria defined within the programs: only statistically valid models were returned and used.

Arrhenius data are modeled by applying the laboratory step-heating schedule (excluding steps above 1100 °C where K-feldspar melts and ceases to follow Arrhenius Law diffusive loss) to model domain distributions with the purpose of creating a domain distribution that will reproduce the Arrhenius data generated in the laboratory. Domain

distributions, expressed as log r/r_o vs. $\%^{39}Ar$ released plots, are also produced during this modeling. A correlation between the log r/r_o plots and age spectra is then determined to quantify the applicability of laboratory diffusion parameters to those in nature, with acceptable correlations of $C_{fg} > 0.8$ (Lovera et al., 2002). Since the age spectrum is a function of natural diffusion during geologic cooling, and the log r/r_o plot is generated in the laboratory (during a much shorter time scale) during heating, a high correlation indicates that laboratory diffusion is via the same mechanism as that in nature. When the lab and model distributions are in good agreement, cooling histories may be modeled to find those that produce an internal argon distribution that would reproduce the laboratory age spectra when modeled. A minimum of 20 cooling histories was used to define an acceptable cooling curve for a sample.

U-Th/He Geochronology

One of the first systems used by geochronologists to determine the ages of rocks was the production of ^4He from the decay of ^{238}U, ^{235}U, and ^{232}Th isotopes (^4He is also produced by decay of ^{147}Sm to ^{143}Nd, but this in insignificant amounts) (Rutherford, 1905; Strutt, 1905; Reiners, 2002). However, early studies yielded ages that were unexpectedly young (Hurley, 1954), leading to limited application and near abandonment of the U-Th/He method of dating. Renewed interest in the technique was inspired after Durango fluorapatite (Zeitler et al., 1987) and apatites from multiple geochemical environments (Lippolt et al., 1994) showed evidence suggesting ^4He ages may record cooling through a lower closure temperature (~100 °C) rather than crystallization ages. Further investigation by Wolf et al. (1996) found that He diffusion in apatite followed a

linear Arrhenius relationship below 290 °C with an activation energy of ~150 kJ/mol, indicating a closure temperature of ~75 °C. This temperature was thought to be independent of chemical composition and grain size suggesting possible application of a single closure temperature to a broad range of samples. Applicability of the U-Th/He system to low temperature thermochronology (~70 to 200 °C) has presently been demonstrated using several mineral phases including apatite, zircon, and titanite (House et al., 1998; Reiners and Farley, 1999; Farley, 2000; Reiners et al., 2002).

Apatite U-Th/He analyses were done at the California Institute of Technology. The ^{4}He is extracted by degassing crystals encased in a small foil packet with a CO_2 or Nd-YAG laser. Measurements are made using a quadropole mass spectrometer (to ~1% precision) following ^{3}He isotope dilution and cryogenic purification (Reiners, 2002). Following degassing, crystals are retrieved, dissolved, and analyzed by isotope dilution for U and Th using an ICP-MS with similar uncertainties. An additional step involved in calculating He ages is determining the α-ejection correction (Farley et al., 1996). Radiogenic ^{4}He is separated from parent U, Th, and decay chain isotopes with high kinetic energies (~4-5 MeV), resulting in long stopping distances (~10 to ~30μm depending on density/ composition of stopping medium) (Farley et al., 1996; Reiners, 2002). The importance of α-stopping distances for He dating is the potential ejection of a significant portion of the total ^{4}He produced from the crystal leading to underestimated ages. The correction for α-ejection (known as F_t correction) is based on the surface to volume ratio of the crystal and the α-stopping distance where crystals with larger surface to volume ratios require larger corrections (Farley et al., 1996).

CHAPTER 5

GEOBAROMETRY RESULTS

Pressures were estimated using calibrations of Hollister et al. (1987) and Schmidt (1992). The Hollister et al. (1987) calibration (P (± 1 kbar) = -4.76 + 5.64Al_T) was used for direct comparison with previous studies (Young and Wooden, 1988; Foster et al., 1989) where their equation was demonstrated to be applicable. The Schmidt (1992) calibration (P (± 0.6 kbar) = -3.01 + 4.76Al_T) represents an improvement to the Hollister et al. (1987) calibration and was used to demonstrate any significant difference in pressure estimates between the two. Although more recent calibrations have been published, (Chapter 4), Schmidt (1992) was selected because other recent calibrations (Anderson and Smith, 1995; and Ague, 1997) require plagioclase analyses, which were not obtained in this study and the experimental calibration of Schmidt (1992) is consistent with earlier empirical and experimental calibrations of the barometer. The Johnson and Rutherford (1989) calibration focused on volcanic rocks (this study focuses on plutonic rocks), whereas Rutter et al. (1989) applied barometry to igneous rocks at pressures greater than 10 kbar, significantly deeper than the mid-crustal rocks exposed in the Mojave Desert region (Young and Wooden, 1988).

All crystal rims represent conditions at the final stage of crystallization when all required phases (plagioclase + K-feldspar + quartz + hornblende + biotite + sphene + magnetite) are most likely present, and are therefore most ideal for estimating pressures

at emplacement. For plutons in the Granite Mountains, the mean Al_T values from all analyses and those found using only rim analyses are indistinguishable demonstrating that rim Al_T values are representative. Mean rim Al_T values (1σ errors) are 1.63 ± 0.04 for the SW monzogranite sample, 1.62 ± 0.08 for the central granodiorite sample, and 1.56 ± 0.09 for NE quartz monzonite sample (Table 1). Of 10 rim analyses, 9 were used in calculating the mean value for the monzogranite. One analysis ($Al_T = 1.12$) was excluded because it is more than 2σ lower than the mean. Hornblende from the syenogranite in the southern Providence Mountains yielded Al_T values ranging from 1.07 to 1.29 based on five analyses across one hornblende from rim to rim. These data yield a mean Al_T of 1.14 ± 0.09 (1σ) (Table 1).

Using the Hollister et al. (1987) and Schmidt (1992) equations, these Al_T values yield pressures of ~4.0 to 4.8 kbar for the Granite Mountains samples and ~1.7 to 2.4 kbar for the southern Providence Mountains sample (Table 1). Pressures for the Granite Mountains samples all overlap at 1σ error, corresponding to mid-crustal depths of emplacement (14.5 to 17.1 km) assuming a 3.6 km/kbar lithostatic gradient (Table 1). Of these three samples, the northeastern quartz monzonite sample yields a slightly lower mean Al_T value. Although pressure/depth estimates overlap for all Granite Mountains samples, the lower Al_T value may be indicative of a slightly shallower emplacement depth than the central granodiorite and SW monzogranite, which appear to have been emplaced at equal depths (Table 1). The implications of these data are discussed in Chapter 8. Mid-crustal emplacement depths are consistent with estimates for Cretaceous plutons in this region based on previous studies (Foster et al., 1989; Young and Wooden, 1988).

Table 1. Mean Al_T values from rim analyses for Granite and Providence Mountains samples, mean pressures with 1σ total uncertanties (quadratic summation of analytical and calibration errors), and depth ranges using calibrations by Hollister et al. (1987) and Schmidt (1992). Depths were calculated using a 3.6 km/kbar lithostatic gradient. Both calibrations indicate mid-crustal emplacement for Granite Mountains plutons and shallow crustal levels for the southern Providence Mountains pluton

Sample	Mean Al_T	Mean Pressure (kbar)		Depth (3.6km/kbar)	
		Hollister et al. (1989)	Schmidt (1992)	Hollister et al. (1989)	Schmidt (1992)
SW monzogranite	1.63 ± 0.04	4.43 ± 1.02	4.75 ± 0.63	15.95 ± 3.67	17.10 ± 2.27
central granodiorite	1.62 ± 0.08	4.40 ± 1.04	4.72 ± 0.66	15.84 ± 3.74	16.99 ± 2.38
NE quartz monzonite	1.56 ± 0.09	4.03 ± 1.03	4.41 ± 0.67	14.51 ± 3.71	15.88 ± 2.41
Providence syenogranite	1.14 ± 0.09	1.68 ± 1.02	2.42 ± 0.64	6.05 ± 3.67	8.71 ± 2.30

Shallow crustal emplacement depths have been determined for Jurassic plutons in the southern Providence Mountains by Young and Wooden (1988) and Fox and Miller (1990). Five analyses from the syenogranite sample yield pressures of 1.68 ± 1.02 kbar (Hollister et al., 1987) and 2.42 ± 0.64 kbar (Schmidt, 1989) (Table 1). These data correspond to emplacement depths ranging from 6.05 to 8.71 km, which is consistent with the previous studies.

CHAPTER 6

GEOCHRONOLOGY RESULTS

U/Pb Zircon

The following sections refer to data tables in Appendix C for ion microprobe U/Pb analyses on zircons from the southwest monzogranite (Calvin), central granodiorite (Floyd), northeast quartz monzonite (Yoshi), and southern Providence syenogranite (Omar). All ages are uncorrected and errors are quoted at ± 1σ.

Southwest monzogranite

Ten analyses were made from the SW monzogranite sample (Calvin). Two zircons with inherited cores yielding $^{238}U/^{206}Pb$ ages of 93.4 and 134.8 Ma (appendix C) were discovered. These two analyses were excluded after statistically invalid linear regressions were obtained. The remaining eight analyses ranging from 75 to 87 Ma define a concordia intercept age of 71.6 ± 2.7 Ma (1σ, MSWD = 1.30) (Fig. 6). Based on these data the age of intrusion and crystallization for the monzogranite pluton is 71.6 ± 2.7 Ma.

Central granodiorite

Nine zircon spots were analyzed from the granodiorite sample (Floyd). An inherited core with a $^{238}U/^{206}Pb$ age of 119.6 Ma (appendix C) was excluded after linear regression of all 9 analyses resulted in a high MSWD of 5.6. The remaining 8 analyses

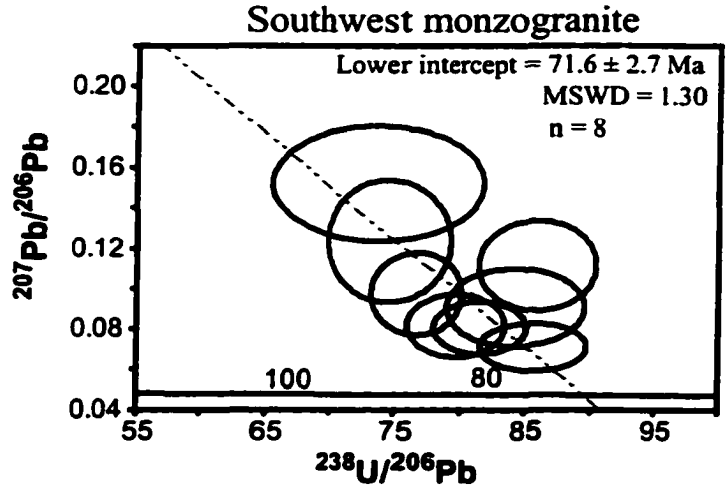

Figure 6. Tera-Wasserburg U/Pb diagram for monzogranite zircons. Eight analyses yield a concordia intercept age of 71.6 ± 2.7 Ma. All errors reported are at 1 σ.

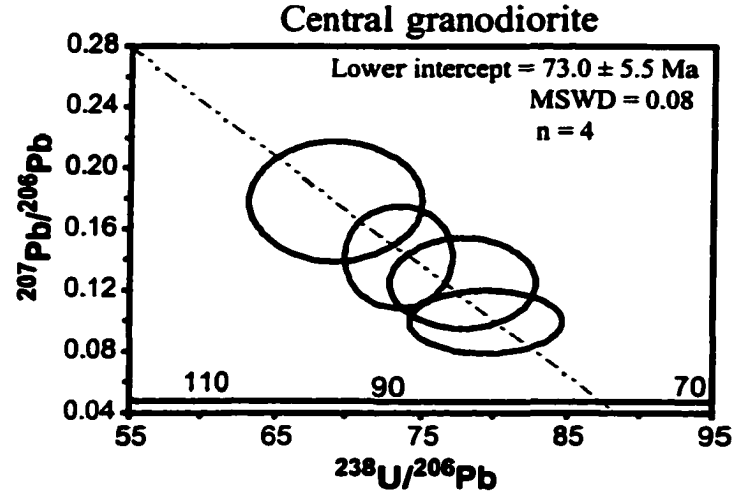

Figure 7. Tera-Wasserburg U/Pb diagram for granodiorite zircons. Four analyses yields a concordia intercept age of 73.0 ± 5.5 Ma. All errors reported at 1 σ.

ranging from ~73 to ~93 Ma, define a statistically valid intercept age of 67.5 ± 2.4 Ma (1σ) with an MSWD of 0.46. However, based on a $^{40}Ar/^{39}Ar$ age of 74.8 ± 0.4 Ma for hornblende from this sample (discussed in the next section) a crystallization age of 68 Ma is unlikely. Within this eight-point data set are two subsets (4 analyses in each) with age ranges of 73 to 76 Ma and 80 to 93 Ma. The younger subset consists of analyses with higher and very similar radiogenic yields. The older set defines a wider range of radiogenic yields and thus a better constrained line fit. The four younger analyses yield a concordia intercept age of 71.2 ± 4.5 Ma (1σ) with an MSWD of 0.24, which is concordant with the $^{40}Ar/^{39}Ar$ data. A linear regression using the older data points yields an indistinguishable intercept age of 73.0 ± 5.5 Ma (1σ) with an MSWD of 0.08 (Fig. 7). As this latter age is defined by a better-constrained linear regression because of the larger spread of the data points, it is therefore interpreted as the age of crystallization for the granodiorite.

Northeast quartz monzonite

Twelve spots were analyzed on zircons from the NE quartz monzonite sample (Yoshi). Four inherited Jurassic cores were found (157, 164, and 179 Ma) along with a young outlier yielding an age of ~61 Ma (appendix C). This anomalously young age is most likely a result of Pb loss. The remaining eight analyses ranging from 76 to 93 Ma yield a concordia intercept age of 76.0 ± 3.3 Ma (1σ) with an MSWD of 1.80 (Fig. 8). This sample was collected from a pluton mapped as Jurassic spotted quartz monzonite (Jsq) by Miller et al. (1985), however, these data indicate the pluton is Cretaceous. The age of crystallization for this pluton is interpreted as 76.0 ± 3.3 Ma.

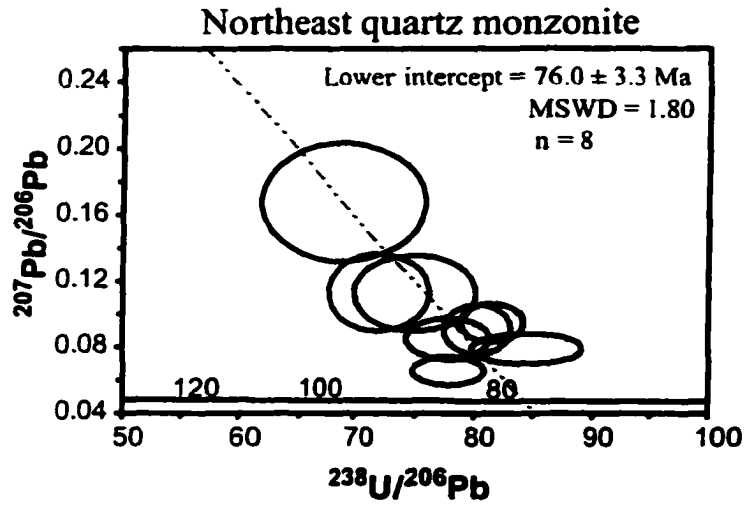

Figure 8. Tera-Wasserburg U/Pb diagram for quartz monzonite zircons. Eight zircon analyses yield a concordia intercept age of 76.0 ± 3.3 Ma. All errors reported at 1σ.

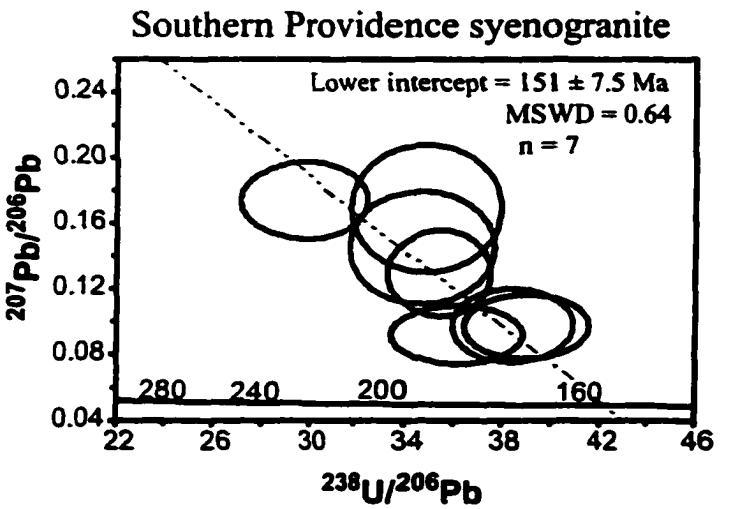

Figure 9. Tera-Wasserburg U/Pb diagram for quartz monzonite in the southern Providence Mountains. Seven zircon analyses give a linear regression with a concordia intercept age of 151 ± 7.5 Ma. All errors reported at 1σ.

Syenogranite

Seven analyses from the syenogranite sample (Omar) from the Providence Mountains yield ages ranging from 163 to 212 Ma. These data define a concordia intercept age of 151 ± 7.5 Ma (1σ) with an MSWD of 0.64 (Fig. 9). This age is consistent within errors of U/Pb zircon and K/Ar biotite ages (162 to 164 Ma and 157 ± 4 respectively) reported by Miller et al. (1985) and is considered as the crystallization age for this pluton.

The zircon ages presented for the Granite Mountains plutons are all concordant with their $^{40}Ar/^{39}Ar$ hornblende ages, which are reported in the following section. The zircon age determined for the syenogranite in the southern Providence Mountains is consistent with ages determined in previous studies of other Jurassic plutons in the region.

$^{40}Ar/^{39}Ar$ Results

Hornblende

The following sections refer to data tables in Appendix D for $^{40}Ar/^{39}Ar$ analyses on hornblende and K-feldspar from the SW monzogranite (Calvin), granodiorite (Floyd), NE quartz monzonite (Yoshi), and syenogranite of Quail Spring (Omar). All errors are quoted at ± 1σ.

Southwest monzogranite

Hornblende from the SW monzogranite sample gave an ideal flat age spectrum after four slightly younger initial steps (Fig. 10). Steps 7 through 16 define a plateau age of 74.80 ± 0.42 Ma, accounting for 88.8% of ^{39}Ar released. This is indistinguishable

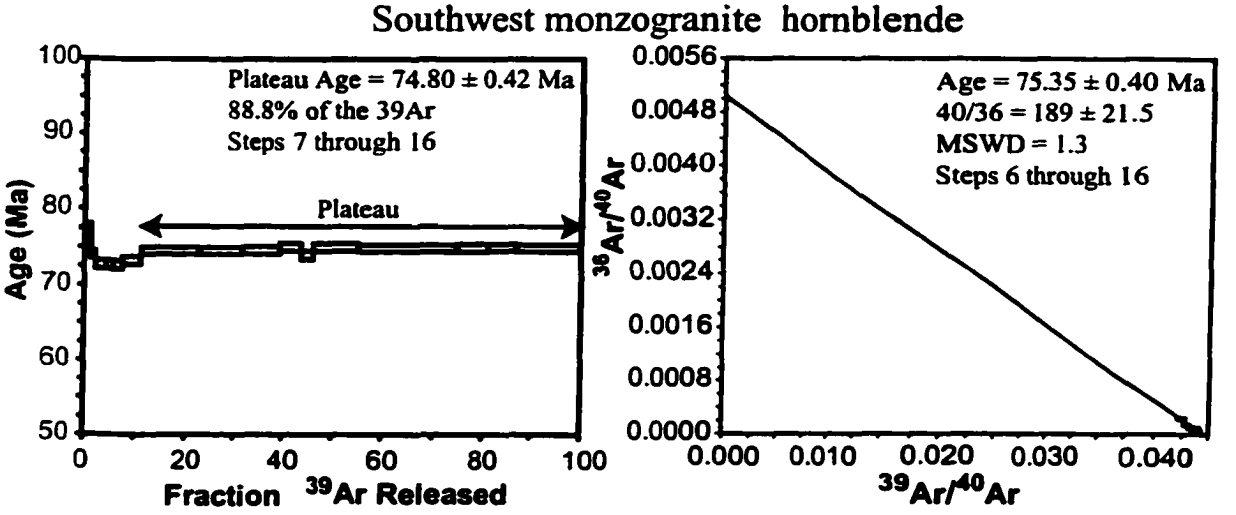

Figure 10. $^{40}Ar/^{39}Ar$ age spectrum and isochron for hornblende from monzogranite. Errors are quoted at 1σ.

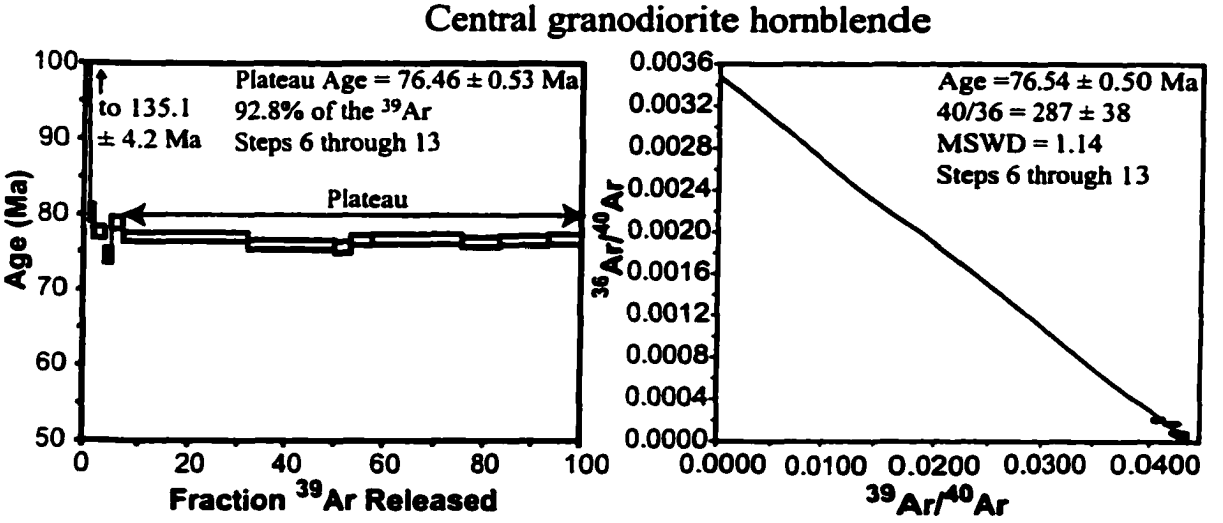

Figure 11. $^{40}Ar/^{39}Ar$ age spectrum and isochron for hornblende from granodiorite. Errors are quoted at 1σ.

from the total gas age of 74.65 ± 0.42 Ma (appendix D). A valid isochron using steps 6 through 16 (92.3% of ^{39}Ar released) gave an age of 75.35 ± 0.40 Ma with an MSWD of 1.3. Due to the high radiogenic yields for these steps, the initial $^{40}Ar/^{36}Ar$ of 189 ± 21.5 is poorly constrained and significantly below the atmospheric ratio of 295.5, indicating it is clearly spurious. Because of the questionable $^{40}Ar/^{36}Ar$ intercept of the isochron and the high radiogenic yields indicating insensitivity to excess argon, the plateau age of 74.80 ± 0.42 Ma is interpreted as the timing of cooling through ~500 °C for the pluton. This age is nearly indistinguishable within 1σ errors from the U/Pb crystallization age of 71.6 ± 2.7 Ma which suggests intrusion and very rapid cooling through 500 °C.

Central granodiorite

After high initial ages of ~135 Ma and ~80 Ma, hornblende from the granodiorite sample gave a concordant flat age spectrum (Fig. 11). A plateau using 92.8% of the ^{39}Ar released during steps 6 through 13 gave an age of 76.46 ± 0.53 Ma, indistinguishable at 1σ errors from the 77.35 ± 0.53 Ma total gas age (appendix D). An isochron using the same steps as the plateau, gave an age of 76.54 ± 0.50 Ma with an MSWD of 1.14. Similar to hornblende from the southwest monzogranite pluton, the high radiogenic yields result in a poorly constrained initial $^{40}Ar/^{36}Ar$ of 287 ± 38, but indicate no excess argon is present. Although the plateau and isochron ages are identical, the plateau age of 76.46 ± 0.53 Ma is taken as the best age for the pluton cooling through ~500 °C, because of the high radiogenic yields. The hornblende plateau age and the U/Pb zircon age of 73.0 ± 5.5 Ma are indistinguishable within 1σ uncertainty suggesting cooling through 500 °C upon intrusion.

Northeast quartz monzonite

A flat concordant age spectrum was obtained for hornblende from the quartz monzonite sample after a high initial age of ~104 Ma (Fig. 12). Steps 7 through 14, representing 77% of the ^{39}Ar released, yield a plateau age of 77.38 ± 0.11 Ma, which is slightly younger than the total gas age of 78.65 ± 0.43 Ma (appendix D). An isochron was obtained using steps 6 through 9, accounting for 39.5% of the ^{39}Ar released, giving an age of 76.57 ± 0.90 Ma. The isochron $^{40}Ar/^{36}Ar$ intercept of 388 ± 40 indicates the presence of excess argon in this sample. The isochron for the sample is considered the best estimate of the age because of the presence of excess argon. Within 1σ errors the isochron age and the U/Pb zircon age of 76.0 ± 3.3 Ma are concordant. These ages suggest that the quartz monzonite pluton intruded, crystallized, and rapidly cooled through ~500 °C.

Southern Providence syenogranite

Hornblende from a syenogranite sample from the southern Providence Mountains yielded a very discordant age spectrum with ages ranging from ~755 Ma to ~168 Ma (Fig. 13). The total gas age for the sample is 286.23 ± 1.42 Ma and there is no plateau (appendix D). The "saddle-shape" of the age spectrum may indicate the presence of excess argon in the sample, however no valid isochron was obtained to verify this. For samples such as this, the minimum age on the spectrum (168.3 ± 1.5 Ma) is interpreted as a maximum age for the sample. This interpretation is consistent with the younger U/Pb zircon age of 151 ± 7.5 Ma. Since zircon has a higher closure temperature for Pb (>900 °C) than hornblende does for Ar (500 °C), the older ages recorded in the $^{40}Ar/^{39}Ar$ age spectra are likely to be artifacts due to excess argon.

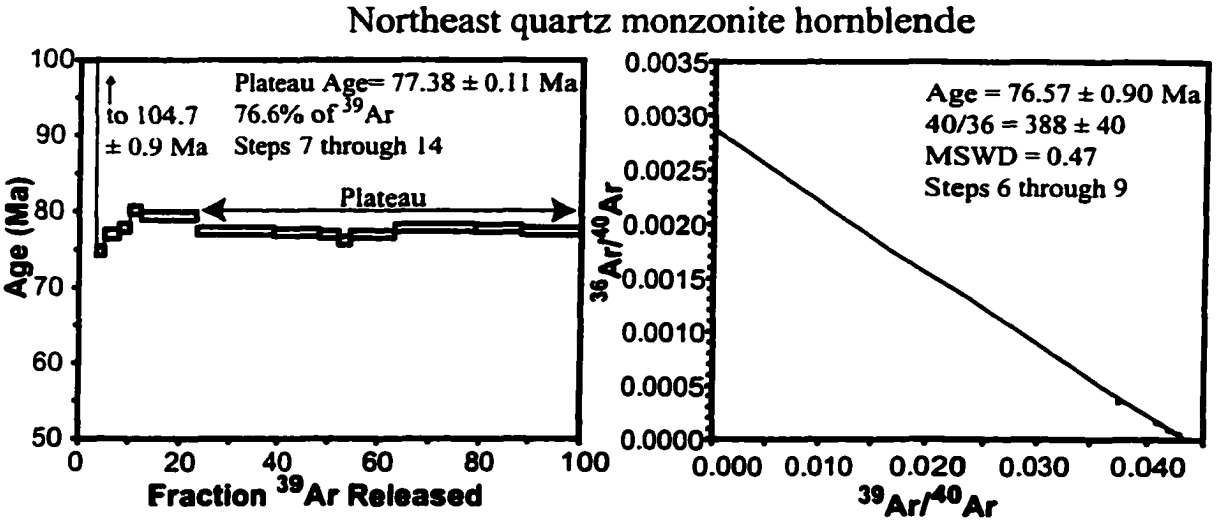

Figure 12. $^{40}Ar/^{39}Ar$ age spectrum and isochron for hornblende from NE Granite Mountains quartz monzonite. Errors are quoted at 1σ.

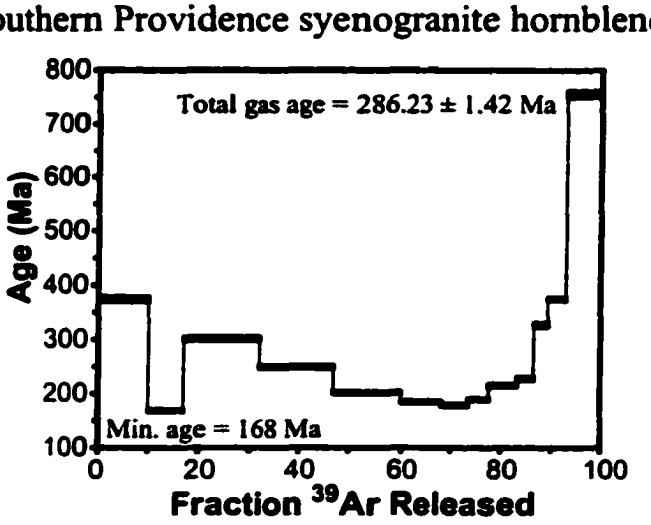

Figure 13. $^{40}Ar/^{39}Ar$ age spectrum for hornblende from quartz monzonite in the southern Providence Mountains. Errors are quoted at 1σ.

K-feldspar

Southwest monzogranite

K-feldspar from the SW monzogranite sample gave a relatively flat age spectrum (Fig. 14). The first 0.5% of the ^{39}Ar released showed an age variation from ~106 Ma to ~64 Ma (appendix D), which is probably a result of low temperature release of a very small amount of fluid inclusion hosted excess argon. The second of the isothermal duplicates (555 – 720 °C) gave lower ages (~1-2 Ma) than the first step ages (appendix D). Apparent ages from the 761 °C step through melting and fusion (> 1100 °C) gave a subtly increasing ages from ~70 to ~72 Ma for the remaining 90% of the ^{39}Ar released. The resulting flat age spectrum gave a total gas age of 71.01 ± 0.35 Ma and is indicative of fast cooling, which is further discussed in chapter 7.

Central granodiorite

After an initial ~98 Ma step (0.2% of ^{39}Ar), the apparent age spectrum exhibits ages increasing in age from ~65 in low temperature steps to ~73 Ma in high temperature steps (Fig. 15). Isothermal duplicates showed very little variation in apparent ages indicating no excess argon (appendix D). The age spectrum yields a total gas age of 70.73 ± 0.35 Ma. Although this age spectrum is not as flat as the age spectrum for K-feldspar from the SW monzogranite, it also suggests relatively rapid cooling.

Northeast quartz monzonite

A gradually increasing age spectrum from ~67 to ~75 Ma resulted after a high initial step (~220 Ma) and minor variation in apparent ages during early isothermal duplicates (473-596 °C; appendix D) (Fig. 16). Apparent ages for this pluton are slightly older than those for the monzogranite and the granodiorite after step 25 (1002 °C)

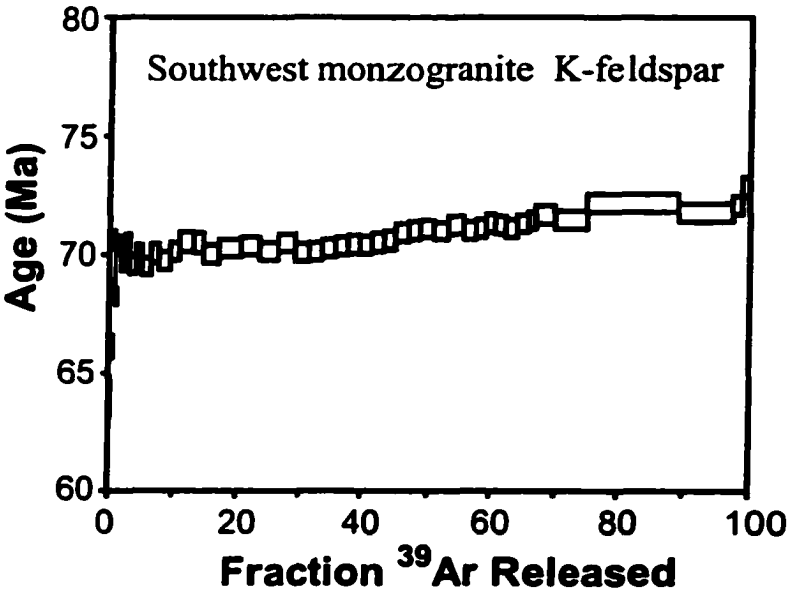

Figure 14. The $^{40}Ar/^{39}Ar$ age spectrum for K-feldspar from monzogranite. Errors are quoted at 1σ.

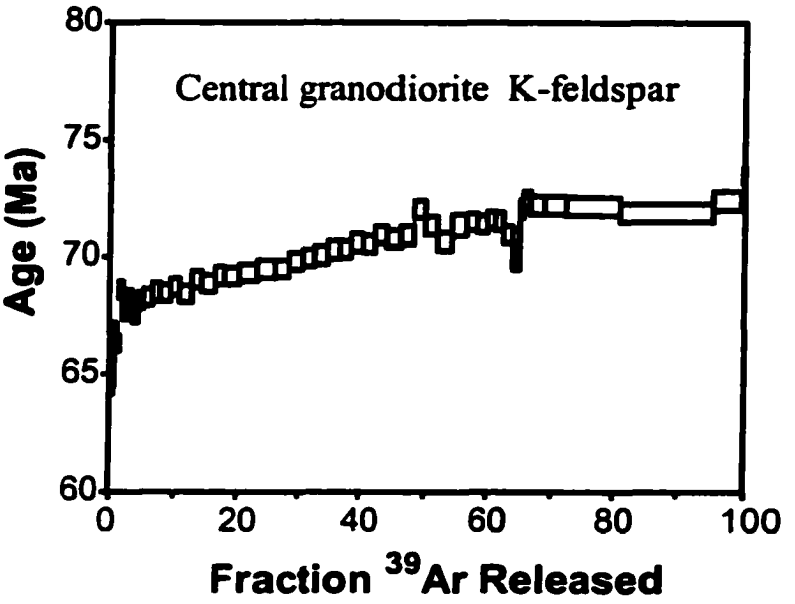

Figure 15. The $^{40}Ar/^{39}Ar$ age spectrum for K-feldspar from granodiorite. Errors are 1σ.

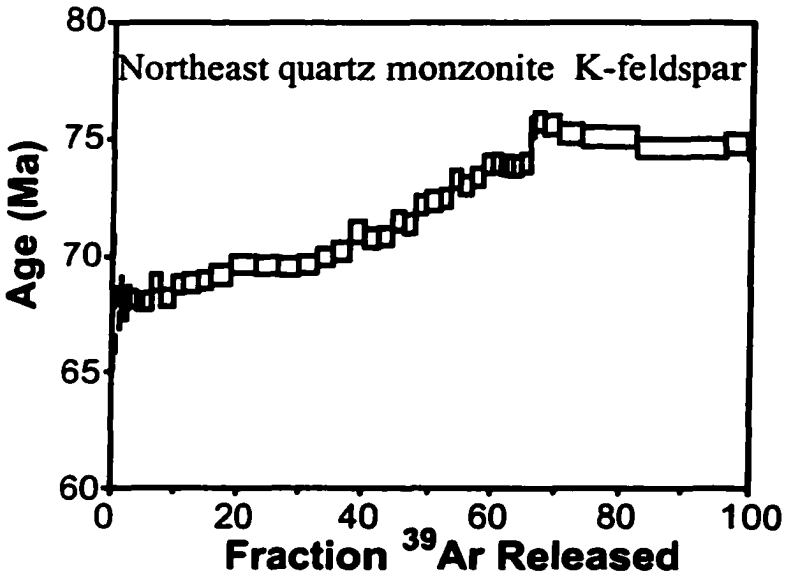

Figure 16. The $^{40}Ar/^{39}Ar$ age spectrum for K-feldspar from Granite Mountains quartz monzonite. Errors are 1σ.

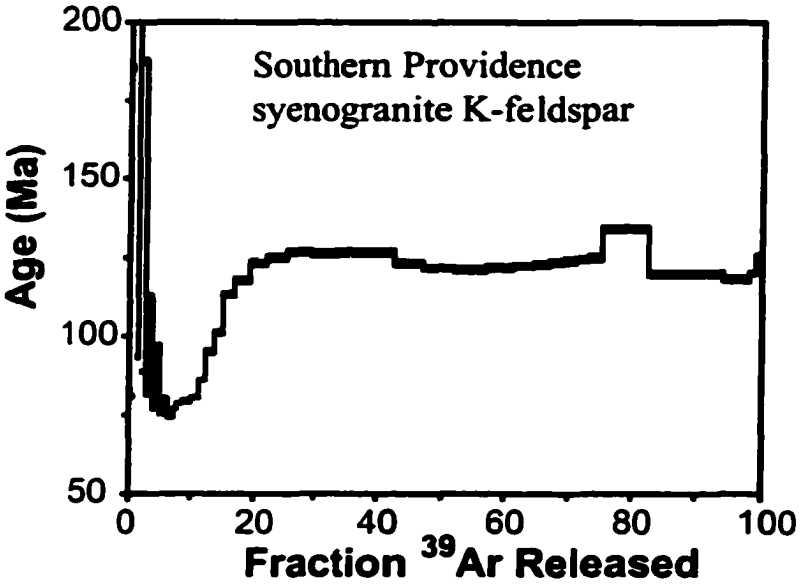

Figure 17. The $^{40}Ar/^{39}Ar$ age spectrum for K-feldspar from southern Providence Mts quartz monzonite of Goldstone. Errors are 1σ.

resulting in a steeper age gradient in the spectrum and an older total gas age; 72.32 ± 0.36 Ma. The slope of the age spectrum suggests somewhat slower cooling than the other plutons.

Southern Providence syenogranite

K-feldspar from the syenogranite in the southern Providence Mountains shows ages ranging from 294 Ma to 75 Ma over the first 6% of ^{39}Ar released (appendix D; Fig. 17). The highest ages are during the first of the isothermal duplicates and represent a relatively large amount of excess argon being released from inclusions. After the varying initial isothermal steps, apparent ages increase from ~77 to ~127 Ma over the next 35.5% of ^{39}Ar released (appendix D). The total gas age for the sample is 119.9 ± 0.6 Ma. Overall this age spectrum is very discordant compared to the Granite Mountains samples. A weighted mean age of 86.49 ± 0.24 Ma corresponding to a closure temperature of 210 ± 40 °C was calculated using steps 2 through 5. This age is significantly older than those from Granite Mountains K-feldspar samples. The relatively low radiogenic yields obtained for steps 2 through 5 may indicate these ages are affected by excess Ar (appendix D) (Chapter 7) and is discussed further in chapter 7.

U-Th/He Apatite

The ages determined using two single crystal analyses for each sample are: 23.6 ± 0.8 Ma from the SW monzogranite pluton:, 40.2 ± 3.3 Ma from the central granodiorite pluton:, 21.2 ± 2.2 Ma from a NE quartz monzonite pluton:, and 35.1 ± 2.3 Ma from syenogranite in the southern Providence Mountains: (all errors at 1σ; appendix E). These data exhibit a positive correlation between age and elevation (Fig. 18), which may

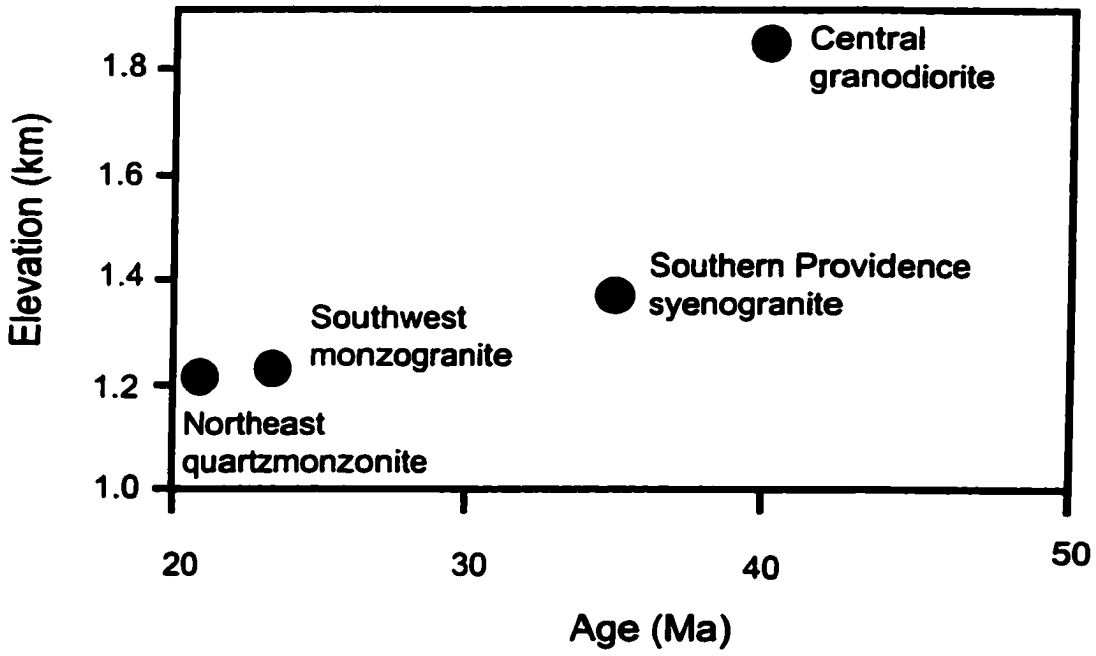

Figure 18. Plot showing correlation between U-Th/He ages and present elevation for samples from the Granite and southern Providence Mountains.

be explained by either very slow cooling following Late Cretaceous tectonics or a prolonged residence in the He partial retention zone.

CHAPTER 7

THERMAL HISTORIES

K-feldspar Multidomain Modeling

Southwest monzogranite

The initial low temperature linear array of the Arrhenius plot (steps 2 through 6) gave an activation energy (E) and D_o/r^2 of 168.6 kJ/mol and 755.4 s^{-1}, respectively (Fig. 19a). The model Arrhenius data, log r/r_o (domain distribution plot), and age spectra all show good agreement with the sample data (Fig 19 a-c). A high correlation coefficient of 0.87 between the log r/r_o plot and age spectrum indicates the relevance of the laboratory diffusion with that in nature (Lovera et al., 2002). The modeled age spectra (Fig. 19c) corresponding to the 20 cooling histories are shown in Fig. 19d. The upper and lower limits of model cooling curves are constrained by closure temperatures calculated for the estimated diffusion domains (Table 2). The model cooling histories are highly reproducible (Fig. 20a) and define a well-constrained cooling curve showing rapid cooling from 303 to 183 °C between 71.0 and 69.1 Ma (Fig. 19d & 20a). This corresponds to a cooling rate of 63.2 °C/Ma, and a denudation rate of 2.1 mm/yr (assuming a 30 °C/km geothermal gradient) between 71.0 and 69.1 Ma.

Figure 19. A: Arrhenius plot for K-feldspar from SW monzogranite showing sample data (diamonds) and model (filled circles). B: Domain size distribution plot with sample data (black) and model (gray). C: Sample age spectrum (black) with modeled age spectra overlying. D: 20 thermal histories corresponding to the age spectra in C. Gray box indicates interval during which the sample was recording.

Figure 19.

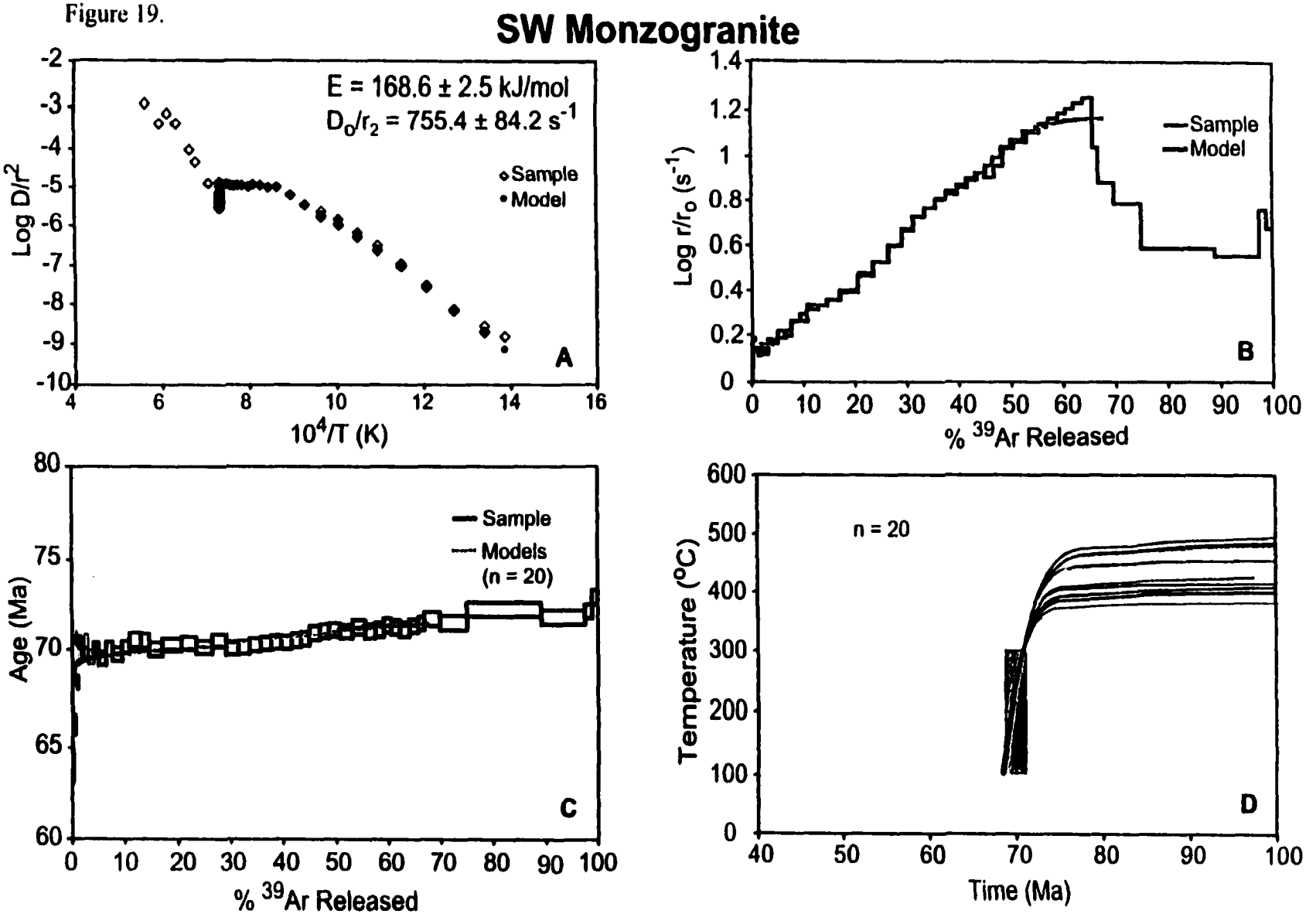

Table 2. Diffusion parameters and calculated closure temperatures for Granite Mountains K-feldspars. E is activation energy, D is diffusion coefficient, ρ is volume fraction of each domain, Tc is closure temperatures, r^1, r^2, r^3....r^6 are relative domain sizes.

Diffusion Parameters	Southwest monzogranite	Central Granodiorite	Northeast quartz monzonite
E, kJ/mol	168.6	160.0	151.0
log (D/r^1)	5.2874870	5.1472083	4.2585685
ρ_1	0.0289459	0.0481174	0.0094906
Tc_1	183 °C	157 °C	145 °C
log (D/r^2)	4.1555758	3.8883916	3.1323605
ρ_2	0.0649949	0.0936750	0.1012080
Tc_2	210 °C	185 °C	170 °C
log (D/r^3)	3.5816602	3.2248793	2.7432369
ρ_3	0.1160971	0.0936750	0.1179123
Tc_3	225 °C	201 °C	179 °C
log (D/r^4)	2.5721137	2.1715751	1.8950039
ρ_4	0.1547621	0.1419780	0.2069467
Tc_4	253 °C	229 °C	201 °C
log (D/r^5)	1.0089939	1.5257370	0.1865962
ρ_5	0.6352001	0.1721033	0.5644425
Tc_5	303 °C	248 °C	251 °C
log (D/r^6)		0.1352336	
ρ_6		0.4651074	
Tc_6		293 °C	

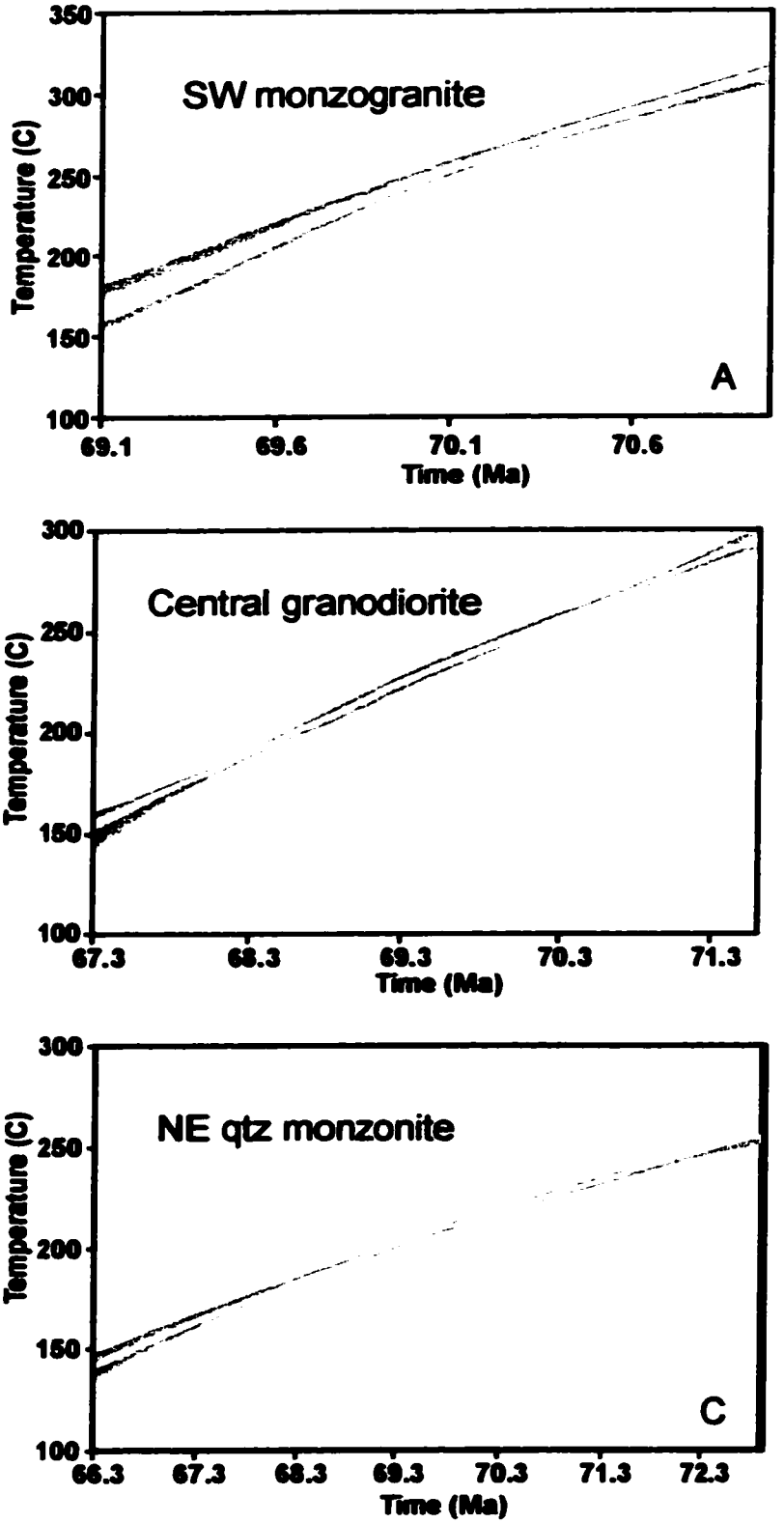

Figure 20. 90% confidence intervals for K-feldspar cooling curves for SW (A), central (B), and NE (C) plutons. Blue indicates 90% confidence that a modelled cooling curve will fall within the region. Yellow shows 90% confidence where the mean of a new series of models will fall.

Central granodiorite

An activation energy of 160.0 kJ/mol and D_o/r^2 of 820.2 s^{-1} was determined from steps 1 through 4 on the Arrhenius plot for K-feldspar from the central granodiorite (Fig. 21a). As with K-feldspar from the SW monzogranite pluton, modeled Arrhenius data, log r/r_o plot, and age spectra for the granodiorite show very good agreement with sample data (Fig. 21a-c). Log r/r_o and age spectra plots have a correlation coefficient of 0.93 supporting consistency between diffusion in the laboratory during step heating and diffusion in nature. Thirty-three modeled cooling histories were produced along with their corresponding age spectra (Fig. 21c,d). The cooling curves define a tightly constrained thermal history (Figs. 21d & 20b) indicating cooling from 293 to 157 °C between 71.6 and 67.3 Ma. This corresponds to a cooling rate of 31.6 °C/Ma or denudation rate of 1.1 mm/yr.

Northeast quartz monzonite

Steps 2 through 12 of the Arrhenius plot for K-feldspar from the quartz monzonite pluton yield an activation energy and D_o/r^2 values of 151.0 kJ/mol and 46.3 s^{-1}, respectively (Fig. 22a). Laboratory and modeled Arrhenius data, log r/r_o plot, and age spectrum are in very good agreement (Fig. 22a-c). The log r/r_o plot and age spectrum have a correlation coefficient of 0.98, supporting confidence in the models and the relevance of laboratory diffusion properties to nature. Along with their respective age spectra, twenty-eight modeled cooling histories were obtained, defining a well-constrained (Figs. 22d, 20c) thermal history from 251 to 145 °C between 72.9 and 66.2 Ma (Fig. 20d). A cooling rate of 15.8 °C/Ma and denudation rate of 0.5 mm/yr can be interpreted from these cooling curves.

Figure 21. A: Arrhenius plot for K-felspar from granodiorite showing sample data (diamonds) and model (filled circles). B: Domain size distribution plot for sample (black) and model (gray). C: Sample age spectrum (black) with modeled age spectra overlying. D: Thermal histories corresponding to the age spectra in C. Gray box indicates interval during which the sample was recording.

Figure 21.

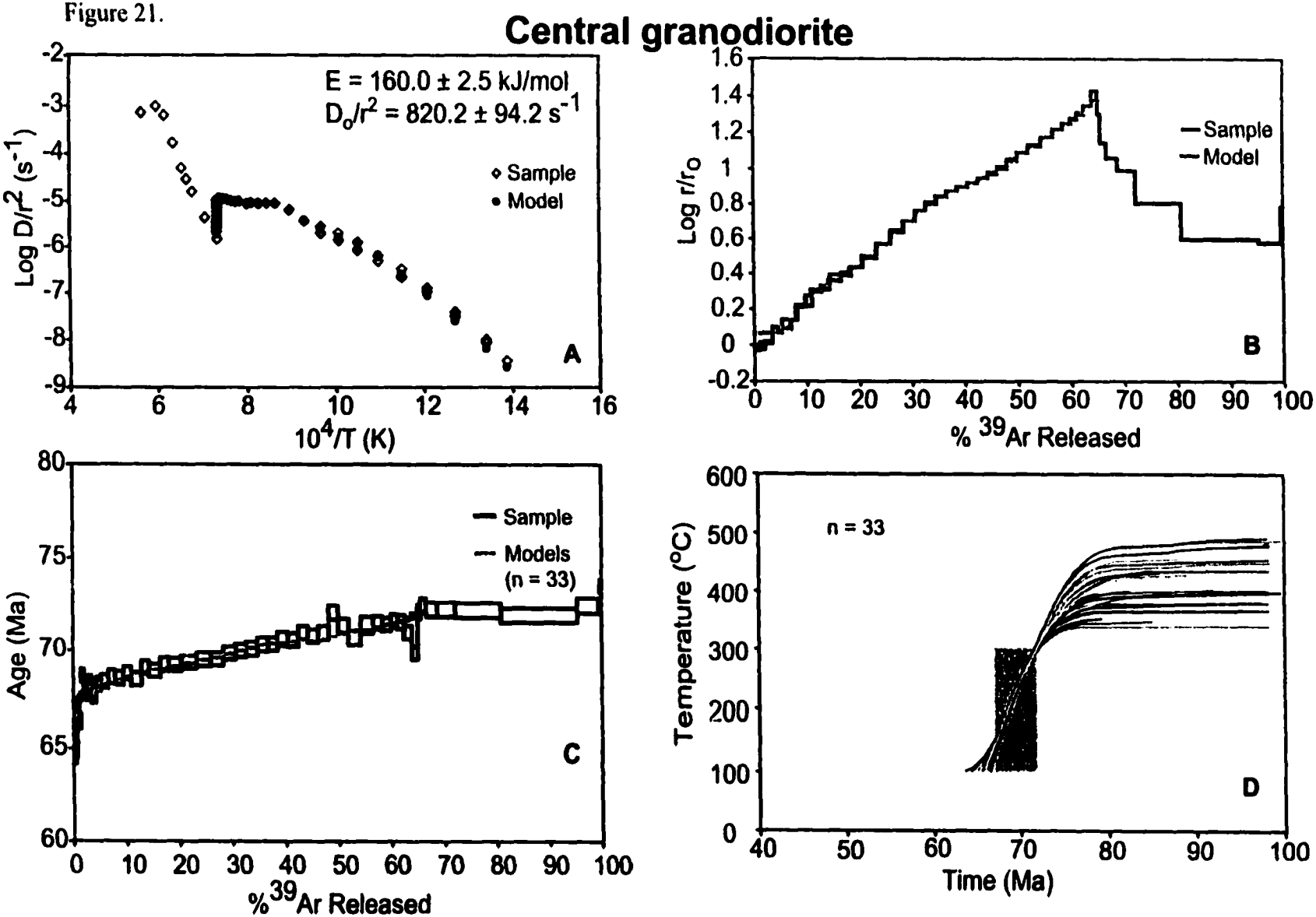

Figure 22. A: Arrhenius plot for K-feldspar from a NE quartz monzonite pluton showing sample data (diamonds) and model (filled circles). B: Domain size distribution plot for sample (black) and model (gray). C: Sample age spectrum (black) with modeled age spectra overlying. D: Thermal histories corresponding to the 28 age spectra in C. Gray box indicates the interval during which the sample was recording.

Figure 22

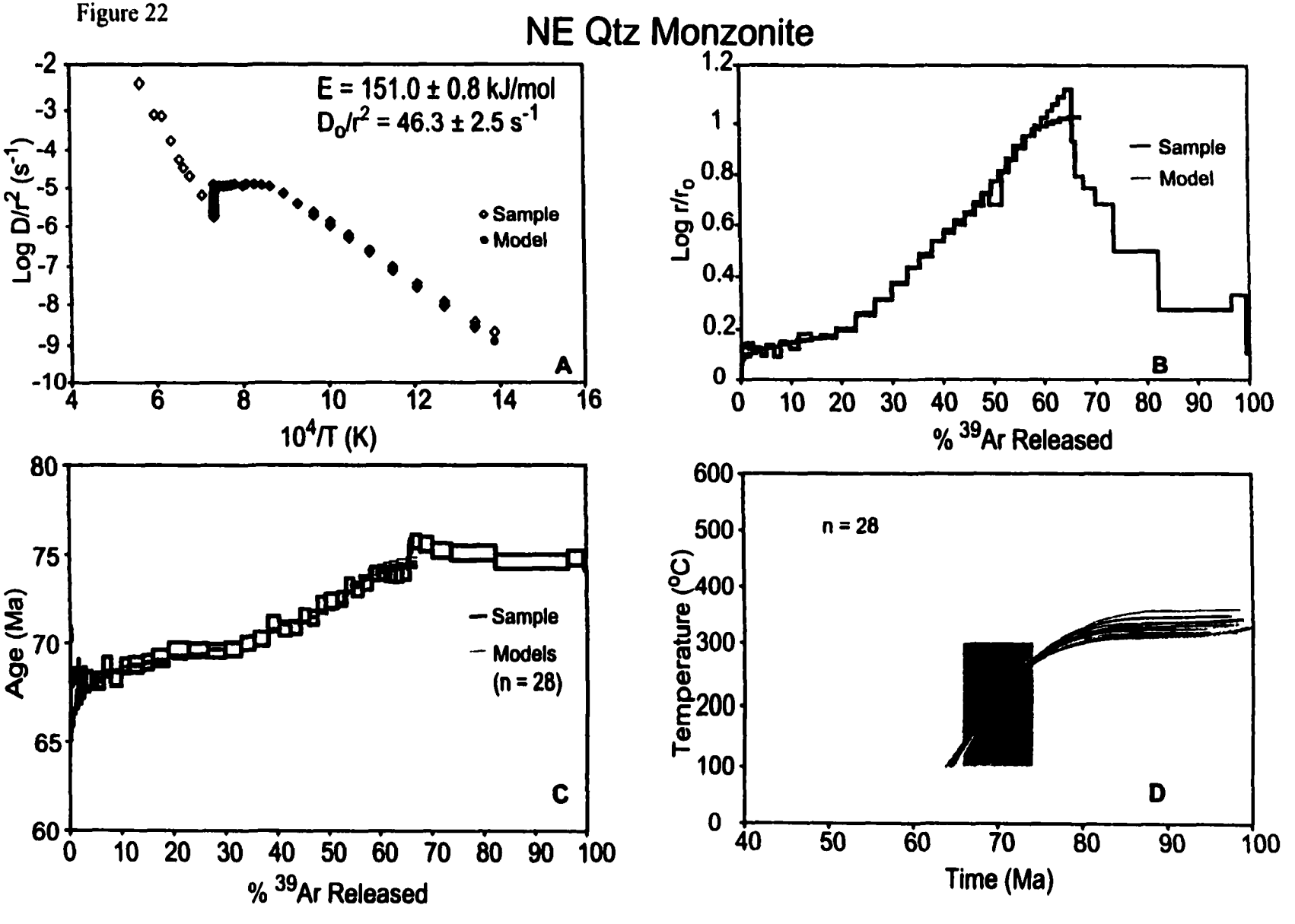

Southern Providence syenogranite

K-feldspar from the syenogranite in the southern Providence Mountains was not suitable for multi-domain modeling. The log r/r_o and age spectra correlation was very poor at 0.19 indicating this sample does not conform to the assumptions of the multi-diffusion domain model (Fig. 23). However, the low temperature diffusion data do provide for an interpretation of this sample. An activation energy of 150.6 kJ/mol and D_o/r^2 of 42.3 s^{-1} was obtained from the steps 2 through 5 of the Arrhenius plot corresponding to the second of the isothermal duplicates from 473 to 596 °C (Fig. 23a). These diffusion parameters were used to calculate a closure temperature of 210 ± 41 °C (Dodson, 1973; Harrison and McDougall, 1982). These steps yield a weighted mean age of 86.5 ± 0.2 Ma, which is associated with the calculated closure temperature. However, due to the relatively low radiogenic yields of these steps, it is possible that this age is affected by excess argon and thus, older than the actual age.

Construction of Thermal Histories

Isotopic ages combined with closure temperatures specific to the phases dated allow reconstruction of the thermal histories for these samples. When used together, the three isotopic systems; U/Pb, $^{40}Ar/^{39}Ar$, and U-Th/He, yield a cooling history from intrusion and crystallization at depth to cooling through 70 °C (near surface). Cooling rates from sections of the cooling curves can be used to identify periods of rapid tectonic denudation (rapid cooling) as well as slower regional erosional exhumation (slower cooling), estimate the rates at which these events occur, and the timing of transitions

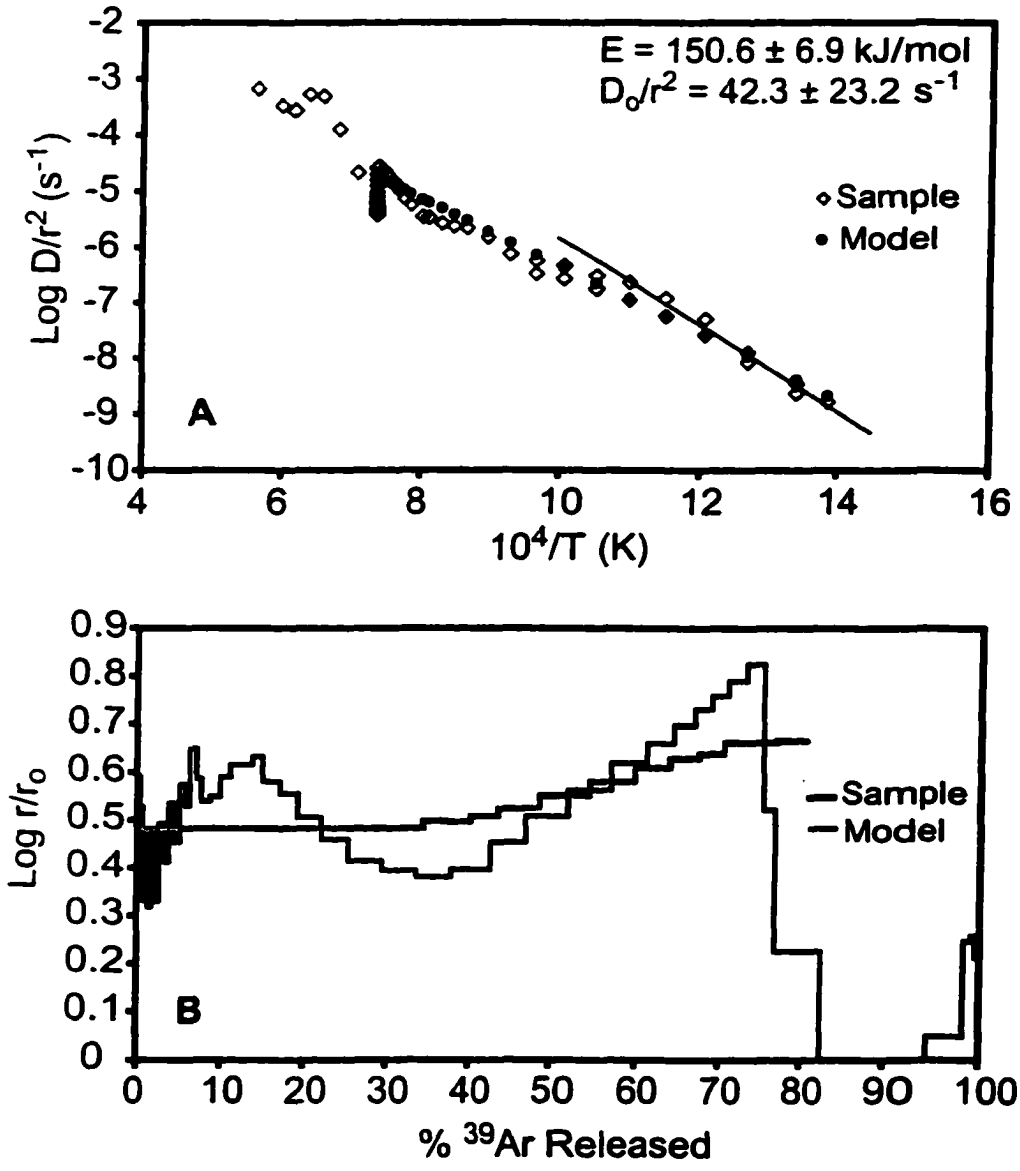

Figure 23. Arrhenius plot (A) and domain size distribution diagram (B) for K-feldspar from syenogranite in the southern Providence Mountains. Poor agreement between model and sample is apparent. The correlation coefficient of 0.19 between the age and log r/r_o spectra supports the inapplicability this K-feldspar for multi diffusion domain modeling.

between them. A description of the thermal histories obtained is presented here while implications for these histories will be discussed in chapter 8.

Southwest monzogranite

The reconstructed thermal history for the SW monzogranite sample is presented in Figure 24. Zircon and hornblende ages are indistinguishable, indicating intrusion and geologically instantaneous cooling from 750 to 500 °C. From ~75 to 71.0 Ma the pluton underwent rapid cooling at ~49 °C/Ma down through ~303 °C, where the K-feldspar began recording. This was followed by an interval of cooling at ~63 °C/Ma from 71.0 to 69.1 Ma as defined by the K-feldspar (Fig. 24). Slow cooling through ~70 °C at ~1.8 °C/Ma is indicated by the ~23.6 Ma U-Th/He apatite age. These data define a significant break in the cooling history at ~69 Ma from rapid cooling through K-feldspar closure to very slow cooling (1.8 °C/Ma) over the interval of ~69 to ~24 Ma.

Central granodiorite

Figure 25 shows the reconstructed thermal history for the granodiorite pluton. As for the southwest monzogranite pluton, emplacement, crystallization, and geologically instantaneous cooling through 500 °C upon intrusion is suggested by the indistinguishable zircon and hornblende ages. Cooling from 500 °C through 293 °C between ~75 and 71.6 Ma occurred at a rate of ~60 °C/Ma K-feldspar models suggests a rate of cooling from 71.6 to 67.3 Ma at ~32 °C/Ma over a temperature interval of 293 to 157 °C. An apatite age of ~40.2 Ma indicates cooling through 70 °C occurred following a period of slow cooling (3.2 °C/Ma) from ~67 to ~40 Ma.

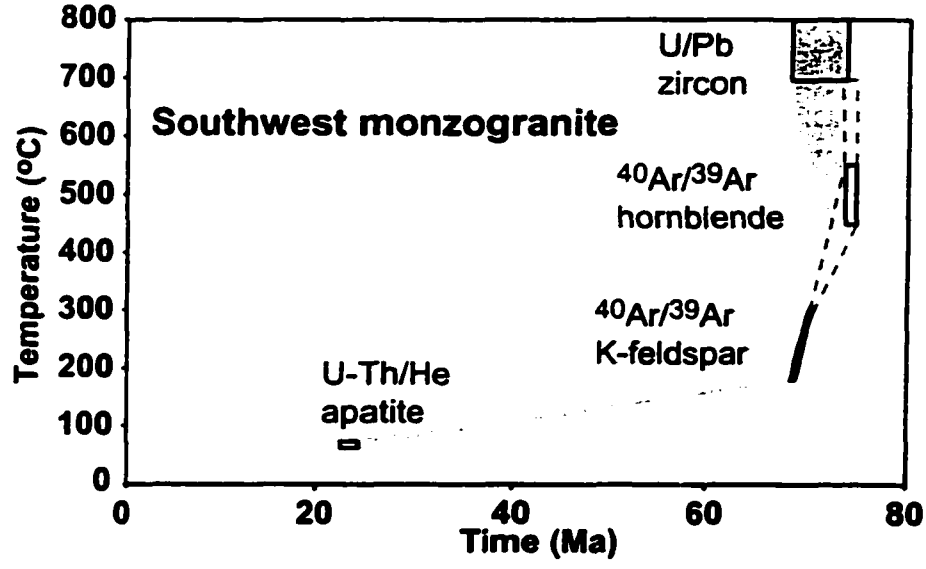

Figure 24. Thermal history for a sample from the southwest Granite Mountains. Error boxes for ages are 1σ. Dark gray region indicates the path of cooling through data points for the pluton. Dashed light gray region indicates most probable cooling path during emplacement. Initial rapid cooling was followed by final slow cooling episode.

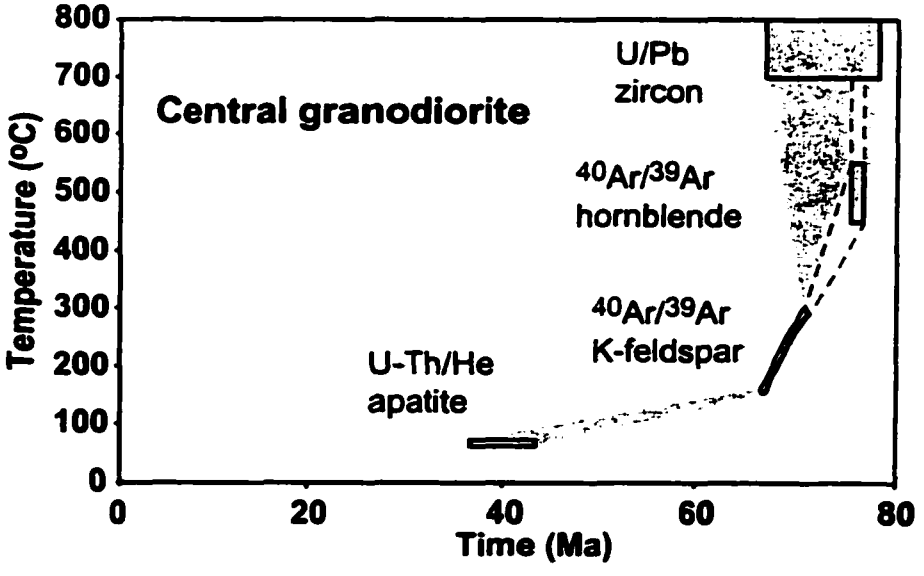

Figure 25. Thermal history for a sample in the central Granite Mountains. Error boxes for ages are 1σ. Dashed light gray region indicates the most likely path of cooling for the pluton from intrusion through 500 °C. The rapid cooling recorded in the K-feldspar is followed by a break to slow cooling through 70 °C.

Northeast quartz monzonite

The thermal history for the NE quartz monzonite (Fig. 26) is similar to the other Granite Mountains plutons, suggesting emplacement and instantaneous cooling through 500 °C at ~75 Ma. Following this initial cooling continued rapid cooling occurred (>100 °C/Ma) through ~251 °C for this sample. K-feldspar modeling indicates cooling from ~251 to ~145 °C occurred at a somewhat lower rate of ~16 °C/Ma from 72.9 to 66.3 Ma. The ~21.2 Ma apatite age (indistinguishable from that of the SW monzogranite) indicates an interval (~66 to 21 Ma) of slow cooling (1.7 °C/Ma) prior to cooling through ~70 °C.

Southern Providence syenogranite

The thermal history for the syenogranite from the southern Providence Mountains is shown in figure 27. Intrusion occurred at 151 Ma as defined by the U/Pb zircon age. Figure 27 shows a dark and light gray path for cooling down to 210 °C (K-feldspar closure). The darker path is a simple connection of data points; the dashed light gray path is a more probable path. The K-feldspar closure temperature of 210 °C corresponds to 7 km depth (assuming 30 °C/ km geothermal gradient) and may define a lower boundary for depth of emplacement whereas the upper boundary is defined by geobarometry indicating intrusion at < 10 km (300 °C). Thus, a pluton intruded within this temperature range would undergo geologically instantaneous thermal equilibration with country rock, at ~300 to 210 °C (Chapter 8) and would remain isothermal or continue cooling at an extremely slow rate (dependent upon regional surface erosion rates). The syenogranite pluton underwent continued slow cooling at ~2.8 °C/Ma following K-feldspar closure from 86 to 35 Ma when the pluton cooled through U-Th/He apatite closure at ~70 °C.

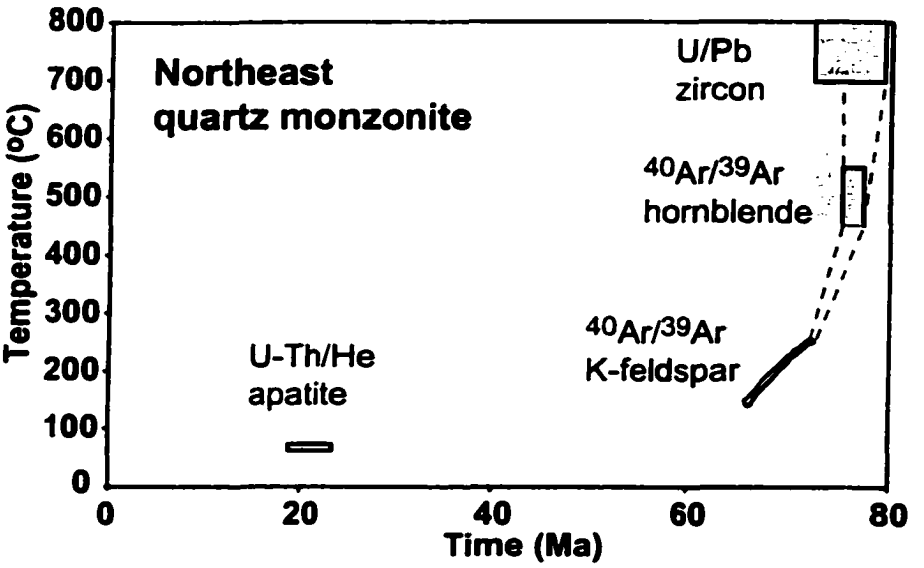

Figure 26. Thermal history for a sample from the northeast Granite Mountains. Error boxes for ages are 1σ. Dark gray region shows cooling path. Dashed light gray area indicates the likely cooling path upon emplacement. Rapid initial cooling followed by slow cooling over ~40 Ma through 70 °C.

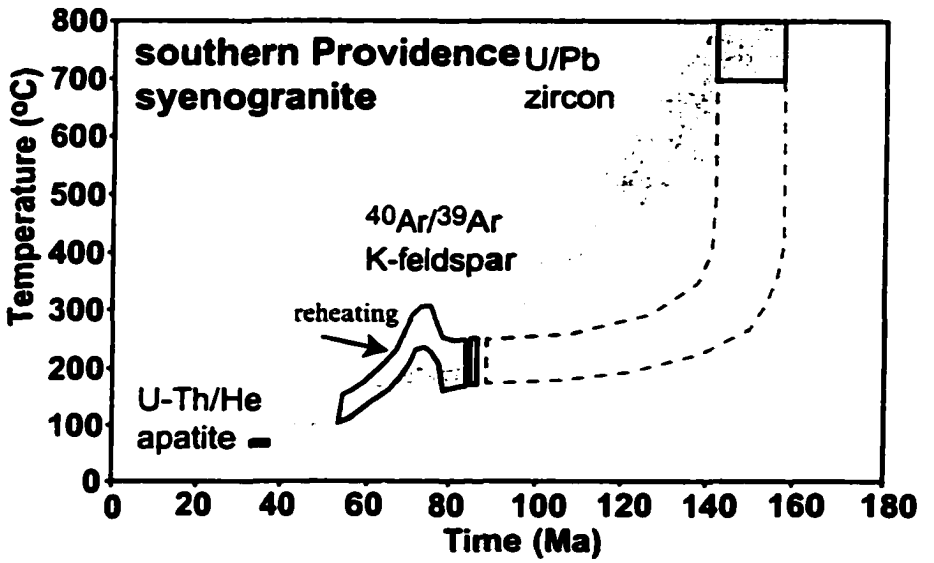

Figure 27. Thermal history for a sample from the southwest Providence Mountains. Dark gray region is inferred cooling history by simply connecting data points. Dashed light gray region is the more likely path, due to shallow crustal emplacement depths. Minimum age of ~74 Ma for K-feldspar likely indicates complete degassing of a domain due to reheating by Granite Mountains plutons. Error boxes for ages are 1σ.

As mentioned in chapter 6, the 86 Ma age for the K-feldspar may be an overestimate caused by excess argon. Another interpretation may be that the slope of the age spectrum is indicative of argon loss during a younger reheating event. The second of several isothermal duplicates yield Late Cretaceous ages with a minimum age of ~74 Ma, which may represent resetting of small domains during this event which at 74 Ma, corresponds with emplacement of Cretaceous plutons in the neighboring Granite Mountains. In this case, the thermal history for this sample would most likely exhibit slow cooling to ~200 °C until ~75 Ma where temperature would increase due to reheating (Fig. 27) before continuing to cool slowly through 70 °C.

Granite Mountains plutons

Common to all three Granite Mountains samples is intrusion at ~75 Ma with geologically instantaneous cooling through 500 °C, followed by continued rapid cooling through ~150 °C at ~66-69 Ma. Geologically instantaneous cooling through ~500 °C upon emplacement is expected for magma bodies intruded at mid-crustal levels (assuming a 30 °C/km geothermal gradient, e.g., 13 km = 390 °C), as indicated by geobarometry (Chapter 8). However, it should be noted that with a lower geothermal gradient of 25 °C/km, cooling would still be interpreted as conductive, but with a slightly higher geothermal gradient of 35 °C/km, cooling through hornblende closure may be interpreted as tectonic. The time interval between hornblende closure and initial K-feldspar closure for the three Granite Mountains samples supports a geothermal gradient >20 °C/Ma. Rapid cooling continues through ~150 °C following thermal equillibration at intrusion. This continuation of rapid cooling is indicative of continued denudation since the plutons continue to cool rapidly to well below mid-crustal temperatures.

Denudation is interpreted as tectonic as opposed to erosional because juxtaposition of different crustal levels (mid and shallow) is involved. This period of extremely fast cooling in the Late Cretaceous was followed by a distinct break to a very slow cooling interval lasting through the Oligocene. Slow cooling during the Tertiary is also seen in the thermal history for the syenogranite in the southern Providence Mountains (Fig. 27), suggesting regional slow cooling during tectonic quiescence.

CHAPTER 8

DISCUSSION

Emplacement depths for plutons

Geobarometry (Chapter 5) indicates mid-crustal emplacement depths for Late Cretaceous plutons of the Granite Mountains (~14 to 17 km) and shallow crustal depths for a Late Jurassic pluton from the southern Providence Mountains (~6 to 9 km). These estimates are similar to those of previous studies of Mesozoic plutons in the area (Young and Wooden, 1988; Fox and Miller, 1990).

Young and Wooden (1988) determined mid-to-deep crustal emplacement depths for both Jurassic and Cretaceous plutons in the Granite Mountains as well as Cretaceous plutons in the nearby Old Woman Mountains (Figs. 2, 3). These estimates were derived using the aluminum-in-hornblende geobarometer, phengite-muscovite, and plagioclase-garnet-muscovite-biotite equilibria barometers, which all yielded pressures of 5 to 7 kbar (19 to 25 km) for the Old Woman granodiorite (Young and Wooden, 1988). Jurassic and Cretaceous plutons in the Granite Mountains yield crystallization pressures of 6.0 to 7.5 kbar based on aluminum-in-hornblende barometry (Young and Wooden, 1988). In this study, analyses on hornblende from Late Cretaceous plutons in the Granite Mountains yielded Al_T values ranging from ~1.5 to ~1.6 (Table 1), which suggests slightly shallower depths of emplacement (14 to 17 km) compared to those determined by Young and

Wooden (1988) also using the aluminum-in-hornblende barometer. The Cretaceous pluton studied by Young and Wooden (1988) yielded a U/Pb age of 136 ± 6 Ma and may indicate the Jurassic plutons remained at or near their emplacement depth into at least the Early Cretaceous before regional contractional tectonics occurred placing these plutons at slightly shallower depths by the Late Cretaceous when the ~4.0 to 5.0 kbar plutons analyzed in this study intruded.

Young and Wooden (1988) reported emplacement pressures of ~3 kbar (10.8 km) for plutons in the southern Providence Mountains, whereas emplacement depths of less than 10 km were estimated by Fox and Miller (1990) using field relations and mineralogic data. Emplacement depths determined for the syenogranite pluton in this study (6 to 9 km) are consistent with these previous studies. The $^{40}Ar/^{39}Ar$ K-feldspar data for this pluton, which corresponds to a closure temperature of ~210 °C at 86.5 Ma (Fig. 27), may also provide constraints on emplacement depth. Although the 86.5 Ma age may be an artifact of excess Ar, the reconstructed thermal history (Fig. 27) suggests emplacement at temperatures > 210 °C because K-feldspar closure (~210 °C) didn't occur until ~65 Ma after emplacement at 151 Ma. Foster et al. (1992) suggest a minimum geothermal gradient of 25 °C/km in the nearby Old Woman and Piute Mountains area prior to extensive Late Cretaceous magmatism. Assuming a 30 °C/km geothermal gradient, this suggests emplacement depths greater than 7 km (210 °C). Therefore, the syenogranite pluton in the southern Providence Mountains was likely emplaced between 7 and 9 km depth.

For the Granite Mountains, the Hollister et al. (1987) and Schmidt (1992) results (Table 1) are indistinguishable within the resolution of their calibrations, and are

consistent with previous studies. However, the slightly lower Al_T value for the NE quartz monzonite may be indicative of shallower emplacement relative to plutons to the SW. Present elevations of samples argue against this, as the northeast sample was taken from the lowest elevation (1217 m) and the central granodiorite sample from the highest (1847 m). Without faulting between them or tilting of the entire section, sample elevations should reflect emplacement depth, however, the NE quartz monzonite is separated from the other plutons by a north-to-northwest-striking down-to-the-northeast normal fault (Fig. 2). Therefore, it is possible that the NE pluton was subsequently down dropped from a higher elevation to its present elevation following emplacement. The age-elevation correlation of the U-Th/He apatite ages indicates any displacement along this fault would have occurred before ~40 Ma. If the sample was emplaced shallower than samples to the southwest, >0.6 km of displacement on the fault is necessary. However, these small apparent differences in emplacement depths cannot be resolved with the geobarometry due to uncertainties of ± 1 kbar and ± 0.6 kbar in the Hollister et al. (1987) and Schmidt (1992) calibrations, respectively.

U/Pb zircon and $^{40}Ar/^{39}Ar$ hornblende ages, along with geobarometry, may also have implications for emplacement depths. The geobarometry suggests emplacement of plutons at 14.5 to 17.1 km depth (Table 1) corresponding to country rock temperatures of 435 to 513 °C, assuming a 30 °C/km geothermal gradient. Emplacement at temperatures less than 500 °C could explain the indistinguishable zircon and hornblende ages as rapid cooling due to conductive heat loss. Conductive cooling models for magma bodies ~10 km in diameter with initial temperatures of 750 °C indicate crystallization and cooling through 500 °C after only several 100 ka when emplaced in ~450 °C country rock, which

is within the uncertainties of the zircon and hornblende ages. Due to the uncertainties associated with U/Pb and $^{40}Ar/^{39}Ar$ ages, such a rapid interval of cooling through 500 °C is not resolvable, and thus interpreted as geologically instantaneous. The barometry allows for the plutons to be emplaced at slightly greater than 500 °C (Table 1), in which case denudation would be necessary to explain the rapid cooling through 500 °C. However, the barometry generally suggests emplacement at ~500 °C or lower, thus conductive heat loss upon intrusion is likely the best explanation for the rapid cooling through hornblende closure (500 °C).

Intrusion and exhumation of the Granite Mountains plutons

The three Granite Mountains samples forming a transect from southwest to northeast across the range (Fig. 2) were emplaced at 72 to 76 Ma as indicated by U/Pb zircon ages. Geobarometry and conductive cooling models suggest the rate of cooling through 500 °C following emplacement was very rapid, which is consistent with the indistinguishable hornblende and zircon ages. As a result of the dating techniques, the $^{40}Ar/^{39}Ar$ hornblende ages are significantly more precise than the U/Pb ion probe zircon ages. Thus, these ages suggest intrusion, crystallization, and initial cooling through 500 °C likely occurred at ~75 Ma (74 to 76 Ma) (Figs. 24-26).

Conductive cooling models indicate very rapid cooling to mid-crustal country rock temperatures where, in the absence of tectonic activity, the plutons would remain isothermal. If this occurred, the cooling history would follow an exponential curve with the cooling rate decreasing rapidly as thermal equilibration with country rock is approached (Fig. 28). The continued rapid cooling from 500 °C to initial K-feldspar

Figure 28. Comparison of reconstructed thermal histories with conductive cooling models. SW=southwest monzogranite, CG=central granodiorite, NE=northeast quartz monzonite. Red curves represent conductive cooling paths for plutons emplaced at ~75 Ma at 17 km (510 °C) and 14.5 km (435 °C) with a geothermal gradient of 30 °C/km and green curves represent conductive cooling paths for plutons emplaced at 14.5 km assuming 20 °C/km (300 °C) and 25 °C/km (363 °C) geothermal gradients. With a 30 °C/km gradient, continued rapid cooling following hornblende closure (500 °C) clearly indicates tectonic denudation . The time interval between hornblende closure and initial K-feldspar closure indicates the geothermal gradient was > 20 °C/km. Continued denudation is still evident with a geothermal gradient lower than 30 °C/km.

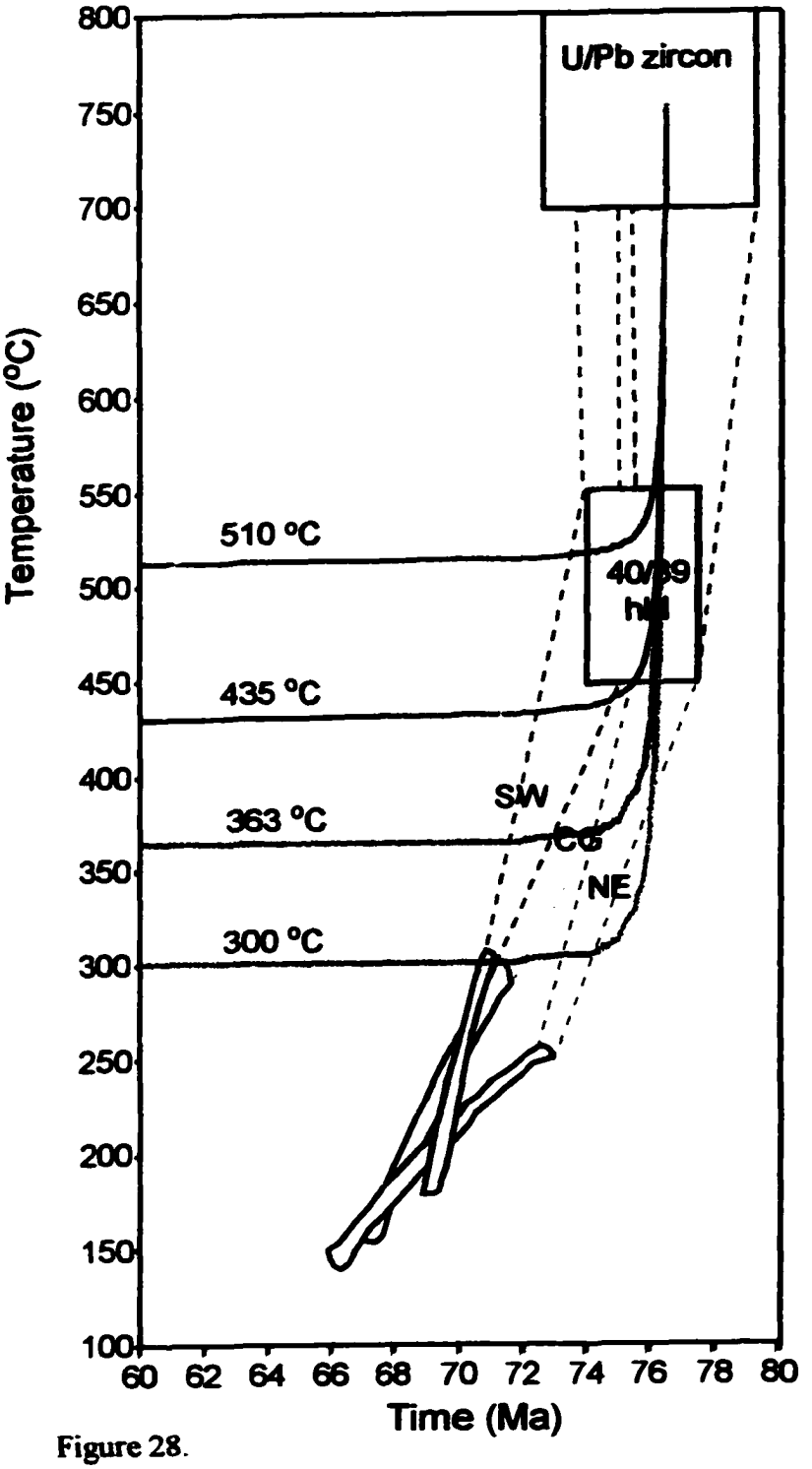

Figure 28.

closure and the cooling intervals (~300 to 150 °C) recorded by the K-feldspar models (63 to 16 °C/Ma) is therefore indicative of exhumation. Tectonic exhumation is favored over erosional exhumation due to the rapid cooling rates as well as the cooling rate gradient across the range. Cooling rates recorded in K-feldspar models do not exceed observed erosional rates. However, the significant change in cooling rate recorded in MDD models (which includes crossing over of cooling curves) across only ~10 –15 km lateral distance, indicates that climatic changes resulting in evolving erosion rates are unlikely. It is therefore interpreted that the three Granite Mountains plutons were intruded syntectonically in the Late Cretaceous at ~75 Ma. Tectonic activity probably ceased around 66 Ma, at the time K-feldspars ceased recording (Fig. 24-26, 28). This interval of rapid cooling was followed by a break to slow cooling (<3.2 °C/Ma) indicating a period of tectonic quiescence through the late Eocene to the early Miocene, when plutons were within a few km's of the surface and beginning to cool through 70 °C (Figs. 24-26).

Rapid tectonic exhumation from ~75 to 66 Ma in the Granite Mountains correlates well in the east Mojave Desert region with timing of rapid exhumation for the Old Woman granodiorite due to movement on the Old Woman shear zone at 73 to 68 Ma (Foster et al., 1989; Foster et al., 1992), extension and unroofing along the Pinto Shear zone from 71 to 65 Ma (Beyene, 2000), movement on the East Providence fault zone at ~70 Ma (Miller et al., 1995), and unroofing in the Funeral Mountains of Death Valley from 72 to 70 Ma (Applegate et al., 1992).

Tectonic implications from K-feldspar multi-domain modeling

During extensional tectonism and normal faulting, footwall rocks are moved up relative to hanging wall rocks. Normal faulting thus places deeper-seated rocks (hotter) in the footwall against shallower rocks (cooler) in the hanging wall. This results in heating of the hanging wall and refrigeration of the footwall due to the temperature gradient between the juxtaposed rocks, a phenomenon that may explain the post-intrusional cooling from 500 °C to ~150 °C in the Granite Mountains. Several possible scenarios may explain the reconstructed thermal histories of the Granite Mountains plutons including exhumation by a single normal fault, tilting of a crustal section, and conjugate normal faulting.

Exhumation by a single normal fault

The extremely rapid K-feldspar cooling curve for the SW pluton suggests a single fault model to be a down-to-the-southwest normal fault with the Granite Mountains in the footwall. Exhumation by such a fault would require the NE quartz monzonite pluton to be emplaced at significantly shallower depths than the central and SW plutons to account for the rapid cooling through initial K-feldspar closure (251 °C at 72.9 Ma) while other samples were at >375 °C (Figs. 20, 24-26). However, the aluminum-in-hornblende geobarometry does not suggest any significant differences in emplacement depth. If the NE pluton was emplaced at 14.5 km (435 °C), which is the minimum depth based on geobarometry (Table 1), with other plutons at deeper levels, proximity to a fault would be necessary to explain the rapid cooling below 300 °C that was not recorded in the central and southwest samples until ~ 2 Ma later (Fig. 24-26). A detachment fault exhibiting flexural rotation of the footwall may accommodate earlier cooling of the NE if the

samples were emplaced at progressively greater depths from NE to SW (Buck, 1988). Upon rotation of the footwall, motion will cease along the low angle portion of the fault accounting for the slow cooling in the NE (Buck, 1988). Isostatic rebound of the footwall due to removal of the upper plate could provide a significant upward motion that may account for the rapid cooling in the SW and also explain the present day sample elevations. However, a single fault model does not seem to account for the juxtaposition of the mid-crustal Granite Mountains and the shallow-crustal southern Providence Mountains. Therefore, a second fault dipping northeast with the Granite Mountains in the footwall appears to be necessary.

A tilted crustal section

Lateral exposure of mid-crustal and shallow-crustal rocks at the surface may be indicative of a tilted crustal section. The four samples used in this study are all located laterally > 4.5 km from each other. Restoration of tilting would result in progressively shallower crustal levels (lateral distances reflected as differences in depth) with the southwest monzogranite sample deepest, and the southern Providence syenogranite shallowest (Fig. 29). A problem with this model is that differences in emplacement depths greater than 4.5 km should be resolvable by the geobarometry, however there is no evidence for significant differences in emplacement depth from the data (Table 1). Significant differences in emplacement depth may be inferred when using upper and lower limits of the uncertainties, however this approach seems to demonstrate poor confidence in the technique.

Alternatively, the plutons of the Granite Mountains could be emplaced next to and progressively (but not significantly) deeper than those in the southern Providence

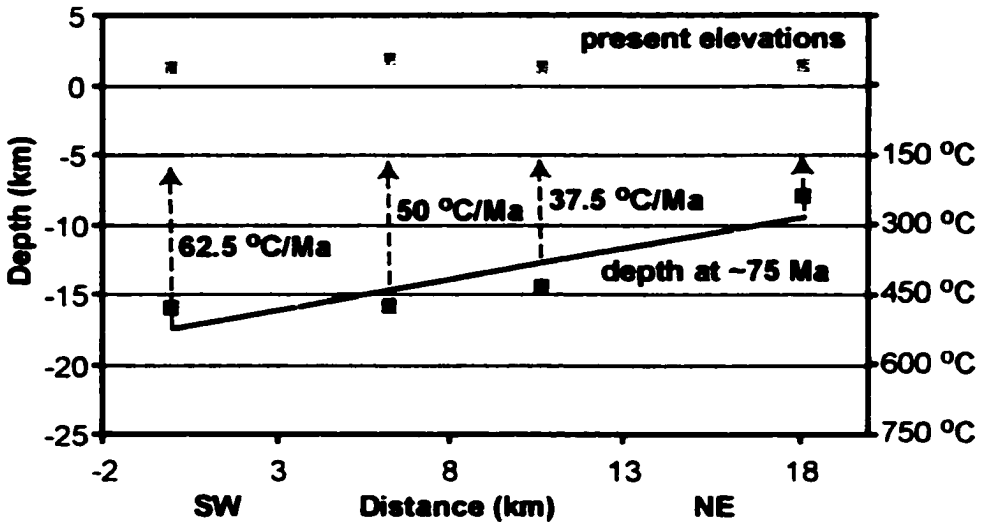

Figure 29. Schematic representing a tilted crustal section with model cooling rates shown. Red squares represent present elevation and map distance between samples from SW to NE. Blue squares represent paleodepth/temperature determined by geobarometry. Linear regression through blue squares represents sample positions before tilting assuming a linear depth profile between samples based on apparent linear relationship between present sample elevations/locations. Cooling rates for each sample are based on interval from 75 to 68 Ma, when the southwest monzogranite would have cooled through ~150 °C. Model cooling rates for the central and northeast Granite Mountains samples are significantly higher than those determined by K-feldspar modeling (Figs. 21, 29, 30). K-feldspar models also suggest earlier cooling through 150 °C for the southwest Granite Mountains, which is not apparent in the tilted section model.

Mountains (Fig. 29). The present day sample locations/elevations allow for the assumption of a linear spatial relationship relative to depth between the samples at the time of emplacement (Fig. 29). Since only hydrothermal alteration has been described in the Providence Mountains, an assumption is made for this model that the plutons are slightly shallower than their original emplacement depth by Late Cretaceous time and have not been significantly buried following intrusion. The U-Th/He ages also provide a lower limit to the depth of the plutons at this time. Tilting, and thus exhumation, of the samples up to ~5 km depth (end of K-feldspar models) over the interval 75 to 68 Ma (timing of southwest sample to cool through 150 °C) suggests cooling rates significantly higher than those indicated by the reconstructed thermal histories for the central and northeast samples (Figs. 29, 30). Also, the southwest sample would be expected to cool through lower temperatures later than samples to the northeast, however K-feldspar models indicate the southwest sample cooled through ~180 °C while other samples were at 200 °C or greater (Fig. 30). Overtilting followed by backtilting would be necessary to accommodate this more rapid cooling through low temperatures in the SW and present day sample elevations. The inconsistency of the reconstructed thermal histories with those expected from the tilted section model suggests lateral juxtaposition of the deeper-seated Granite Mountains with the shallow crustal southern Providence Mountains is most likely a result of faulting between them, and not tilting of a crustal section.

Exhumation by conjugate faulting model

K-feldspar thermal models indicate a distinct cooling rate gradient across the Granite Mountains. From southwest to northeast, samples record cooling rates of 63, 32 and 16 °C/Ma between ~300 and 150 °C (Figs. 2, 20, & 30). These correspond to

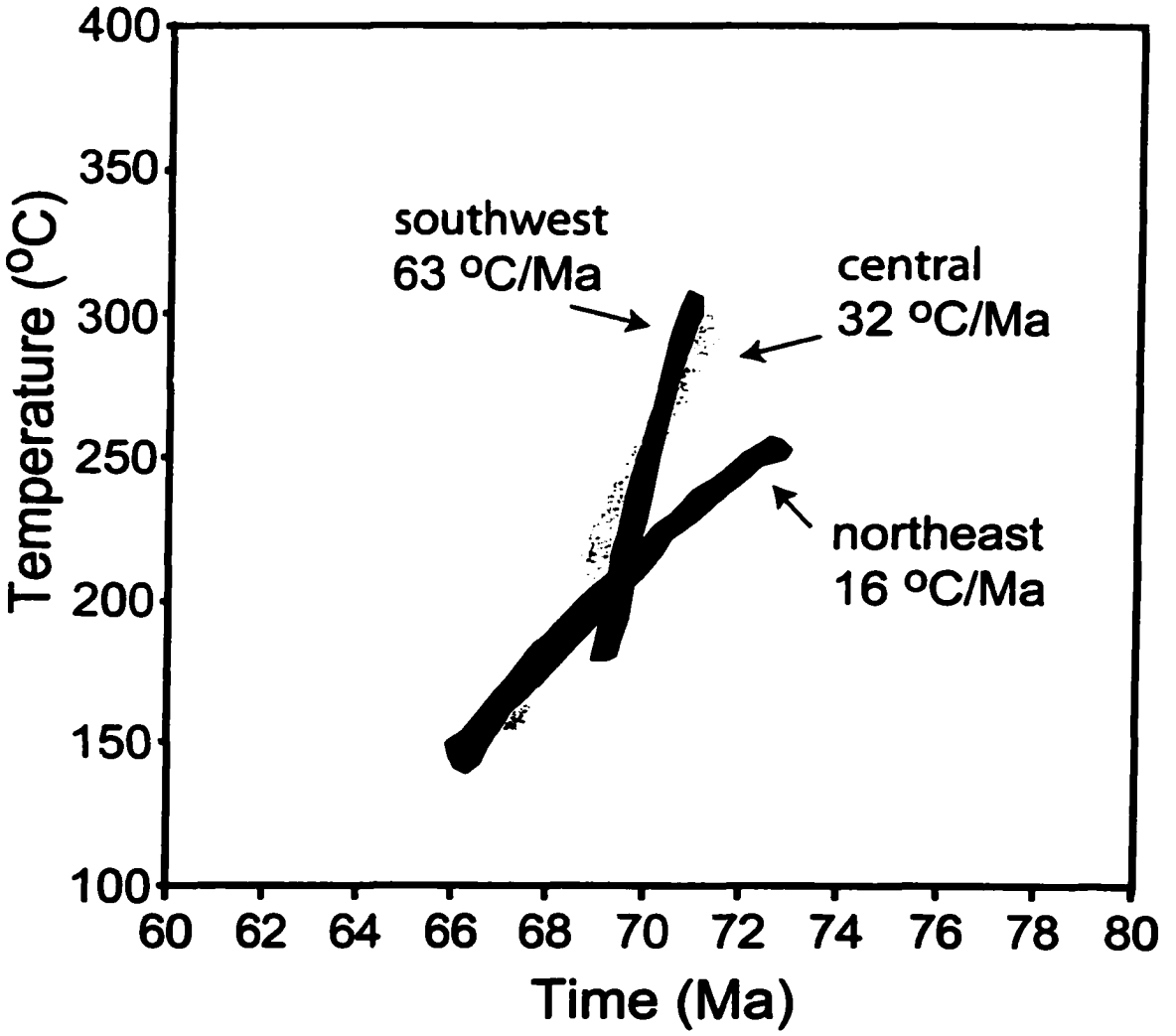

Figure 30. Cooling curves from K-feldspar multidomain modeling for three Granite Mountains plutons. Plot shows the changes in cooling rates across the Granite Mountains from the southwest to the northeast. The northeast began to cool through lower temperatures earlier than the others, whereas samples to the southwest cooled later and faster.

denudation rates of 2.1, 1.1, and 0.5 mm/yr assuming a 30 °C/km geothermal gradient. Advection of geotherms is expected when denudation rates exceed ~1 mm/yr (Stuwe et al., 1994). The implications of advection are that the cooling rates determined from thermochronology may not reflect motion of the plutons to the surface, but rather cooling during relaxation of compressed geotherms after rapid tectonic emplacement in the shallow crust. However, a significant tectonic event is necessary to explain the rapid cooling rates, regardless of which case they represent.

K-feldspar models show that cooling was fastest to the southwest (63 °C/Ma), where K-feldspar recording began later (71.0) and ended earlier (69.1 Ma) than in the northeast. The NE K-feldspar sample indicates the NE Granite Mountains began to cool earlier than the southwest, more slowly, and over a longer period of time (72.9 to 66.2 Ma; 16 °C/Ma) (Figs. 20 & 30). A model in which two faulting events occurred may explain this cooling pattern. It should be noted however, that the structures proposed below that may have existed have since been removed by erosion, although a breccia zone in Granite Pass may be a remnant of one of the proposed faults.

The northeast Granite Mountains cooled through ~250 °C while other samples to the SW were still at >375 °C (Fig. 28). Proximity to a normal fault may explain this earlier stage of cooling, as geobarometry indicates no significant difference in emplacement depth for the three samples. This normal fault would most likely be north to northwest striking with the Granite Mountains in the footwall and the Providence Mountains in the hanging wall. The fault in Granite Pass (Fig. 2) (Howard and Miller, 1992) may represent this structure. Two-dimensional thermal modeling indicates a normal fault dipping ~65 ° NE with a slip rate of 3.5 mm/yr from 76 to 74 Ma will

accommodate juxtaposition of the Granite Mountains with the southern Providence Mountains and reproduce the higher temperature segments (~500 to 350 °C) of the reconstructed thermal histories (Figs. 31 and 32). The interval 76 to 74 Ma represents cooling through 500 °C and initial K-feldspar closure for the NE sample. The inflection to a slower rate of cooling for the NE quartz monzonite while rapid cooling continued in the SW (Fig. 28) suggests motion probably stopped on this fault, and extension changed to down-to-the-west on a separate fault. Flexural rotation and isostatic rebound of the footwall of this second fault during exhumation (Buck, 1988) may explain the change in cooling rate across the Granite Mountains that was recorded in the K-feldspars (Fig. 33). The isostatic response of the footwall may result in an increase in exhumation rate and accommodate the narrow interval between initial K-feldspar closure between the SW monzogranite and central granodiorite samples (Figs. 28 and 30). Footwall refrigeration due to displacement along this fault would only effect the SW and central Granite Mountains samples, as the NE sample would be >10 km from the fault. Motion on this fault may have lasted until ~66 Ma, when NE K-feldspar ceased recording (Figs. 28 and 30). Following exhumation along this top-to-the-southwest normal fault, the Granite Mountains samples were likely in the upper 5 km of the crust where they remained while slow erosional denudation proceeded through the Oligocene.

Figures 32 and 33 summarize this conjugate fault model for the exhumation of Granite Mountains plutons. Faults are north-to northwest striking dipping outward from the Granite Mountains at angles of 65 ° in the NE and 30 ° in the SW. The steeply dipping fault in the NE is proposed to accommodate a significant amount of displacement to juxtapose the Granite Mountains and southern Providence Mountains. Whereas a

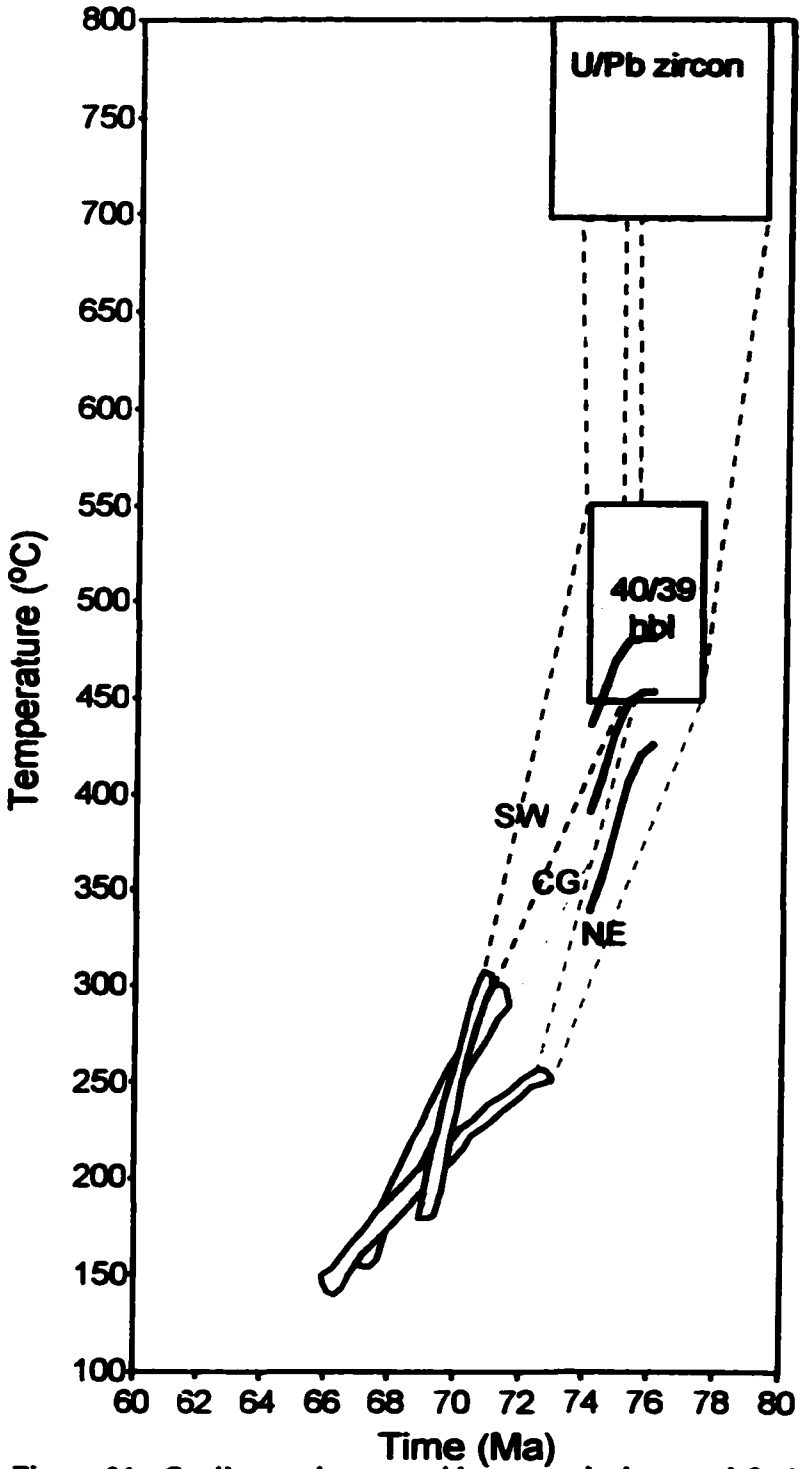

Figure 31. Cooling paths created by numerical normal fault modeling (solid black lines) are in agreement with reconstructed thermal histories based on thermochronology. The model cooling paths correspond to the fault model shown in figure 33.

Figure 32. Two-dimensional numerical model for cooling of rocks during normal faulting. a. Initial sample positions based on geobarometry and map distance with a 30 °/km geothermal gradient. Fault is dipping 65° northeast. b. Post faulting positioning of samples with compressed geotherms. Fault was modelled from 76 to 74 Ma with a slip rate of 3.5 mm/yr. This event may explain juxtaposition of the mid-crustal Granite Mountains next to the shallow-crustal southern Providence Mountains.

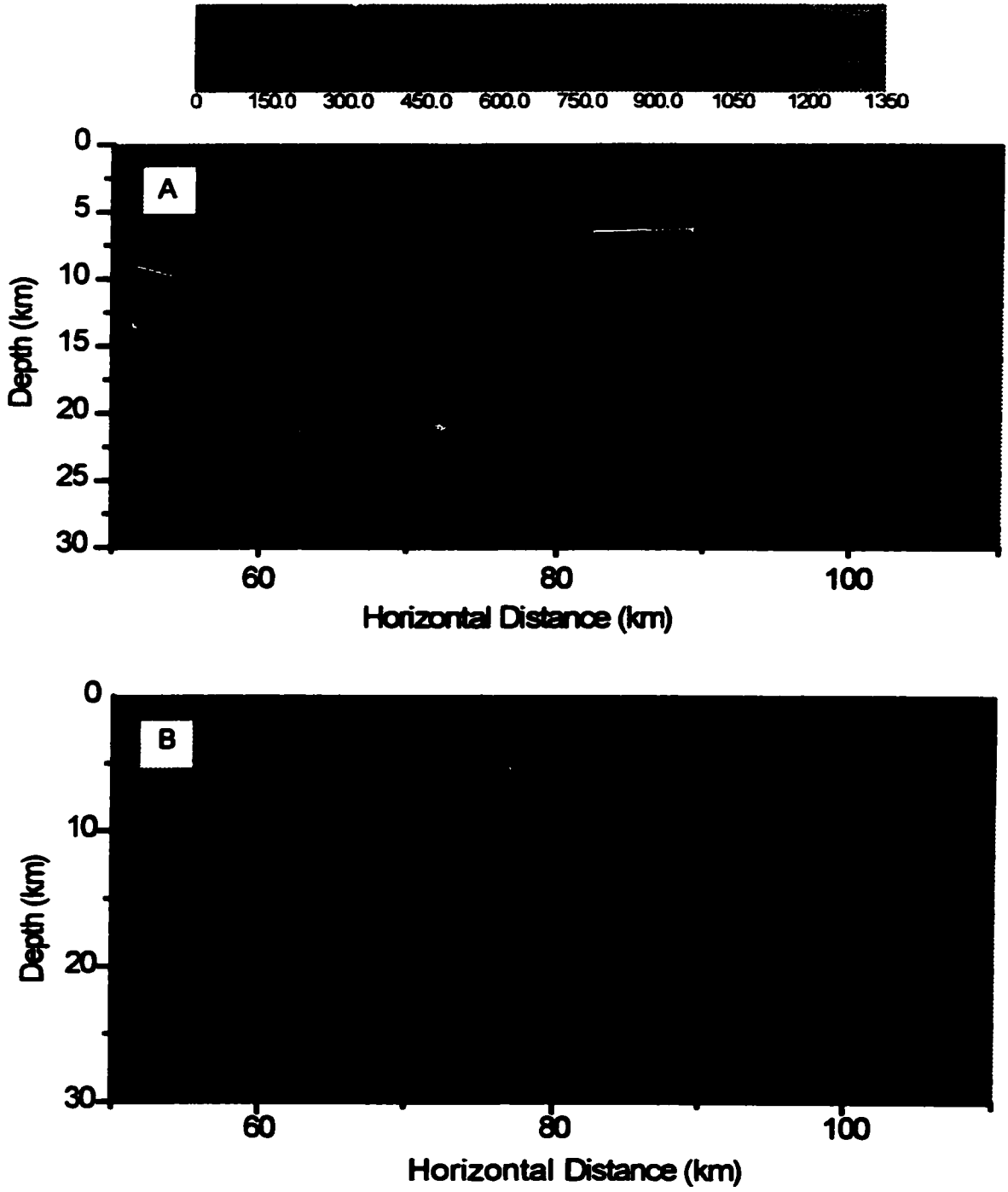

Figure 32.

Figure 33. Schematic of SW dipping detachment fault. a. Samples are in positions following exhumation along the NE fault. At ~74 Ma motion ceases on the NE fault and begins on the SW fault. b and c. Samples are exhumed along the SW fault. d. Following removal of the upper plate, the footwall rebounds isostatically accounting for the increase in exhumation rate and rapid cooling recorded in the SW and central K-feldspar samples. The fault trace at the surface is proposed to be far enough to the SW so that the NE and Providence Mountains samples decrease in cooling rate and are not affected by the isostatic response of footwall unroofing.

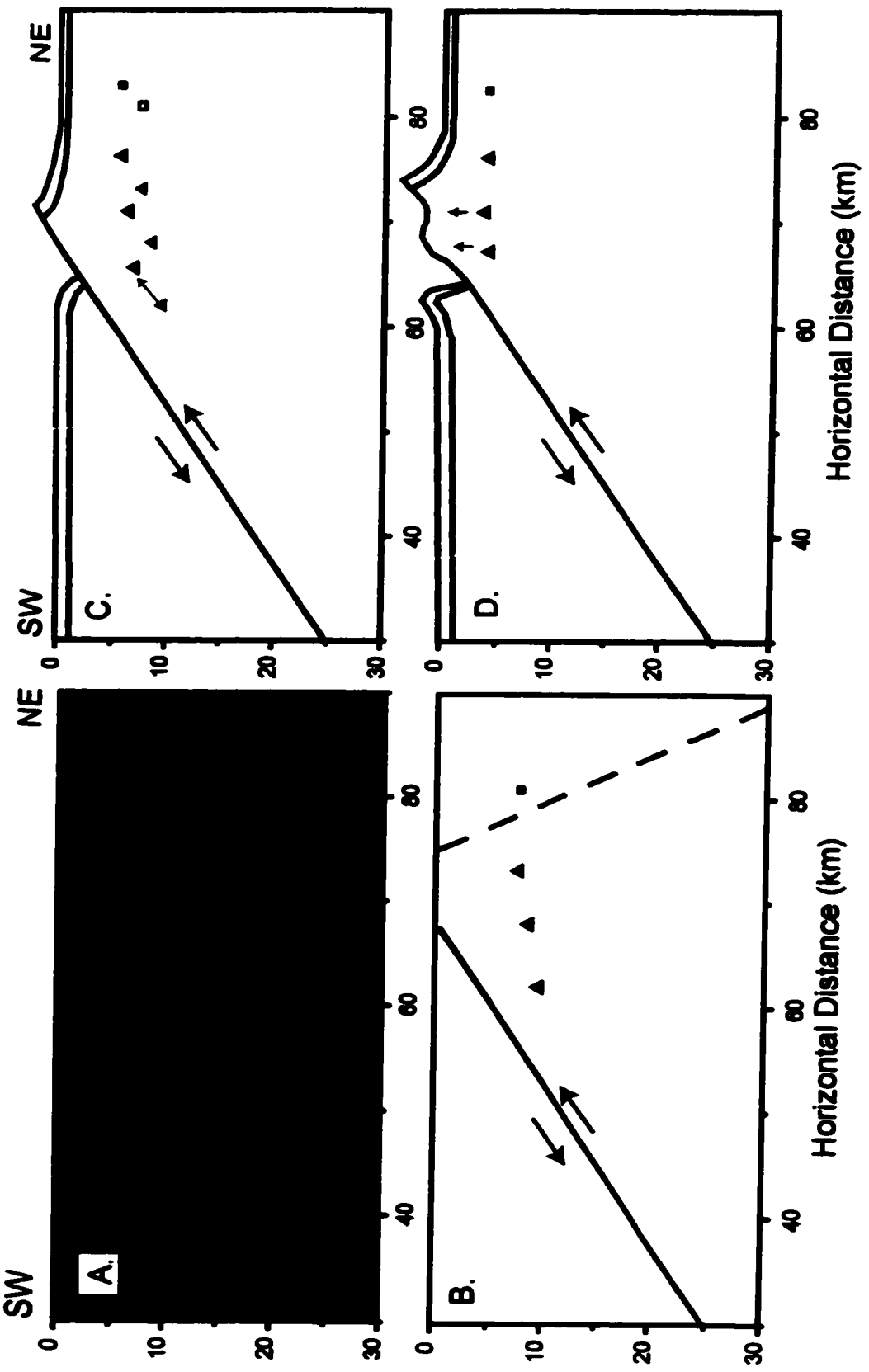

Figure 33.

reverse fault with a similar geometry to the modeled NE normal fault would also accommodate initial cooling and juxtaposition of the two complexes, the regional extensional tectonism that is related both spatially and temporally to the data in this study suggests extensional faulting is a more likely explanation. The SW dipping fault accommodated more extension than the NE fault with a shallower dip (?), a longer interval of activity, and more rapid cooling indicating faster exhumation.

For Late Cretaceous Granite Mountains plutons, intrusion and extensional tectonics appear to be temporally related. Relationships between magmatism and extensional deformation have been suggested in the formation of many metamorphic core complexes (Hill et al., 1995; Walker et al., 1995; Foster and Fanning, 1997). Igneous intrusions have been proposed to provide a heat source to thermally weaken overlying crust and trigger rock failure, i.e. detachment faulting, which exhumes the metamorphic core complex. Although the Granite Mountains may not represent a metamorphic core complex (any structures that may have existed have been removed by erosion), they are similar in that they represent mid-crustal rocks emplaced in the shallow crust due to (most likely) low angle detachment faulting. The syntectonic intrusion of Granite Mountains plutons, indicated by reconstructed thermal histories, suggests magmatism may have been a driving force in initiating extensional faulting.

Exhumation dominantly by a top-to-the-southwest low angle fault is consistent with Late Cretaceous low-angle shear zones in the region. Foliations in the Pinto shear zone in the New York Mountains (Fig. 3) dip 20 to 65° south and southwest with top to the SW motion and was active from ~71 to 65 Ma (Beyene et al., 2000). This interval of tectonic activity is synchronous with the time intervals recorded in K-feldspar from the

SW monzogranite and the central granodiorite. The proximity of this shear zone (~65-70 km) to the Granite Mountains and the similarity of K-feldspar models suggest a possible link to the same top-to-the-southwest extensional structure. Motion on a low-angle top-to-the-southwest shear zone also occurred ~65 km to the southwest of the Granite Mountains in the Old Woman Mountains (Fig. 3) during the interval 73 to 68 Ma (Foster et al., 1989). Extension occurring at 72 to 70 Ma in the Funeral Mountains of Death Valley was also accommodated by a low-angle west dipping shear zone (Applegate et al., 1992; Hodges and Walker, 1992). The East Providence fault zone, although steeply dipping, was also a down-to-the-west structure active at ~70 Ma. Rapid cooling recorded in K-feldspars from Granite Mountains plutons from 71 to 66 Ma (Fig. 20) further supports regional top-to-the-southwest extensional deformation in this part of the southern Sevier belt.

Implications from U-Th/He ages

Apatite U-Th/He ages indicate a period of very slow cooling through 70 °C from the Late Cretaceous to the Tertiary (Fig. 24-27). Ages range from 40 to 21 Ma and are correlative with elevation (Fig. 18). The central granodiorite pluton has the highest elevation and the oldest age and was therefore cooled through 70 °C by erosional denudation first, followed by samples at lower elevations.

Although at least one fault separates the syenogranite pluton in the southern Providence Mountains from the Granite Mountains, the apatite age fits within the overall age-elevation correlation (Fig. 18). This suggests a period of tectonic quiescence and slow cooling from ~40 to 21 Ma during which the Granite Mountains and southern

Providence Mountains were exhumed as a single block during slow erosional denudation. Therefore, motion on the Granite Pass fault, which separates the Providence and Granite Mountains and may be a remnant of the proposed NE fault in this study, likely occurred pre-Oligocene. The apatite ages indicate the plutons were near the upper 2 km of the crust prior to the onset of Basin and Range extension (~25 Ma), which may have supplied the final movement upward through He closure temperature (70 °C) for the lower elevation samples.

U-Th/He data may also help to constrain timing of faulting within the Granite Mountains. The NE quartz monzonite pluton is separated from the other Granite Mountains plutons by a north-northwest striking down-to-the-northeast normal fault (Howard et al., 1987; Miller et al., 1991) (Fig. 2). If the age-elevation correlation is indicative of slow cooling through 70 °C as a single tectonic block, movement on this fault must have occurred pre-Oligocene. Although this is a short fault suggesting minimal displacement, U-Th/He ages are sensitive to as little as ~100 m (Fig. 18) indicating any significant movement on the fault likely predated passage through the He closure temperature. If the pluton were down dropped subsequent to cooling through 70 °C, an older age (such as that of the central granodiorite or Providence syenogranite) would have been recorded. No crystal size to age correlation exists in the apatite data, which further supports the age relationships to be structurally controlled, and suggests this fault may be Cretaceous.

Information on erosion rates may also be inferred from apatite ages. Figure 34 is a plot of paleodepth/ temperature vs. age at 40 Ma, when the central granodiorite cooled through 70 °C. Paleodepths are inferred from the present sample elevations and

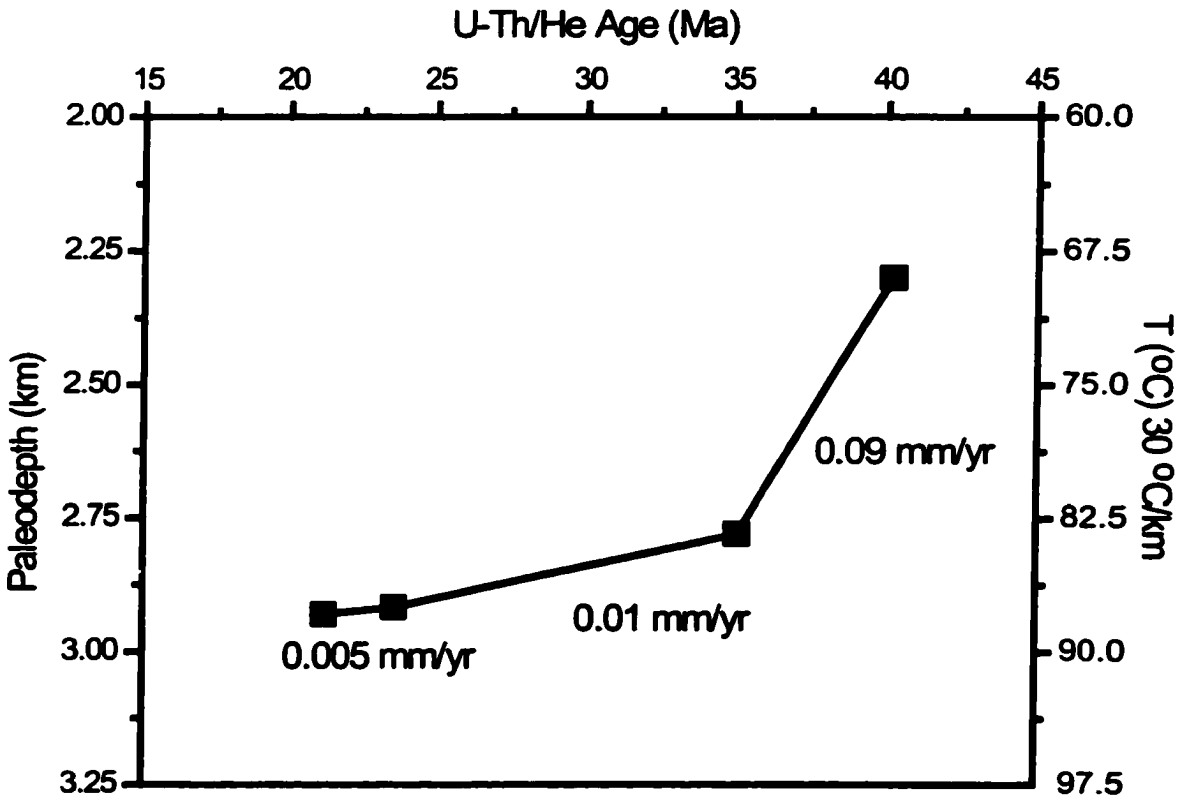

Figure 34. Paleodepth vs. age plot for Granite and Southern Providence Mountains samples (boxes). Sample elevations are reflected as paleodepth with respective temperature based on 30 °C/km geothermal gradient at 40 Ma when the central granodiorite cooled through 70 °C. Exhumation rates due to erosional denudation are shown for each interval between samples. Plot indicates erosion rates decreased between 40 and 20 Ma.

temperatures are based on 30 °C/km geothermal gradient. Erosion rates can be determined based on the difference in depth and timing of He closure between each sample. These data indicate that erosion rates decreased from 0.09 mm/yr at ~40 Ma to 0.005 mm/yr at ~20 Ma.

Relations between the Granite and southern Providence Mountains

One goal of this project was to determine if there was a structural or tectonic relationship between the Granite Mountains and the southern Providence Mountains. Any model must explain geobarometry data, which indicate that the Granite Mountains plutons were emplaced at similar mid-crustal depths whereas the southern Providence Mountains plutons were emplaced at shallow depths. One hypothesis of this study was that the two mountains ranges might represent a single crustal section exposed at the surface due to tilting during extension. Geobarometry results showing similar emplacement depths for the three Granite Mountains plutons rather than (significantly) progressively deeper depths to the southwest (reflecting surface distance between samples) do not support a tilted a crustal section.

The tectonic model in figures 32 and 33 provides a more consistent explanation for the data, and suggests the Granite Mountains plutons were emplaced at crustal levels deeper than the southern Providence Mountains plutons. Their present-day juxtaposition can be explained as a single crustal section cut by a normal fault during extensional tectonism, which placed deep and shallow segments adjacent to each other at the surface.

The geobarometry for the syenogranite in the southern Providence Mountains (Fig. 27) indicates that the pluton was quickly cooled as a result of emplacement into cool

shallow crustal rocks. By 75 Ma the pluton had probably cooled below ~200 °C, whereas the Granite Mountains plutons were just being emplaced. Following reheating, the southern Providence Mountains likely underwent slow cooling similar in rate to the interval from ~66 to ~20 Ma in the Granite Mountains. This implies that Late Cretaceous exhumation juxtaposed the deeper-seated Granite Mountains and shallow southern Providence Mountains and the two experienced slow erosional cooling as a single block during a period of Early Tertiary tectonic quiescence.

Extensional collapse of the Sevier Orogen

Extensional collapse of overthickened crust during mountain building events is a well-known phenomenon that has been documented in ancient as well as the active orogens such as the Himalayan orogen. A significant body of evidence indicates widespread extensional tectonics occurred during the Late Cretaceous within the Sevier orogen as a result of gravity-driven collapse of overthickened crust.

Hodges and Walker (1992) suggest that mid-crustal detachment faults and decollements accommodated extension in the Sevier hinterland. Motion on low-angle normal faults in the Raft River Mountains (Utah) and Black Pine Mountains (Idaho) has been constrained between ~100 and 82 Ma based on $^{40}Ar/^{39}Ar$ muscovite ages (Wells et al., 1990). The Mahogany Peaks fault, juxtaposing Ordovician and Proterozoic rocks in the Raft River Mountains is interpreted as a low-angle top-to-the-west normal fault active in the Latest Cretaceous to Paleocene (90 to 47 Ma) and possibly synchronous with $^{40}Ar/^{39}Ar$ ages for cooling of the footwall (~70 to 60 Ma) (Wells et al., 1998). These support low angle extensional tectonics in the central regions of the Sevier hinterland.

In southeast California, low angle shear zones and detachment faults dominate the Late Cretaceous extensional structures supporting Sevier orogenic collapse (Hodges and Walker, 1992). Rapid cooling of plutonic rocks in the Old Woman Mountains (Fig. 3) was accommodated along a west dipping, normal sense, ductile shear zone active from 73 to 68 Ma (Carl et al., 1991; Foster et al., 1992). Miller et al. (1996) correlated three down to the west extensional structures to postulate the East Mojave Fault. This fault zone extends mainly north south and is defined by the Cima fault zone, Pinto Shear zone, and East Providence fault zone. Mylonite in the Cima fault zone suggests normal, down to the west shear active in the Late Cretaceous based on cross cutting relationships (Miller et al., 1996). The Pinto shear zone is a shallow dipping (20 to 65°) down to the west normal sense shear zone in the New York Mountains (Fig. 3) that was active from 71 to 65 Ma (Beyene et al., 2000). Motion on the East Providence fault zone took place between the latest Cretaceous and early Miocene based on cross cutting relationships with 76 to 80 Ma dikes and the Miocene Wildhorse Mesa tuff (Miller et al., 1996). The East Mojave Fault may represent a link between southern extension in the Old Woman Mountains and extension in the Funeral Mountains of Death Valley (Fig. 3) where top the southwest shearing was occurring at 72 Ma, lasting until 70 Ma (Applegate et al., 1992).

The Granite Mountains are located west of the postulated East Mojave Fault. Rapid cooling of Granite Mountains plutons at ~76 to 66 Ma correlates very well with the timing of rapid cooling in the surrounding Cretaceous extensional terrains. Exhumation dominated by a top to the southwest low angle normal fault is consistent with surrounding extensional structures, especially the nearby Pinto Shear zone (71 to 65 Ma) with K-feldspar models almost identical to the central and SW Granite Mountains plutons

(~71 to 67 Ma). The matching time intervals recorded in K-feldspars along with the close proximity (~50 to 60 km) of the Granite Mountains and Pinto Shear zone may be indicative of a single large-scale Late Cretaceous extensional structure, which the postulated East Mojave Fault of Miller et al. (1996) may represent the central portion of. If so, this structure may be a single large-scale top-to-the-southwest extensional zone linking Late Cretaceous extensional structures from the Old Woman Mountains in the south to the Funeral Mountains in the north, accommodating gravitational collapse at the southern extent of the overthickened Sevier Orogen.

CHAPTER 9

CONCLUSIONS

Based on calibrations of the aluminum-in-hornblende geobarometer by Hollister et al. (1987) and Schmidt (1992), three Cretaceous plutons in the Granite Mountains intruded at pressures of 4.0 to 4.8 kbar corresponding to mid-crustal depths of 14.5 to 17.1 km. A syenogranite pluton in the southern Providence Mountains intruded at 1.7 to 2.4 kbar suggesting shallow crustal emplacement levels of 7 to 9 km depth based on both geobarometry and $^{40}Ar/^{39}Ar$ thermochronology.

Emplacement of the Cretaceous plutons in the Granite Mountains was synchronous with Late Cretaceous extension during collapse of the overthickened Sevier Orogen beginning at ~75 Ma. The syenogranite pluton in the southern Providence Mountains was emplaced in the Jurassic at 151 ± 8 Ma as part of earlier extensive arc magmatism throughout the Cordillera.

Rapid cooling of Granite Mountains plutons through hornblende closure (~500 °C) was likely a result of conductive heat loss due to mid-crustal emplacement. Continued rapid cooling can be explained by short-lived (76 to 74 Ma) movement along a top-to-the-NE normal fault juxtaposing these plutons against cooler shallow crustal rocks in the neighboring southern Providence Mountains. Numerical models indicate a fault dipping 65 ° NE with a slip rate of 3.5 mm/yr from 76 to 74 Ma will reproduce the high temperature (~500-300 °C) interval of the reconstructed thermal histories and may

accommodate this juxtaposition. K-feldspar models suggest cooling rates of 63 to 16 °C/Ma from southwest to northeast in the Granite Mountains. This cooling interval (~73 to 66 Ma) was probably accommodated by a top-to-the-southwest normal fault to the southwest of the Granite Mountains, which would be the dominant structure in the exhumation of the plutons. Flexural rotation with isostatic rebound of the footwall during faulting and possibly an increase in exhumation rate may explain the change in cooling rate from SW to NE. It is likely that exhumation dominated by the top-to-the-west fault was similar to unroofing in many metamorphic core complexes where syntectonic plutons provide a heat source to thermally weaken overlying rocks and initiate detachment faulting. This rapid cooling event coincides temporally and spatially with the nearby top-to-the-southwest Pinto Shear zone, which was active from 71 to 65 Ma relating the Granite Mountains to a possible single large scale extensional structure in the Mojave Desert region.

U-Th/He apatite ages indicate that following rapid Late Cretaceous exhumation, Granite Mountains plutons underwent slow cooling lasting through the Oligocene. The southern Providence Mountains also underwent similar slow cooling from Late Cretaceous to ~35 Ma, indicating juxtaposition of the Granite Mountains and southern Providence Mountains occurred during Late Cretaceous extensional tectonics. Apatite ages also indicate the plutons were in the upper crust prior to Basin and Range extension, which may have contributed to their final movement upward.

REFERENCES CITED

Ague, J.J., 1997, Thermodynamic calculation of emplacement pressures for batholithic rocks, California: Implications for the aluminum-in-hornblende barometer: Geology, v. 25, p. 563-566.

Allmendinger, R. W., 1992, Fold and thrust tectonics of the western United States Cordillera, exclusive of the accreted terranes, *in* Burchfiel, B. C., Lipman, P., and Zoback, M. L., eds., The Cordilleran Orogen: Conterminous U.S.: Boulder, Colorado, Geological Society of America, The Geology of North America, v. G-3, p. 583-607.

Allmendinger, R.W., and Jordan, T.E., 1984, Mesozoic structure of the Newfoundland Mountains, Utah: Horizontal shortening and subsequent extension in the hinterland of the Sevier belt: Geological Society of America Bulletin, v. 95, p. 1280-1292.

Anderson, J.L., 1983, Proterozoic anorogenic granite plutonism of North America, *in* Medaris, L.G. ed., Proterozoic Geology: Selected Papers from an International Proterozoic Symposium, Geological Society of America Memoir 161, p. 133-154.

Anderson, J.L. and Smith, D.R., 1995, The effects of temperature and fo_2 on the Al-in-hornblende barometer: American Mineralogist, v. 80, p. 549-559.

Applegate, J.D.R., Walker, J.D., and Hodges, K.V., 1992, Late Cretaceous extensional unroofing in the Funeral Mountains metamorphic core complex, California: Geology, v. 20, p. 519-522.

Armstrong, G.C., and Oriel, S.S., 1965, Tectonic development of Idaho-Wyoming thrust belt: American Association of Petroleum Geologists Bulletin, v. 49, p. 1847-1866.

Armstrong, R.L., 1968, Sevier orogenic belt in Nevada and Utah: Geological Society of America Bulletin, v. 79, p. 429-458.

Beckerman, G.M., Robinson, J.P., and Anderson, J.L., 1982, The Teutonia batholith; A large intrusive complex of Jurassic and Cretaceous age in the eastern Mojave Desert, California. *in* Frost, E.G., and Martin, D.M., eds., Mesozoic-Cenozoic tectonic evolution of the Colorado River region, California, Arizona, and Nevada: San Diego, California, Cordilleran Publishers, p. 205-220.

Bennet, V., and Depaolo, D.J., 1987, Proterozoic crustal history of the western United

States as determined by neodymium isotopic mapping, Geological Society of America Bulletin, v. 90, p. 674-685.

Beyene, M.A., 2000, Kinematics and Timing of the Pinto Shear Zone, New York Mountains, northeastern Mojave Desert, California [M.S. Thesis]: University of Nevada, Las Vegas, Las Vegas, Nevada, 155 p.

Beyene, M.A., Wells, M.L., and Spell, T.L., 2000, Late Cretaceous extension, Pinto Shear Zone, New York Mountains, northeastern Mojave Desert, California: Geological Society of America Abstracts with Programs, v. 32, p. 3.

Bishop, C.C., 1964, Geologic map of California, Needles sheet, scale 1:250,000, California Division of Mines and Geology, Sacramento.

Brady, R.H., III, 1988, Southward continuation of the southern Death Valley fault zone from the Avawatz to the Bristol Mountains, San Bernardino County, California: Geological Society of America Abstracts with Programs, v. 21, p. 59.

Buck, W.R., 1988, Flexural rotation of normal faults: Tectonics, v. 7, p. 959-973.

Burchfiel, B.C., Cowan, D.S., and Davis, G.A., 1992, Tectonic overview of the Cordilleran orogen in the western United States, *in* Burchfiel, B.C., Lipman, P.W., and Zoback, M.L., eds., The Cordilleran Orogen: Conterminous U.S.: Boulder, Colorado, Geological Society of America, The Geology of North America, v. G-3, p. 407-479.

Burchfiel, B.C., and Davis, G.A., 1981, Mojave Desert and environs. *in* Ernst, W.G., ed., The geotectonic development of California: Englewood Cliffs, New Jersey, Prentice-Hall, p. 217-252.

Carl, C.S., Miller, C.F., and Foster, D.A., 1991, Western Old Woman Mountains shear zone: Evidence for late ductile extension in the Cordilleran orogenic belt: Geology, v. 19, p. 893-896.

Cebula, G.T., Kunk, M.J., Mehnert, H.H., Naeser, C.W., Obradovich, J.D., and Sutter, J.F., 1986, The Fish Canyon Tuff, a potential standard for the 40Ar/39Ar and fission-track dating methods: Terra Cognita (6th International Conference on Geochronology, Cosmochronology and Isotope Geology), v. 6, p. 139.

Cherniak, D.J. and Watson, E.B., 2000, Pb diffusion in zircon: Chemical Geology, v. 172, p. 5-24.

Davis, G.A., Shackelford, T.J., Freeman, S.T., Kuniyoshi, S., and West, S.M., 1974, Limitations on southward extent of the Death Valley fault zone, California: Geological Society of America Abstracts with Programs, v. 6, p. 161.

DeWitt, E., Armstrong, R.L., Sutter, J.F., and Zartman, R.E., 1984, U-Th-Pb, Rb-Sr, and Ar-Ar mineral and whole-rock isotopic systematics in a metamorphosed granitic terrane, southeastern California: Geological Society of America Bulletin. v. 95, p. 723-739.

Dodson, M.H., 1973, Closure temperature in cooling geochronological and petrological systems: Contributions to Mineralogy and Petrology, v. 40, p. 259-274.

Dokka, R.K., and Travis, C.J., 1990, Late Cenozoic strike-slip faulting in the Mojave Desert, California: Tectonics, v. 9, p. 311-340.

Farley, K.A., Wolf, R.A., and Silver, L.T., 1996, The effects of long alpha-stopping distances on (U-Th)/He ages: Geochimica et Cosmochimica Acta, v. 60, p. 4223-4229.

Farley, K.A., 2000, Helium diffusion from apatite: General behavior as illustrated by Durango fluorapatite: Journal of Geophysical Research, v. 105, p. 2903-2914.

Fitzgibbon, T.T., and Howard, K.A., 1987, Tectonic significance of middle Proterozoic diabase sheets in southeastern California and Arizona, Geological Society of America Abstracts with Programs, v. 19, p. 377.

Foster, D.A., Harrison, T.M., and Miller, C.F., 1989, Age, inheritance, and uplift history of the Old Woman-Piute Batholith, California and implications for K-feldspar age spectra: Journal of Geology, v. 97, p. 232-243.

Foster, D.A., Harrison, T.M., Miller, C.F., and Howard, K.A., 1990, The $^{40}Ar/^{39}Ar$ thermochronology of the eastern Mojave Desert, California, and adjacent western Arizona with implications for the evolution of metamorphic core complexes: Journal of Geophysical Research, v.95, p. 20,005-20,024.

Foster, D.A., Miller, C.F., Harrison, T.M., and Hoisch, T.D., 1992, $^{40}Ar/^{39}Ar$ thermochronology and thermobarometry of metamorphism, plutonism, and tectonic denudation in the Old Woman Mountains area, California: Geological Society of America Bulletin, v. 104, p. 176-191.

Foster, D.A., and Fanning, C.M., 1997, Geochronology of the northern Idaho batholith and the Bitterroot metamorphic core complex: Magmatism preceding and contemporaneous with extension: Geological Society of America Bulletin, v. 109, p. 379-394.

Fox, L. K., and Miller, D. M., 1990, Jurassic granitoids and related rocks of the southern Bristol Mountains, southern Providence Mountains, and Colton Hills, Mojave Desert, California. *in* Anderson, J.L. (ed) The nature and origin of cordilleran magmatism. Geological Society of America Memoir 174: p. 111-132.

Gamble, J., 1959a, Geology and mineral resources of Township 8 North, Ranges 11 and 12 East, San Bernardino Base and Meridian, San Bernardino County, California: San Francisco, California, Southern Pacific company, unpublished report and 1:24,000-scale map, 22 p.

Gamble, J., 1959b, Geology and mineral resources of Township 9 North, Ranges 11 and 12 East, San Bernardino Base and Meridian, San Bernardino County, California: San Francisco, California, Southern Pacific Company, unpublished report and 1:24,000-scale map, 18 p.

Gerber, M.E., Miller, C.F., and Wooden, J.L., 1995, Plutonism at the interior margin of the Jurassic magmatic arc, Mojave Desert, California, *in* Miller, D.M., and Busby, C., Jurassic Magmatism and Tectonics of the North American Cordillera: Boulder, Colorado, Geological Society of America Special Paper 299, p. 351-374.

Goldfarb, R.J., Miller, D.M., Simpson, R.W., Hoover, D.B., Moyle, P.R., Olson, J.E., and Gaps, R.S., 1988, Mineral resources of the Providence Mountains Wilderness Study Area, San Bernardino County, California: U.S. Geological Survey Bulletin 1712-D, p. 70.

Hamilton, W., and Myers, W.B., 1966, Cenozoic tectonics of the western United States: Reviews of Geophysics, v. 4, p. 509-549.

Hammarstrom, J.M. and Zen, E-an, 1986, Aluminum in hornblende: An empirical igneous geobarometer: American Mineralogist, v. 71, p. 1297-1313.

Harrison, T.M. and McDougall, I., 1982, The thermal significance of potassium feldspar K-Ar ages inferred from $^{40}Ar/^{39}Ar$ age spectrum results: Geochimica et Cosmochimica Acta, v. 46, p. 1811-1820.

Harrison, T.M., 1981, Diffusion of ^{40}Ar in Hornblende: Contributions to Mineralogy and Petrology, v. 78, p. 324-331.

Hazzard, J.C., 1954, Rocks and structures of the northern Providence Mountains, San Bernardino County, California: California Division of Mines Bulletin v. 170, p. 27-35.

Heller, P.L., Bowdler, S.S., Chambers, H.P., Coogan, J.C., Hagen, E.S., Shuster, M.W., and Winslow, N.S., 1986, Time of initial thrusting in the Sevier Orogenic belt, Idaho-Wyoming and Utah: Geology, v. 14, p. 388-391.

Hill, E.J., Baldwin, S.L., and Lister, G.S., 1995, Magmatism as an essential driving force for formation of active metamorphic core complexes in eastern Papua New Guinea: Journal of Geophysical Research, v. 100, p. 10,441-10,451.

Hodges, K.V., and Walker, J.D., 1992, Extension in the Cretaceous Sevier orogen, North

American Cordillera: Geological Society of America bulletin, v. 104, p. 560-569.

Hollister, L.S., Grissom, G.C., Peters, E.K., Stowell, H.H., and Sisson, V.B., 1987, Confirmation of the empirical correlation of Al in hornblende with pressure of solidificaiton of calc-alkaline plutons: American Mienralogist, v. 72, p. 231-239.

House, M.A., Wernicke, B.P., and Farley, K.A., 1998, Dating topography of the Sierra Nevada, California, using apatite (U-Th)/He ages: Nature, v. 396, p. 66-69.

Howard, K.A., Kilburn, J.E., Simpson, R.W., Fitzgibbon, Todd T., Detra, D.E., Raines, G.L, and Sabine, C., 1987, Mineral resources of the Bristol/Granite Mountains Wilderness Study Area, San Bernardino County, California: U. S. Geological Survey Bulletin, Report: B 1712-C, p.C1-C18.

Howard, K.A. and Miller, D.M., 1992, Late Cenozoic Faulting at the Boundary between the Mojave and Sonoran Blocks: Bristol Lake Area, California, *in* Richard, S.M., ed., Deformation associated with the Neogene Eastern California Shear Zone, southeastern California and southwestern Arizona, San Bernardino County Museums Special Publication, p. 37-47.

Howard, K.A., McCaffrey, K.J.W., Wooden, J.L., Foster, D.A., and Shaw, S.E., 1995, Jurassic thrusting of Precambrian basement over Paleozoic cover in the Clipper Mountains, southeastern California, *in* Miller, D.M., and Busby, C., Jurassic Magmatism and Tectonics of the North American Cordillera: Boulder, Colorado, Geological society of America Special Paper 299, p. 375-392.

Howard, K.A., 2000, personal communication

Hurley, P.M., 1954, The helium age method and the distribution and migration of helium in rocks, *in* Faul, H., ed., Nuclear Geology: New York, John Wiley and Sons, p. 301-329.

John, B.E., 1981, Reconnaissance study of Mesozoic plutonic rocks in the Mojave Desert region. *in* Howard, K.A., Carr, M.D., and Miller, D.M., eds., Tectonic framework of the Mojave and Sonoran deserts, California and Arizona: U.S. Geological Survey Open-File Report 81-503, p. 49-51.

John, B.E. and Mukasa, S.B., 1990, Footwall rocks to the Mid-Tertiary Chemehuevi Detachment fault: a window into the middle crust in southern cordillera: Journal of Geophysical Research, v. 95, p. 463-485.

Johnson, M.C., and Rutherford, M.J., 1989, Experimental calibration of the aluminum-in-hornblende geobarometer with application to Long Valley caldera (California) volcanic rocks: Geology, v. 17, p. 837-841.

Lageson, D.R. and Schmitt, J.G., 1994, The Sevier orogenic belt of the western United

States: Recent advances in understanding its structural and sedimentologic framework *in* Caputo, M.V., Peterson, J.A., and Franczyk, K.J., eds., Mesozoic Systems of the Rocky Mountain Region, USA, p. 27-56.

Lanphere, M. A., 1964, Geochronologic studies in the eastern Mojave Desert, California: Journal of Geology, v. 72, p. 381-399.

Lippolt, H.J., Leitz, M., Wernicke, R.S., and Hagedorn, B., 1994, (Uranium+thorium)/ helium dating of apatite: experience with samples from different geochemical environments: Chemical Geology, v. 112, p. 179-191.

Livaccari, R.F., 1991, Role of crustal thickening and extensional collapse in the tectonic evolution of the Sevier-Laramide orogeny, western United States, Geology, v. 19, p. 1104-1107.

Lovera, O.M., Richter, F.M., and Harrison, T.M., 1989, The $^{40}Ar/^{39}Ar$ Thermochronometry for Slowly Cooled Samples Having a Distribution of Diffusion Domain Sizes: Journal of Geophysical Research, v. 94, p. 17,917-17,935.

Lovera, O.M., Richter, F.M., and Harrison, T.M., 1991, Diffusion domains determined by ^{39}Ar released during step heating: Journal of Geophysical Research, v. 96, p. 2057-2069.

Lovera, O.M., 1992, Computer Programs to Model $^{40}Ar/^{39}Ar$ Diffusion Data from Multidomain Samples: Computers and Geosciences, v. 18, p. 789-813.

Lovera, O.M., Heizler, M.T., and Harrison, T.M., 1993, Argon diffusion domains in K-feldspar II: kinetic properties of MH-10: Contribution to Mineralogy and Petrology, v. 113, p. 381-393.

Lovera, O.M., Grove, M., and Harrison, T.M., 2002, Systematic Analysis of K-feldspar $^{40}Ar/^{39}Ar$ step heating results II: Relevance of laboratory argon diffusion properties to nature: Geochimica et Cosmochimica Acta, v.66, p.1237-1255.

Ludwig, K.R., 1998, On the treatment of concordant uranium-lead ages: Geochimica et Cosmochimica Acta, v. 62, p. 665-676.

Ludwig, K.R., 2001, Users Manual for Isoplot/Ex rev. 2.49: Berkely Geochronology Center, Special Publication No. 1, 56 p.

McDougall, I. and Harrison, T.M., 1999, Geochronology and Thermochronology by the $^{40}Ar/^{39}Ar$ Method, 2nd edition, Oxford University Press, New York, NY, 269 p.

Merrihue, C., 1965, Trace-element determinations and potassium-argon dating by mass

spectroscopy of neutron-irradiated samples: Transactions of the American Geophysical Union, v. 46, p. 125.

Merrihue, C., and Turner, G., 1966, Potassium-argon dating by activation with fast neutrons: Journal of Geophysical Research, v. 71, p. 2852-2857.

Miller, D.M., and Howard, K.A., 1985, Bedrock geologic map of the Iron Mountains Quadrangle, San Bernardino and Riverside Counties, California: U.S. Geological Survey Miscellaneous Field Studies Map MF-1736.

Miller, D.M., Glick, L.L., Goldfarb, R., Simpson, R.W., Hoover, D.B., Detra, D.E., Dohrenwend, J.C., and Munts, S.R., 1985, Mineral resources and mineral resource potential of the South Providence Mountains Wilderness Study Area, San Bernardino County, California: U.S. Geological survey Miscellaneous Field Studies Map MF-1780-A, 29 p., scale 1:62,500.

Miller, D.M., Miller, R.J., Nielson, J.E., Wilshire, H.G., Howard, K.A., Stone, P., 1991, Preliminary Geologic Map of the East Mojave National Scenic Area: U.S. Geological Survey Open File Report, OF 91-0435

Miller, D.M., Wells, M.L., Dewitt, E., Walker, J.D., and Nakata, J.K., 1996, Late Cretaceous extensional fault system across the northeastern Mojave Desert: San Bernardino County Museum Association Quarterly, v. 43, p. 77-84.

Moser, D.E. and Scott, D.J., 2000, Towards a more accurate U-Pb geochronology: Chemical Geology, v. 172, p. 1-3.

Paces, J.B. and Miller, J.D., 1993, Precise U-Pb Ages of Duluth Complex and Related Mafic Intrusions, Northeastern Minnesota: Geochronoligcal Insights to Physical, Petrogenetic, Paleomagnetic, and Tectonomagmatic Processes Associated with the 1.1 Ga Midcontinent Rift System: Journal of Geophysical Research, v. 98, p. 13,997-14,013.

Poole, F.G., Stewart, J.H., Palmer, A.R., Sandberg, C.A., Madrid, R.J., Ross, R.J., Hintze, L.F., Miller, M.M., and Wrucke, C.T., 1992, Latest Precambrian to latest Devonian time; development of a continental margin, *in* Burchfiel, B.C., Lipman, P.W., and Zoback, M.L., eds., The Cordilleran Orogen; conterminous U.S.: Boulder Colorado, Geological Society of America, The Geology of North America, v. G-3, p. 9-56.

Reiners, P.W. and Farley, K.A., 1999 Helium diffusion and (U-Th)/He thermochronometry of titanite: Geochimica et Cosmochimica Acta, v. 63, p. 3845-3859.

Reiners, P.W., Brady, R., Farley, K.A., Fryxell, J.E., Wernicke, B., and Lux, D., 2000,

Helium and argon thermochronometry of the Gold Butte block, south Virgin Mountains, Nevada: Earth and Planetary Science Letters, v. 178, p. 315-326.

Reiners, P.W., 2002, (U-Th)/He chronometry experiences a renaissance, Eos, transactions, American Geophysical Union, v. 83, p. 21-27

Reiners, P.W., Farley, K.A., and Hickes, H.J., 2002, He diffusion and (U-Th)/He thermochronometry of zircon: Initial results from Fish Canyon tuff and Gold Butte, Nevada: Tectonophysics, v. p. .

Richter, F.M., Lovera, O.M., Harrison, T.M., and Copeland, P., 1991, Tibetan tectonics from $^{40}Ar/^{39}Ar$ analysis of a single K-feldspar sample: Earth and Planetary Science Letters, v. 105, p. 266-278.

Rodgers, D.W. and Janecke, S.U., 1992, Tertiary paleogeologic maps of the western Idaho-Wyoming-Montana thrust belt, *in* Link, P.K., Kuntz, M.A., and Platt, L.B., eds., Regional geology of eastern Idaho and western Wyoming, Geological Society of America Memoir, v.179, p.83-94.

Rutherford, E., 1905, Present problems in radioactivity: Popular Science Monthly, May, p. 1-34.

Rutter, M.J., Van der Laan, S.R., and Wyllie, P.J., 1989, Experimental data for a proposed empirical igneous geobarometer: Aluminum in hornblende at 10 kbar pressure: Geology, v. 17, p. 897-900.

Schmidt, M.W., 1992, Amphibole composition in tonalite as a function of pressure: an experimental calibration of the Al-in-hornblende barometer: Contributions to Mineralogy and Petrology, v. 110, p. 304-310.

Steven, T.A., Mehnert, H.H, and Obradovich, J.D., 1967, Age of volcanic activity in the San Juan Mountains, Colorado: U.S. Geological Survey Professional Paper, 575-D, p. 47-55.

Stone, P., Howard, K.A., and Hamilton, W., 1983, Correlation of metamorphosed Paleozoic strata of the southeastern Mojave Desert region, California and Arizona, Geological Society of America Bulletin, v. 94, p. 1135-1147.

Strutt, R.J., 1905, On the Radioactive minerals: Proceedings of the Royla Society of London, v. 76, p. 88-101.

Stuwe, K., White, L., and Brown, R., 1994, The influence of eroding topography on steady-state isotherms: Application to fission-track analysis: Earth and Planetary Science Letters, v. 124, p. 63-74.

Tera, F. and Wasserburg, G.J., 1972, U-Th-Pb Systematics in Three Apollo 14 Basalts

and the Problem of Initial Pb in Lunar Rocks: Earth and Planetary Science Letters, v. 14, p. 281-304.

Walker, J.D., Burchfiel, B.C., and Davis, G.A., 1995a, New age controls on initiation and timing of foreland belt thrusting in the Clark Mountains, southern California: Geological Society of America Bulletin, v. 107, p. 742-750.

Walker, J.D., Fletcher, J.M., Fillmore, R.P., Martin, M.W., Taylor, W.J., Glazner, A.F., and Bartley, J.M., 1995b, Connection between igneous activity and extension in the Mojave metamorphic complex, California: Journal of Geophysical Research, v. 100, p. 10,477-10,494.

Wells, M.L., Dallmeyer, R.D., and Allmendinger, R.W., 1990, Late Cretaceous extension in the hinterland of the Sevier thrust belt, northwestern Utah and southern Idaho: Geology, v. 18, p. 929-933.

Wells, M.L., 1997, Alternating contraction and extension in the hinterlands of orogenic belts: An example from the Raft River Mountains, Utah: Geological society of America Bulletin, v. 109, p. 107-126.

Wells, M.L., Hoisch, T.D., Peters, M.T., Miller, D.M., Wolff, E.D., and Hanson, L.M., 1998, The Mahogany Peaks Fault, a Late Cretaceous-Paleocene(?) Normal Fault in the Hinterland of the Sevier Orogen: The Journal of Geology, v. 106, p. 623-634.

Wendt, I. and Carl, C., 1991, The statistical distribtution of the mean squared weighted deviation: Chemical Geology, v. 86, p. 275-285.

Williams, I., 1992, Some observations on the use of zircon U-Pb geochronology in the study of granitic rocks: Transactions of the Royal Society of Edinburgh: Earth Sciences, v. 83, p. 447-458.

Wolf, R.A., Farley, K.A., and Silver, L.T., 1996, Helium diffusion and low-temperature thermochronometry of apatite: Geochimica et Cosmochimica Acta, v. 60, p. 4231-4240.

Wooden, J.L., Miller, D.M., and Howard, K.A., 1988, Early Proterozoic chronology of the eastern Mojave Desert, Geological Society of America Abstracts with Programs, v. 20, p. 243.

Wright, J.E., Howard, K.A., and Anderson, J.L., 1987, Isotopic systematics of zircons from Late Cretaceous intrusive rocks, southeastern California; Implications for a vertically stratified crust: Geological Society of American Abstracts with Programs, v. 19, p. 898.

Young, E.D. and Wooden, J.L., 1988, Mid-crustal emplacement of Mesozoic granitoids,

eastern Mojave Desert; Evidence from crystallization barometry: Geological Society of America Abstracts with Programs, v. 20, p. 244.

Young, E.D., Wooden, J.L., Shieh, Y-N, and Farber, D., 1992, Geochemical evolution of Jurassic diorites from the Bristol Lake region, California, USA and the role of assimilation: Contributions to Mineralogy and Petrology, v. 110, p. 68-86.

Zeitler, P.K., Herczig, A.L., McDougall, I., and Honda, M., 1987, U-Th-He dating of apatite: a potential thermochronometer: Geochimica et Cosmochimica Acta, v. 51, p. 2865-2868.

APPENDIX A

Sample Descriptions

Calvin: 34° 46' 34.8" N, 115° 44' 26.4" W

Calvin was collected in the southwest Granite Mountains from a pluton mapped as Cretaceous porphyritic monzogranite (Kpm) (Miller et al., 1985) (Fig. 2). This unit is known as the Granite of Arrowweed in the southern Providence Mountains (Miller et al., 1985). This pluton makes up the southern half of the range and is the largest pluton found in the Granite Mountains. The granite is coarsely crystalline (~2-3 mm), containing K-feldspar phenocrysts and large biotite crystals in hand sample. Plagioclase, quartz, K-feldspar, biotite, and hornblende are all widely present in thin section. Sphene and apatite are also abundant with zircons commonly found as inclusions within biotite.

Floyd: 34° 48' 51.0" N, 115° 41' 40.2"W

Floyd was collected from a Cretaceous granodiorite (Kgd) (Miller et al., 1985) near the center of the Granite Mountains. This unit is exposed in the interior of the range and also in the southwest (Fig. 2) and may be described as an equigranular hornblende-biotite granodiorite (~1-2 mm). Thin section shows quartz, plagioclase, K-feldspar, and abundant hornblende and biotite. Zircon is present as inclusions within biotite and there is also apatite and large sphene crystals.

Yoshi: 34° 49' 58.0" N, 115° 39' 11.5" W

Yoshi was taken from a pluton in the northeast Granite Mountains described by Miller et al. (1985) as a Jurassic spotted quartz monzonite (Fig. 2). The sample has a visible fabric, which has been determined as magmatic (boundary flow) rather than metamorphic due to a lack of prominent foliation and metamorphic minerals in thin section. The sample is a medium to fine-grained (~1-2 mm with large ~3-5 mm mafic clots) hornblende-biotite quartz monzonite (Miller et al., 1985). Thin section shows abundant plagioclase with quartz and K-feldspar. Sample is also rich in biotite and hornblende, zircon common as inclusions and scattered apatite.

Omar: 34° 52' 11.7" N, 115° 34' 52.1" W

Omar was collected in the southern Providence Mountains from the Jurassic quartz monzonite of Goldstone (Miller et al., 1985) (Fig. 2). The hand sample is darker in color than those from the Granite Mountains and is medium to coarse grained (~1-3 mm). The mafic phases appear as clusters. Thin section shows plagioclase, quartz and K-feldspar with large biotite and hornblende with pyroxene (?). Apatite and zircon are scattered throughout with zircon common as inclusions in biotite.

APPENDIX B

Electron Microprobe hornblende chemical analyses

Appendix B consists of the standards used for calibration along with chemical data for Kakanui Hornblende, which was the standard, used during analyses. Data tables of hornblende chemical analyses are listed in sequence from a to e representing rim-to-core-to-rim analyses where a and e are rims and c is core. SEM images of hornblendes with respective spots analyzed are also included.

Standards used in calibration

Analysis	Lab Number	Supplier	Mineral Name	Standard Number
Al_2O_3	UNLV-44	Harvard	Green's Creek Almandine	HMM 112140
FeO	UNLV-45	Harvard	Green's Creek Almandine	HMM 112141
K_2O	UNLV-49	USNM(1)	Microcline	USNM 143966
Na_2O	UNLV-76	MAC-EMS	Jadeite	
SiO_2	UNLV-43	USNM(1)	Kakanui Hornblende	USNM 143965
CaO	UNLV-72	MAC-EMS	Natural Wollastonite	
MgO	UNLV-63	Harvard	Chandrika Wewa Enstatite	HMM 131709
MnO	UNLV-54	USNM(1)	Ilmen Ilmenite	USNM 96189
TiO_2	UNLV-55	USNM(1)	Ilmen Ilmenite	USNM 96190

Kakanui Hornblende

Al_2O_3	FeO_T	K_2O	Na_2O	SiO_2	CaO	MgO	MnO	TiO_2	Total
14.90	11.25	2.05	2.60	40.37	10.30	12.80	0.09	4.72	99.08

Hornblende analyses				Weight Percent						23 OXYGEN FORMULA	
Sample	**Al_2O_3**	**FeO**	**K_2O**	**Na_2O**	**SiO_2**	**CaO**	**MgO**	**MnO**	**TiO_2**	**Total**	**Al(T)**	
SW monzogranite												
Calvin-1a	8.636	16.967	0.872	1.309	44.799	11.729	11.550	0.515	0.364	96.741	**1.521**	Calvin-1a
Calvin-1b	8.797	17.083	0.942	1.359	44.897	11.658	11.282	0.508	0.754	97.280	**1.541**	Calvin-1b
Calvin-1c	9.046	17.041	0.993	1.368	44.706	11.648	11.369	0.474	0.913	97.558	**1.581**	Calvin-1c
Calvin-1d	9.118	17.054	1.073	1.324	44.370	11.726	11.182	0.516	0.749	97.112	**1.603**	Calvin-1d
Calvin-1e	9.370	17.549	0.999	1.376	44.215	11.607	10.832	0.512	0.631	97.091	**1.650**	Calvin-1e
Calvin-2a	9.448	17.735	0.996	1.483	43.959	11.440	11.084	0.556	0.833	97.534	**1.659**	Calvin-2a
Calvin-2b	8.891	17.414	0.958	1.378	44.745	11.654	11.442	0.488	0.790	97.760	**1.553**	Calvin-2b
Calvin-2c	8.940	17.296	1.020	1.328	45.122	11.600	11.476	0.529	0.887	98.198	**1.553**	Calvin-2c
Calvin-2d	9.187	17.122	1.005	1.404	44.366	11.456	11.318	0.492	0.814	97.164	**1.613**	Calvin-2d
Calvin-2e	9.465	17.340	1.091	1.314	44.019	11.647	10.923	0.534	0.834	97.167	**1.666**	Calvin-2e
Calvin-3a	9.255	17.365	1.090	1.599	44.086	11.602	11.593	0.500	0.800	97.890	**1.619**	Calvin-3a
Calvin-3b	9.271	17.320	1.041	1.397	44.173	11.347	11.154	0.494	0.800	96.997	**1.632**	Calvin-3b
Calvin-3c	9.593	17.758	1.124	1.421	43.957	11.662	10.918	0.528	1.181	98.142	**1.676**	Calvin-3c
Calvin-3d	8.736	16.932	1.007	1.257	44.879	11.443	11.536	0.467	0.788	97.045	**1.532**	Calvin-3d
Calvin-3e	9.238	17.160	0.974	1.343	44.242	11.725	11.272	0.527	0.668	97.149	**1.624**	Calvin-3e
Calvin-5a	9.380	17.521	1.092	1.304	44.466	11.654	11.035	0.479	0.677	97.608	**1.642**	Calvin-5a
Calvin-5b	9.252	17.571	1.068	1.493	43.871	11.576	11.397	0.558	0.767	97.553	**1.625**	Calvin-5b
Calvin-5c	8.596	16.785	0.944	1.225	45.068	11.690	11.710	0.451	0.682	97.151	**1.505**	Calvin-5c
Calvin-5d	8.371	16.915	0.953	1.205	45.165	11.644	11.713	0.509	0.702	97.177	**1.466**	Calvin-5d
Calvin-5e	9.334	17.507	0.968	1.197	44.386	11.765	11.111	0.525	0.567	97.360	**1.638**	Calvin-5e

	Weight Percent										23 OXYGEN FORMULA	
Sample	**Al_2O_3**	**FeO**	**K_2O**	**Na_2O**	**SiO_2**	**CaO**	**MgO**	**MnO**	**TiO_2**	**Total**	**Al(T)**	
Calvin-6a	9.428	17.202	1.099	1.508	44.414	11.735	11.023	0.507	0.774	97.690	**1.649**	Calvin-6a
Calvin-6b	9.101	17.464	1.056	1.341	44.441	11.764	11.437	0.536	1.075	98.215	**1.585**	Calvin-6b
Calvin-6c	8.691	16.975	0.981	1.441	45.385	11.657	11.772	0.541	0.983	98.426	**1.504**	Calvin-6c
Calvin-6d	8.820	16.907	1.032	1.404	44.995	11.612	11.315	0.485	0.894	97.464	**1.542**	Calvin-6d
Calvin-6e	6.558	15.362	0.492	0.886	48.833	12.201	13.191	0.478	0.147	98.148	**1.120**	Calvin-6e
Central granodiorite												
Floyd-1a	9.743	17.286	1.009	1.164	44.406	11.652	11.033	0.492	0.644	97.429	**1.705**	Floyd-1a
Floyd-1b	8.506	15.768	0.782	1.213	46.194	11.915	12.203	0.518	0.798	97.897	**1.469**	Floyd-1b
Floyd-1c	8.652	16.207	0.960	1.252	45.188	11.762	11.836	0.542	1.101	97.500	**1.507**	Floyd-1c
Floyd-1d	9.262	15.718	0.976	1.259	44.187	11.684	11.330	0.580	1.036	96.032	**1.638**	Floyd-1d
Floyd-1e	10.007	16.765	0.996	1.223	44.454	11.668	10.859	0.539	0.614	97.125	**1.753**	Floyd-1e
Floyd-2a	9.046	17.332	0.917	1.245	44.294	11.730	10.689	0.472	0.523	96.248	**1.604**	Floyd-2a
Floyd-2b	8.467	16.606	0.861	1.178	45.338	11.778	11.598	0.477	0.973	97.276	**1.479**	Floyd-2b
Floyd-2c	7.694	15.178	0.760	1.153	46.506	11.761	12.501	0.492	1.262	97.307	**1.333**	Floyd-2c
Floyd-2d	8.770	16.017	0.799	1.197	44.811	11.649	11.811	0.496	1.356	96.906	**1.535**	Floyd-2d
Floyd-2e	9.561	17.015	0.909	1.170	44.604	11.674	10.935	0.511	0.643	97.022	**1.677**	Floyd-2e
Floyd-3a	8.968	15.830	0.897	1.274	45.338	11.716	11.854	0.547	0.725	97.149	**1.564**	Floyd-3a
Floyd-3b	8.163	15.584	0.872	1.033	45.996	11.840	12.527	0.504	0.974	97.493	**1.415**	Floyd-3b
Floyd-3c	7.538	14.929	0.789	0.988	46.168	11.794	12.399	0.455	1.175	96.235	**1.319**	Floyd-3c
Floyd-3d	9.000	16.256	0.945	1.008	44.857	11.785	11.572	0.497	1.010	96.930	**1.576**	Floyd-3d
Floyd-3e	8.642	15.745	0.956	0.997	45.841	11.867	12.044	0.568	1.202	97.862	**1.494**	Floyd-3e

	Weight Percent										23 OXYGEN FORMULA	
Sample	**Al_2O_3**	**FeO**	**K_2O**	**Na_2O**	**SiO_2**	**CaO**	**MgO**	**MnO**	**TiO_2**	**Total**	**Al(T)**	
Floyd-4a	9.533	17.735	0.850	1.107	44.306	11.900	10.867	0.551	0.239	97.088	**1.677**	Floyd-4a
Floyd-4b	9.406	16.816	1.012	1.168	44.734	11.760	11.153	0.525	1.001	97.575	**1.641**	Floyd-4b
Floyd-4c	7.914	15.860	0.856	1.105	46.438	11.788	12.118	0.581	1.015	97.675	**1.370**	Floyd-4c
Floyd-4d	9.138	16.800	1.004	1.209	44.426	11.833	11.571	0.558	0.904	97.443	**1.599**	Floyd-4d
Floyd-4e	9.303	16.586	1.010	1.173	44.808	11.625	11.196	0.522	0.778	97.001	**1.630**	Floyd-4e
Floyd-5a	8.811	16.622	0.920	1.211	45.036	11.651	11.494	0.479	0.826	97.050	**1.543**	Floyd-5a
Floyd-5b	8.933	16.415	0.985	1.249	45.159	11.775	11.424	0.486	1.035	97.461	**1.557**	Floyd-5b
Floyd-5c	8.517	17.721	0.882	1.198	44.709	11.627	11.538	0.444	1.223	97.859	**1.487**	Floyd-5c
Floyd-5d	8.783	16.532	0.942	1.225	44.237	11.685	11.363	0.576	1.327	96.670	**1.548**	Floyd-5d
Floyd-5e	8.974	16.624	1.002	1.268	43.669	11.271	10.983	0.526	1.139	95.456	**1.602**	Floyd-5e
NE quartz monzonite												
Yoshi-1a	9.087	17.157	0.962	1.128	44.561	12.030	11.178	0.362	1.004	97.469	**1.590**	Yoshi-1a
Yoshi-1b	8.409	16.287	0.840	1.139	45.619	11.782	12.060	0.384	1.372	97.892	**1.456**	Yoshi-1b
Yoshi-1c	8.307	16.238	0.821	1.059	45.748	11.994	12.032	0.401	0.952	97.552	**1.443**	Yoshi-1c
Yoshi-1d	6.022	14.634	0.446	0.855	49.043	11.973	14.079	0.423	0.636	98.111	**1.026**	Yoshi-1d
Yoshi-1e	8.762	16.566	0.919	1.055	45.397	12.009	11.877	0.365	1.167	98.117	**1.517**	Yoshi-1e
Yoshi-2a	8.496	16.174	0.902	1.148	44.963	12.081	12.169	0.401	0.884	97.218	**1.485**	Yoshi-2a
Yoshi-2b	8.920	17.072	0.905	1.133	44.909	11.901	11.441	0.368	1.064	97.713	**1.554**	Yoshi-2b
Yoshi-2c	8.701	16.433	1.008	1.224	44.320	11.477	11.647	0.446	1.309	96.565	**1.533**	Yoshi-2c
Yoshi-2d	8.823	16.560	0.928	1.187	45.328	11.914	11.847	0.353	1.299	98.239	**1.526**	Yoshi-2d
Yoshi-2e	8.937	16.888	0.831	1.102	45.531	12.046	11.449	0.349	0.860	97.993	**1.549**	Yoshi-2e

	Weight Percent										23 OXYGEN FORMULA	
Sample	**Al_2O_3**	**FeO**	**K_2O**	**Na_2O**	**SiO_2**	**CaO**	**MgO**	**MnO**	**TiO_2**	**Total**	**Al(T)**	
Yoshi-4a	8.912	16.374	0.940	1.171	45.350	11.998	11.942	0.358	1.064	98.109	**1.542**	Yoshi-4a
Yoshi-4b	8.128	15.474	0.670	1.166	46.081	11.538	12.582	0.382	1.318	97.339	**1.408**	Yoshi-4b
Yoshi-4c	8.423	15.699	0.825	1.059	45.679	11.887	12.344	0.370	1.220	97.506	**1.461**	Yoshi-4c
Yoshi-4d	8.560	16.543	0.740	1.082	45.842	12.017	12.052	0.380	0.955	98.171	**1.478**	Yoshi-4d
Yoshi-4e	8.744	16.289	0.892	1.151	45.277	11.959	11.892	0.374	0.804	97.382	**1.524**	Yoshi-4e
Yoshi-6a	8.812	16.720	0.887	1.047	45.554	12.044	11.718	0.346	0.653	97.781	**1.530**	Yoshi-6a
Yoshi-6b	9.032	16.935	0.943	1.176	44.757	11.742	11.199	0.371	0.682	96.837	**1.587**	Yoshi-6b
Yoshi-6c	8.543	16.382	0.849	1.045	46.068	11.978	11.989	0.388	0.761	98.003	**1.476**	Yoshi-6c
Yoshi-6d	7.418	15.703	0.716	1.028	46.679	11.874	12.583	0.416	0.824	97.241	**1.287**	Yoshi-6d
Yoshi-6e	10.153	17.588	1.098	1.173	43.704	11.941	10.286	0.332	0.673	96.948	**1.791**	Yoshi-6e
Yoshi-7a	8.987	17.076	0.976	1.104	45.321	11.723	11.107	0.368	0.863	97.525	**1.566**	Yoshi-7a
Yoshi-7b	8.659	16.856	0.839	1.110	45.627	11.778	11.686	0.361	1.193	98.109	**1.498**	Yoshi-7b
Yoshi-7c	8.740	17.022	0.937	1.133	45.461	11.691	11.615	0.389	1.019	98.007	**1.516**	Yoshi-7c
Yoshi-7d	10.198	17.498	1.113	1.167	43.180	11.800	10.557	0.393	1.648	97.554	**1.790**	Yoshi-7d
Yoshi-7e	8.482	16.921	0.950	1.137	44.403	11.846	11.489	0.382	1.387	96.997	**1.491**	Yoshi-7e
So. Providence quartz monzonite of Goldstone												
Omar-1a	2.467	12.847	0.187	0.452	52.726	12.012	15.868	0.540	0.279	97.378	**0.417**	Omar-1a
Omar-1b	5.809	15.307	0.589	1.077	48.429	11.737	13.454	0.607	0.923	97.932	**0.997**	Omar-1b
Omar-1c	1.283	12.367	0.098	0.213	54.164	12.158	16.789	0.593	0.112	97.777	**0.215**	Omar-1c
Omar-1d	0.567	11.766	0.065	0.168	54.903	11.679	17.409	0.753	0.062	97.372	**0.095**	Omar-1d
Omar-1e	0.773	11.509	0.062	0.181	55.069	11.738	17.345	0.675	0.030	97.382	**0.129**	Omar-1e

	Weight Percent										23 OXYGEN FORMULA	
Sample	**Al_2O_3**	**FeO**	**K_2O**	**Na_2O**	**SiO_2**	**CaO**	**MgO**	**MnO**	**TiO_2**	**Total**	**Al(T)**	
Omar-3a	0.857	14.530	0.044	0.105	54.284	13.003	14.619	0.470	0.024	97.936	**0.145**	Omar-3a
Omar-3b	2.873	12.813	0.000	0.430	52.694	12.012	15.576	0.364	0.469	97.231	**0.485**	Omar-3b
Omar-3c	0.672	15.158	0.024	0.040	53.929	12.661	14.410	0.540	0.003	97.437	**0.114**	Omar-3c
Omar-3d	0.562	14.165	0.037	0.040	54.584	12.844	14.945	0.458	0.002	97.637	**0.095**	Omar-3d
Omar-3e	0.355	14.980	0.016	0.037	54.867	12.648	14.574	0.478	0.000	97.955	**0.060**	Omar-3e
Omar-4a	0.490	11.278	0.062	0.130	55.094	12.076	17.542	0.721	0.050	97.443	**0.082**	Omar-4a
Omar-4b	0.622	11.078	0.042	0.163	55.747	11.798	17.948	0.857	0.059	98.314	**0.103**	Omar-4b
Omar-4c	0.564	10.862	0.056	0.179	55.575	11.290	18.219	0.878	0.055	97.678	**0.094**	Omar-4c
Omar-4d	0.841	11.925	0.070	0.167	54.847	12.173	16.971	0.697	0.077	97.768	**0.141**	Omar-4d
Omar-4e	4.934	14.932	0.395	0.577	49.623	12.168	13.646	0.590	0.288	97.153	**0.849**	Omar-4e
Omar-7a	6.156	15.263	0.638	1.251	47.439	11.806	13.057	0.471	1.059	97.140	**1.068**	Omar-7a
Omar-7b	7.347	16.275	0.852	1.375	45.532	11.310	12.575	0.413	1.095	96.774	**1.288**	Omar-7b
Omar-7c	6.198	15.497	0.677	1.009	47.804	11.943	13.151	0.516	0.902	97.697	**1.069**	Omar-7c
Omar-7d	6.508	14.670	0.632	0.971	47.867	11.825	13.622	0.411	1.021	97.527	**1.119**	Omar-7d
Omar-7e	6.782	15.044	0.702	0.984	47.742	12.047	13.233	0.409	0.982	97.925	**1.164**	Omar-7e
Omar-8a	0.446	13.404	0.010	0.050	54.657	13.518	15.544	0.494	0.014	98.137	**0.075**	Omar-8a
Omar-8b	0.294	7.529	0.000	0.169	53.232	24.233	13.390	0.546	0.027	99.420	**0.050**	Omar-8b
Omar-8c	0.512	9.045	0.001	0.257	52.644	22.296	14.642	0.514	0.096	100.007	**0.086**	Omar-8c
Omar-8d	3.157	13.806	0.248	0.400	52.024	12.349	14.944	0.298	0.428	97.654	**0.535**	Omar-8d
Omar-8e	2.485	13.751	0.085	0.223	53.179	12.887	15.141	0.279	0.006	98.036	**0.418**	Omar-8e

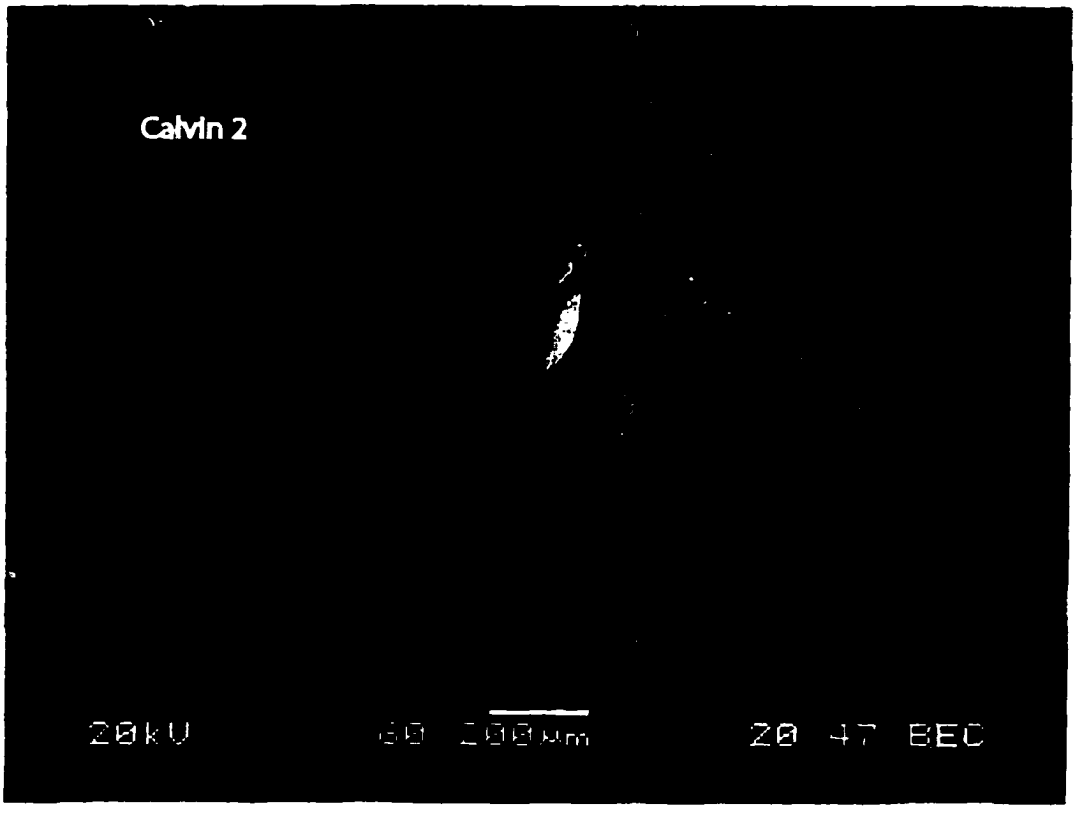

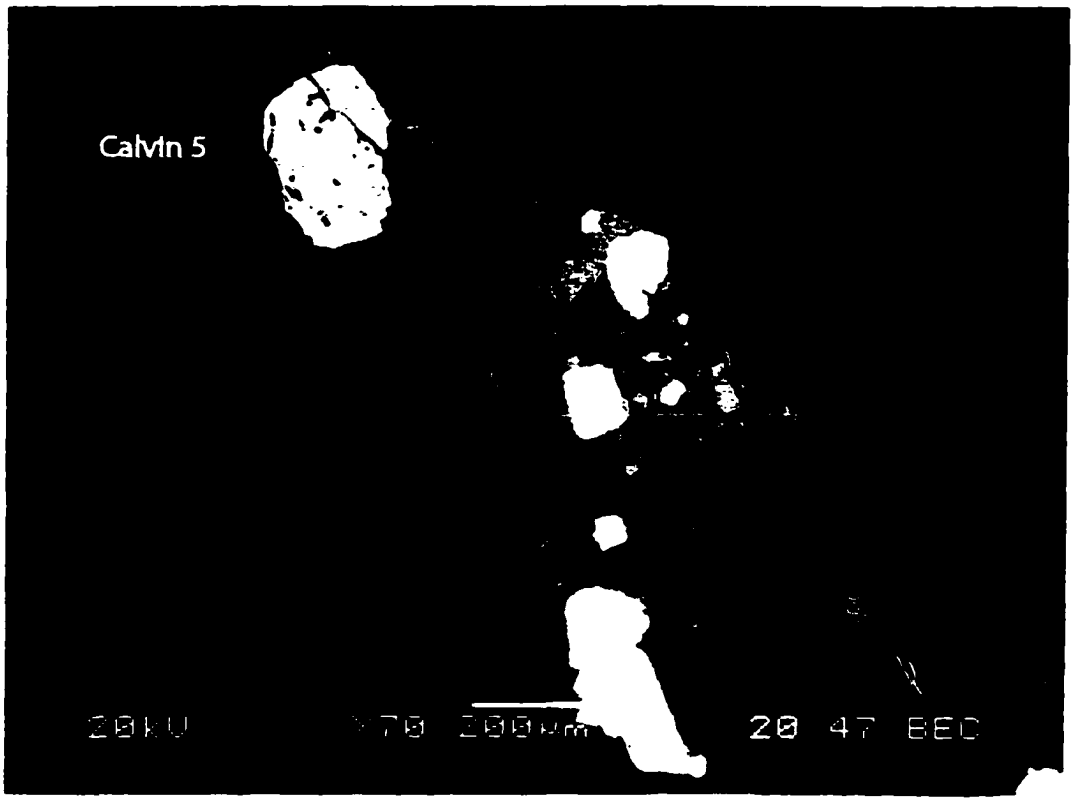

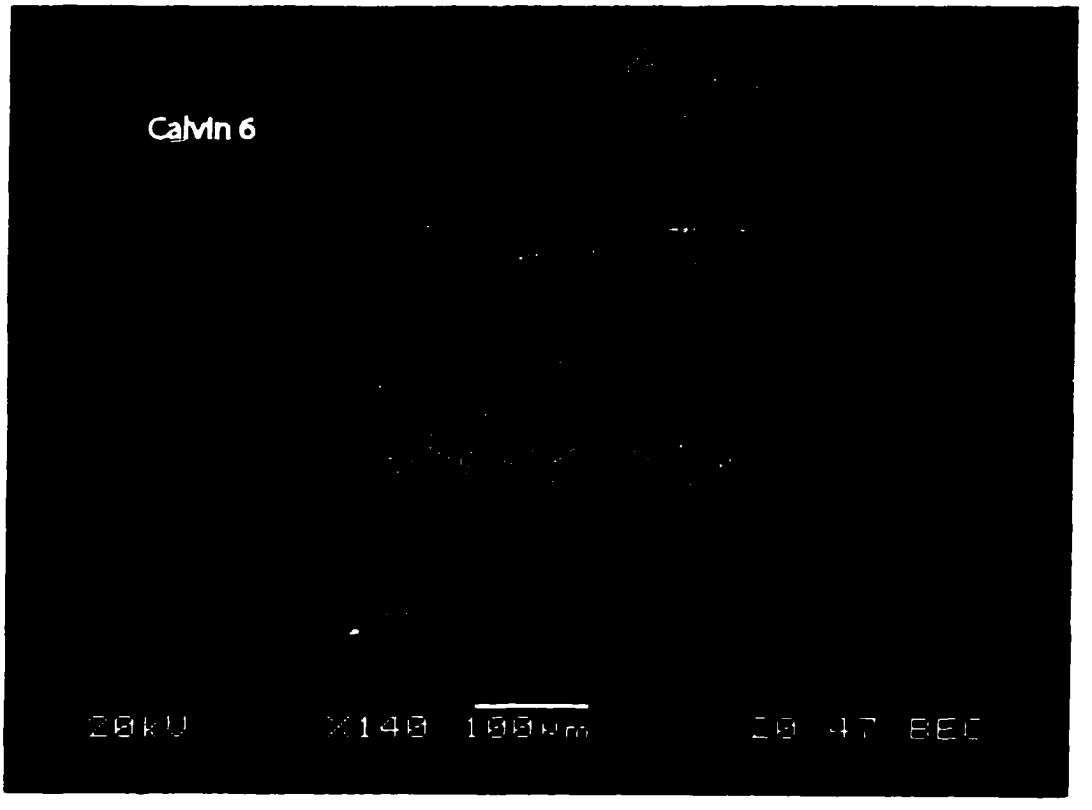

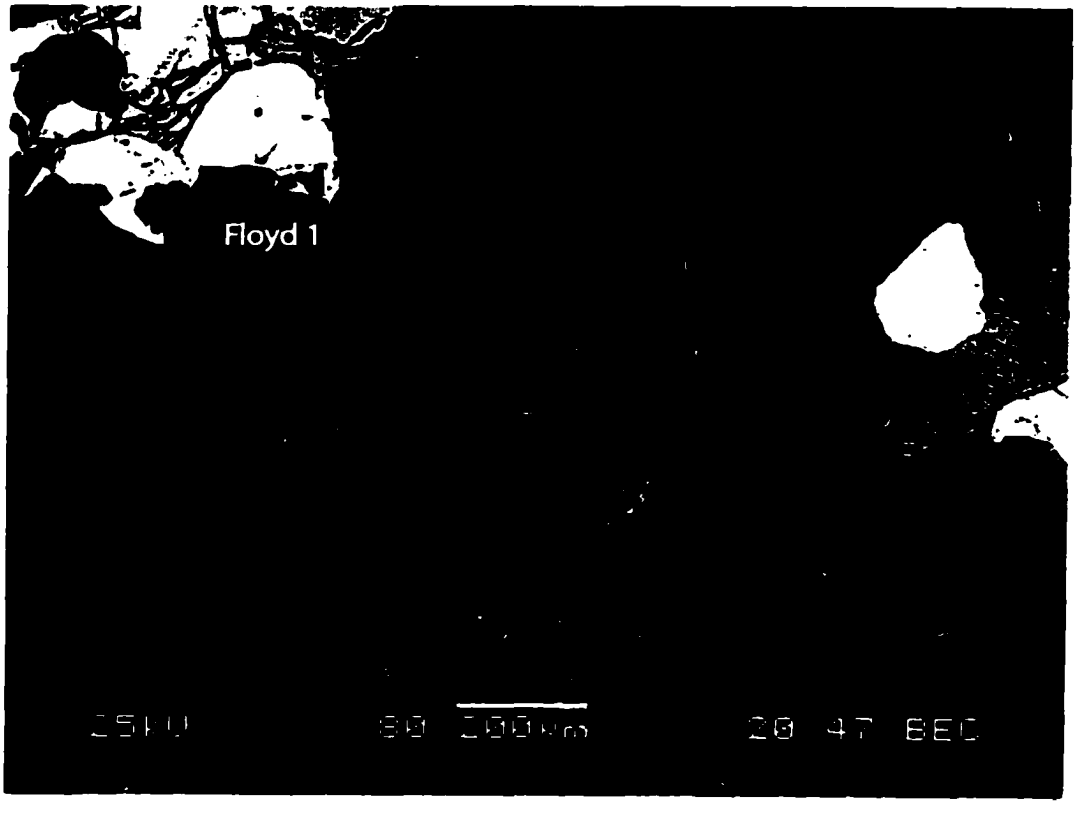

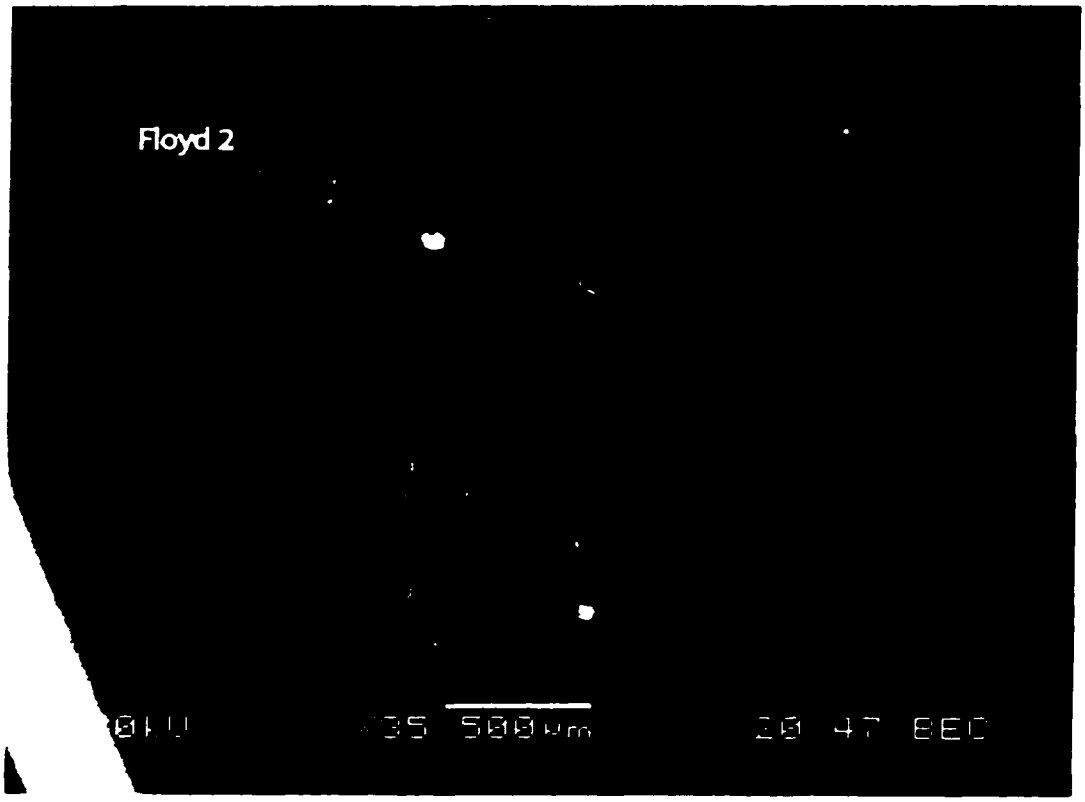

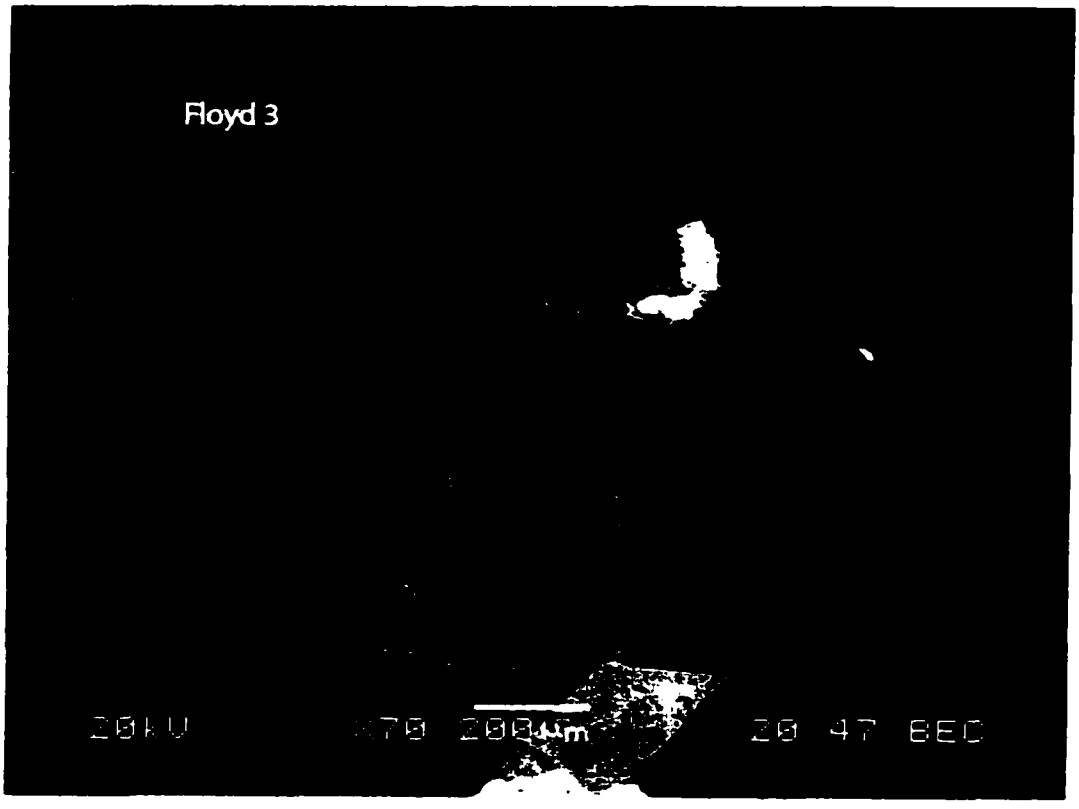

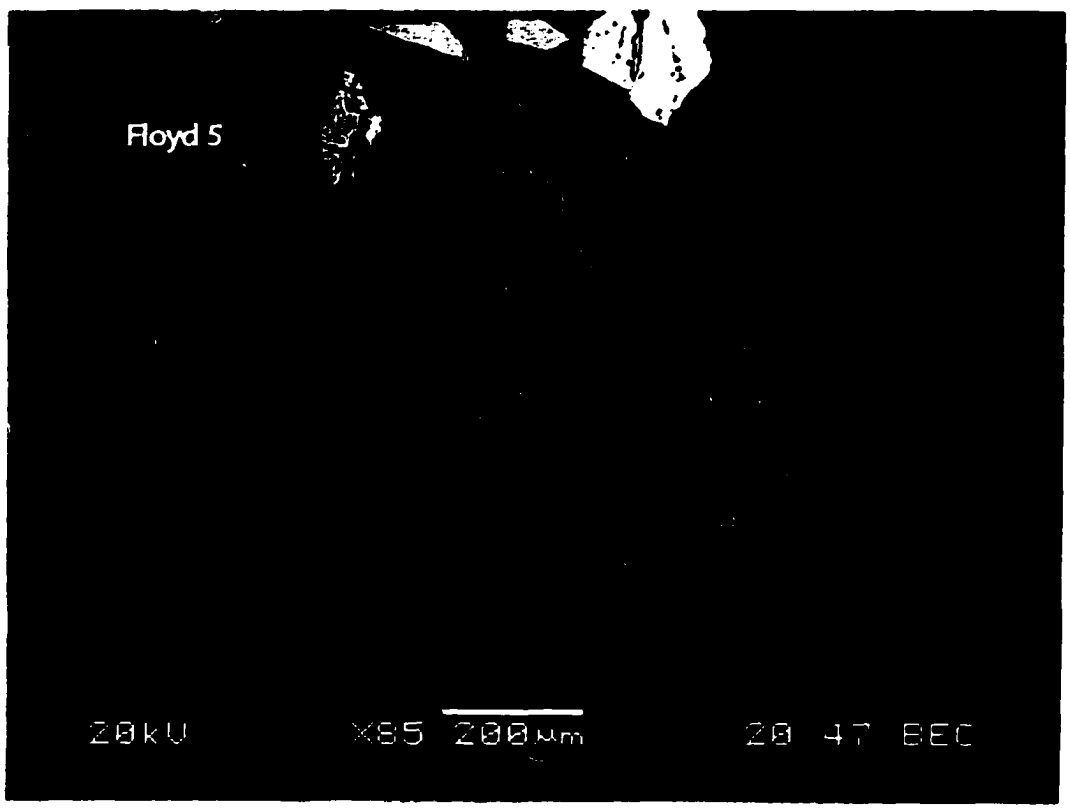

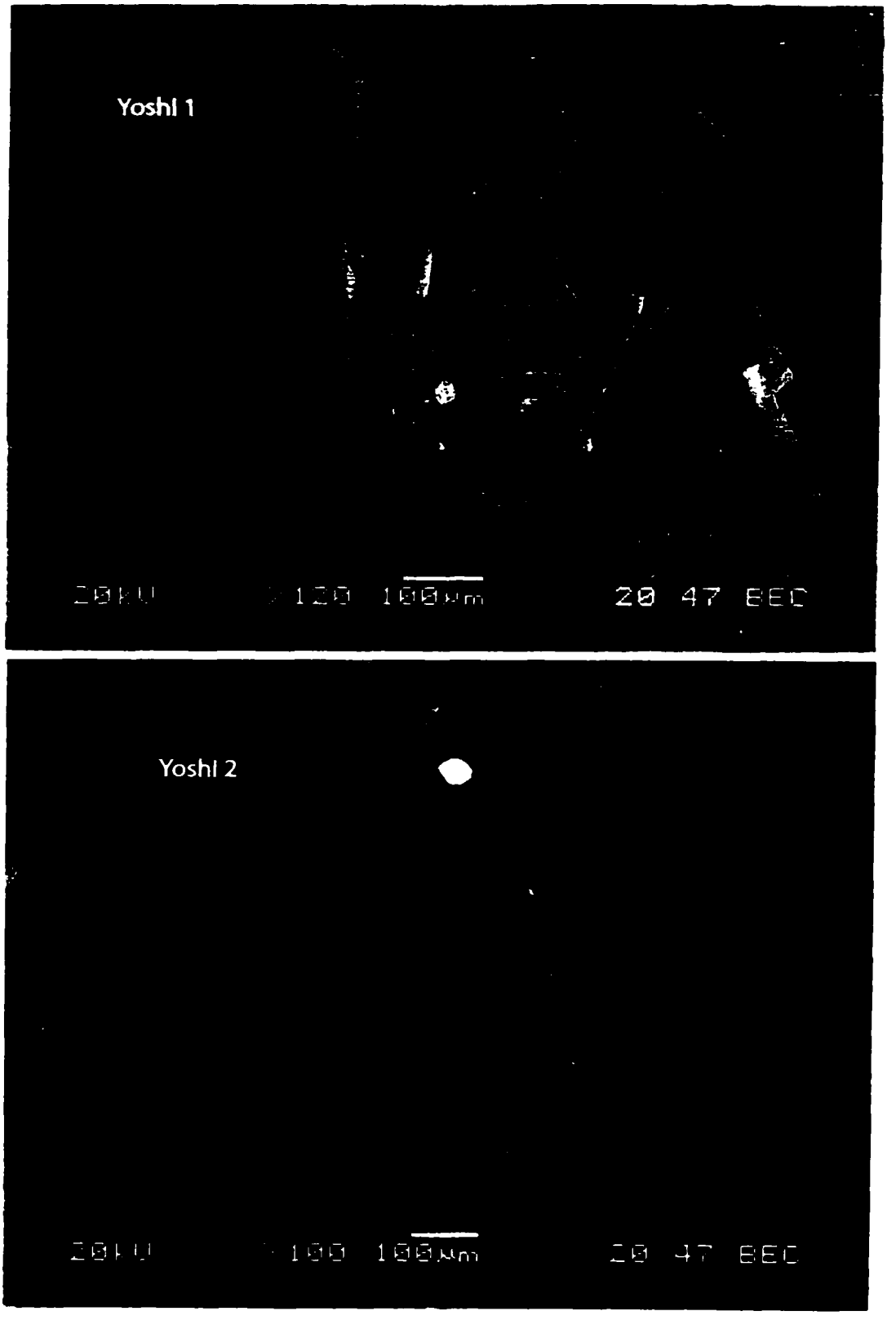

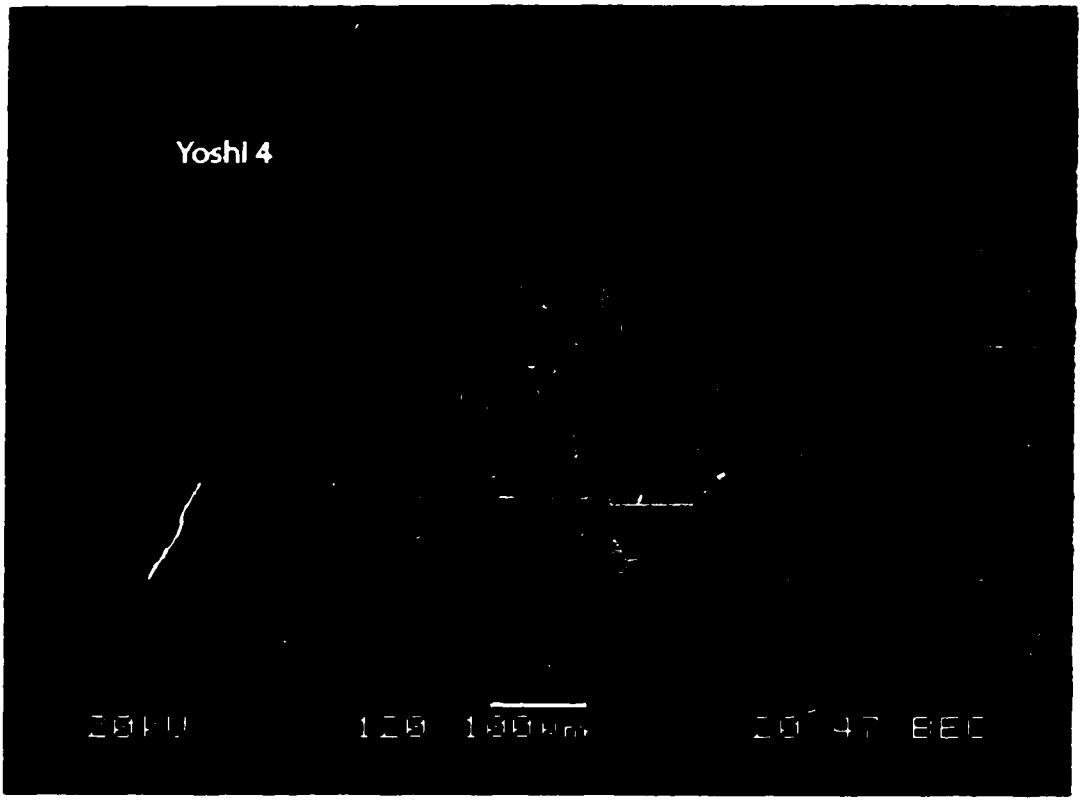

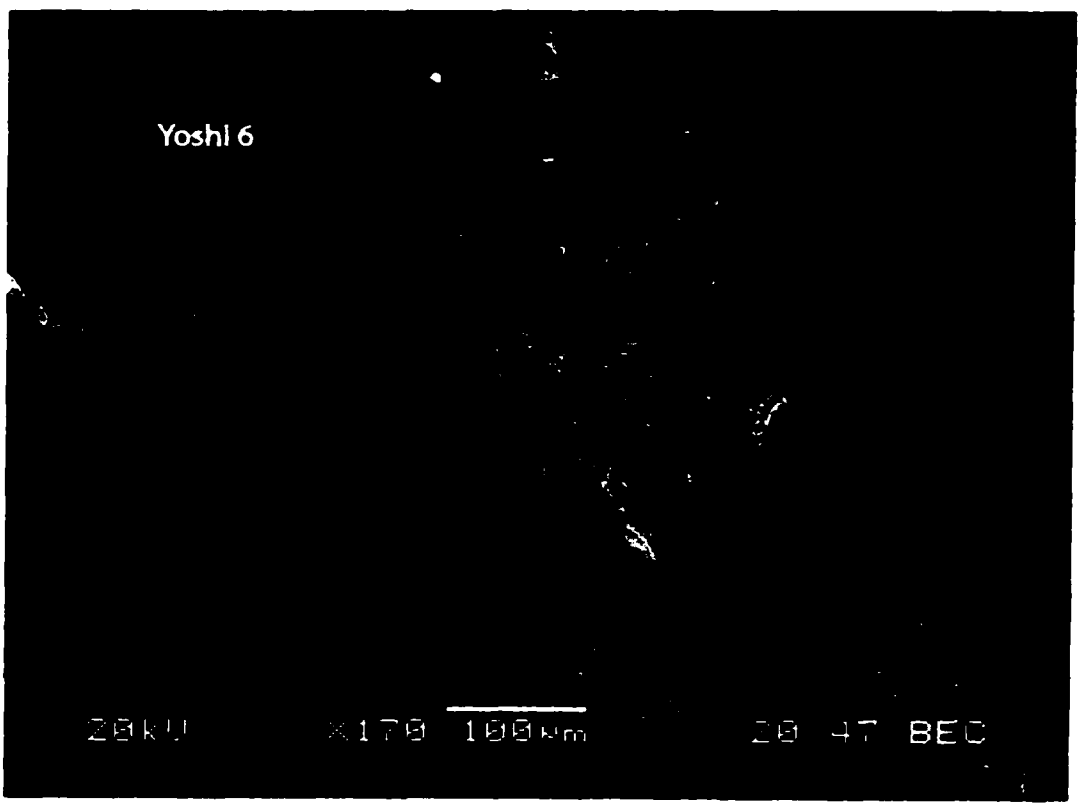

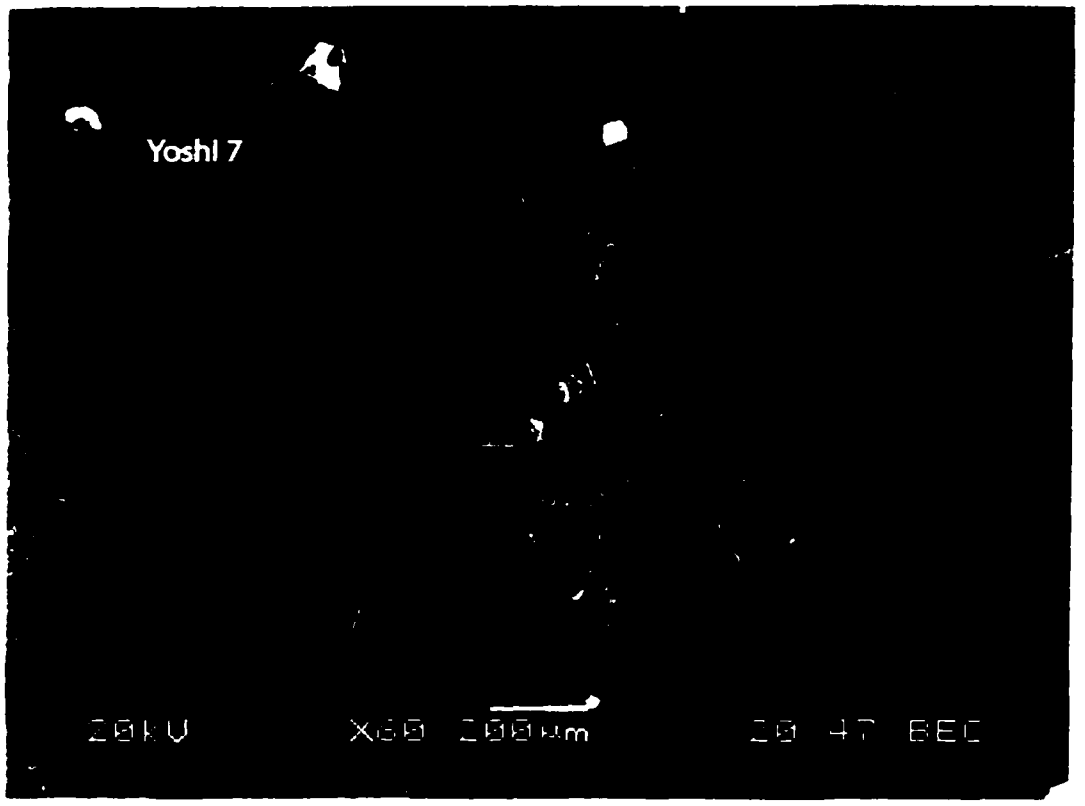

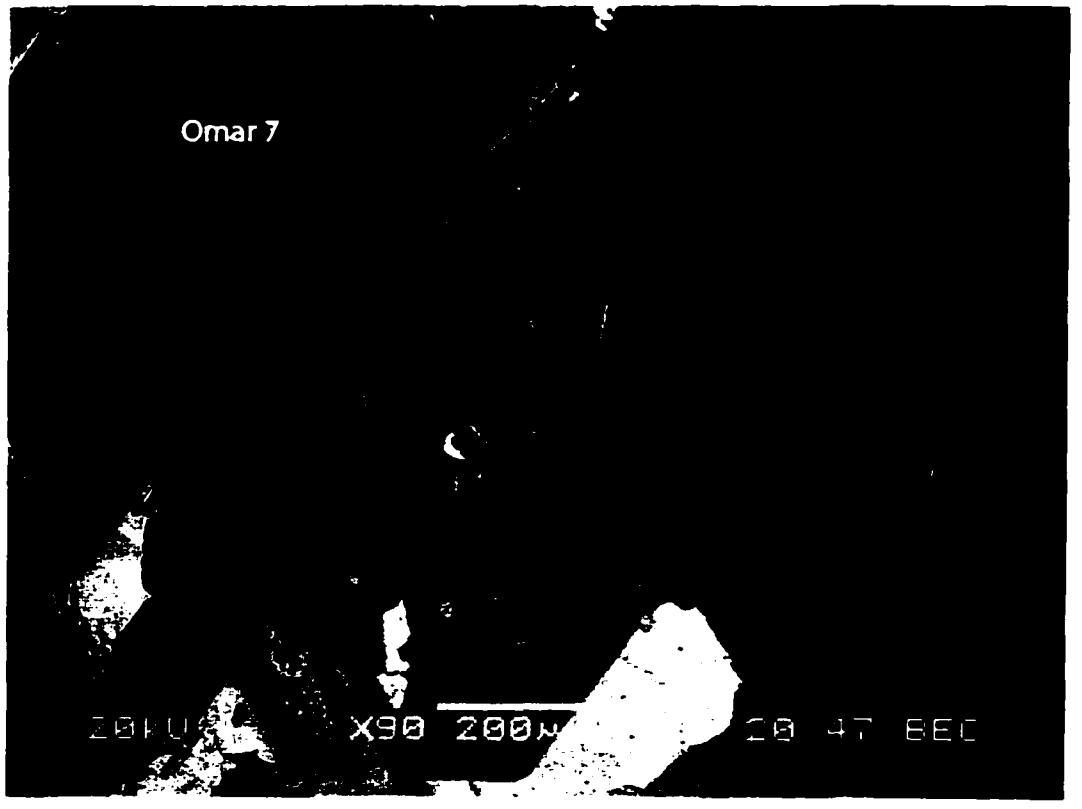

APPENDIX C

Data tables and SEM images of ion microprobe U/Pb isotopic analyses

SW Monzogranite	CALVIN Ratios[a]			(uncorrected) Age (Ma)
Sample	$\frac{^{207}Pb^*}{^{235}U}$	$\frac{^{207}Pb^*}{^{206}Pb^*}$	$\frac{^{206}Pb^*}{^{238}U}$	$\frac{^{206}Pb}{^{238}U}$
Calvin_g11_1	0.1142 ± 13.1	0.07087 ± 11.0	0.01168 ± 3.1	74.90 ± 2.3
Calvin2_g5_1	0.1752 ± 15.8	0.09742 ± 13.9	0.01304 ± 2.9	83.52 ± 2.4
Calvin_g5_1	0.2286 ± 19.6	0.1236 ± 16.2	0.01342 ± 4.1	85.93 ± 3.5
Calvin2_g6_1	0.1159 ± 5.1	0.05763 ± 4.6	0.01459 ± 1.5	93.35 ± 1.4
Calvin2_g11_1	0.1412 ± 15.0	0.08157 ± 12.7	0.01255 ± 3.1	80.40 ± 2.5
Calvin2_g10_1	0.1362 ± 12.4	0.08054 ± 10.7	0.01227 ± 2.9	78.59 ± 2.3
Calvin_g1_1	0.2848 ± 16.0	0.1521 ± 12.3	0.01358 ± 7.3	86.95 ± 6.3
Calvin_g6_1	0.1789 ± 15.5	0.1115 ± 13.2	0.01164 ± 3.5	74.57 ± 2.6
Calvin2_g3_1	0.4631 ± 19.8	0.1589 ± 15.8	0.02113 ± 5.0	134.8 ± 6.7
Calvin_g7_1	0.1483 ± 16.6	0.09052 ± 14.1	0.01188 ± 4.2	76.13 ± 3.2

[a] 1σ % uncertainties.

Central Granodiorite Sample	FLOYD Ratios[a] $\frac{^{207}Pb^*}{^{235}U}$	$\frac{^{207}Pb^*}{^{206}Pb^*}$	$\frac{^{206}Pb^*}{^{238}U}$	(uncorrected) Age (Ma) $\frac{^{206}Pb}{^{238}U}$
Floyd_g1_1	0.1191 ± 10.7	0.07524 ± 8.5	0.01148 ± 3.3	73.60 ± 2.4
Floyd_g2_1	0.1669 ± 7.5	0.1023 ± 6.8	0.01183 ± 2.7	75.80 ± 2.0
Floyd_g2_2	0.1531 ± 3.6	0.09702 ± 3.3	0.01144 ± 3.3	73.36 ± 2.4
Floyd_g6_1	0.3556 ± 18.8	0.1782 ± 14.7	0.01447 ± 5.6	92.61 ± 5.2
Floyd_g20_1	0.2203 ± 19.1	0.1245 ± 15.7	0.01284 ± 4.18	82.22 ± 3.4
Floyd2_g1_1	0.2654 ± 17.1	0.1416 ± 15.5	0.01360 ± 3.2	87.05 ± 2.8
Floyd_g2_3	0.1301 ± 4.9	0.05036 ± 1.0	0.01873 ± 4.7	119.6 ± 5.6
Floyd_g15_1	0.1343 ± 14.6	0.08506 ± 12.0	0.01145 ± 3.9	73.41 ± 2.8
Floyd_g13_1	0.1722 ± 16.0	0.09919 ± 13.6	0.01259 ± 4.3	80.68 ± 3.5

[a] 1σ % uncertainties

NE Qtz Monzonite Sample	YOSHI Ratios[a] $\frac{^{207}Pb^*}{^{235}U}$	$\frac{^{207}Pb^*}{^{206}Pb^*}$	$\frac{^{206}Pb^*}{^{238}U}$	(uncorrected) Age (Ma) $\frac{^{206}Pb}{^{238}U}$
Yoshi_4_1	0.2534 ± 9.8	0.07471 ± 8.9	0.0246 ± 4.2	156.70 ± 6.5
Yoshi_5_1	0.1176 ± 13.6	0.08896 ± 11.6	0.00959 ± 4.4	61.53 ± 2.7
Yoshi_9_1	0.1602 ± 9.2	0.09479 ± 8.1	0.01226 ± 2.2	78.52 ± 1.7
Yoshi_11_1	0.1508 ± 11.2	0.08506 ± 9.6	0.01285 ± 3.0	82.33 ± 2.4
Yoshi_11_2	0.2070 ± 16.3	0.11270 ± 13.4	0.01332 ± 4.5	85.30 ± 3.8
Yoshi_13_1	0.2169 ± 15.9	0.11320 ± 13.6	0.01390 ± 3.9	88.98 ± 3.5
Yoshi2_10_1	0.3349 ± 12.6	0.09375 ± 10.7	0.02591 ± 3.3	164.9 ± 5.3
Yoshi_19_1	0.1292 ± 8.7	0.07910 ± 7.5	0.01184 ± 3.6	75.90 ± 2.7
Yoshi_10_1	0.4641 ± 20.9	0.11960 ± 17.2	0.02814 ± 5.4	178.90 ± 9.6
Yoshi2_7_1	0.1164 ± 9.6	0.06570 ± 8.4	0.01285 ± 2.6	82.34 ± 2.1
Yoshi_1_1	0.3364 ± 17.3	0.16780 ± 14.1	0.01454 ± 6.8	93.05 ± 6.3
Yoshi_7_1	0.1556 ± 12.0	0.09063 ± 10.9	0.01245 ± 2.4	79.77 ± 1.9

[a] 1σ % uncertainties

So. Prov. Qtz Monzonite Sample	OMAR Ratios[a]			(uncorrected) Age (Ma)
	$\frac{^{207}Pb^*}{^{235}U}$	$\frac{^{207}Pb^*}{^{206}Pb^*}$	$\frac{^{206}Pb^*}{^{238}U}$	$\frac{^{206}Pb}{^{238}U}$
Omar2_g13_1	0.8038 ± 13.0	0.1739 ± 9.0	0.03352 ± 6.0	212.5 ± 12.4
Omar2_g11_1	0.3501 ± 16.2	0.09186 ± 12.7	0.02764 ± 4.9	175.8 ± 8.5
Omar_g10_1	0.5031 ± 16.1	0.1294 ± 13.4	0.02820 ± 3.9	179.3 ± 6.9
Omar_g3_1	0.3503 ± 17.3	0.09757 ± 15.1	0.02604 ± 4.2	165.7 ± 6.9
Omar2_g16_1	0.6681 ± 19.4	0.1691 ± 15.2	0.02866 ± 5.8	182.2 ± 10.4
Omar2_g16_2	0.5763 ± 18.3	0.1451 ± 15.6	0.02880 ± 5.6	183.0 ± 10.1
Omar2_g5_1	0.3428 ± 16.0	0.09694 ± 13.2	0.02565 ± 4.3	163.3 ± 6.9

[a] 1σ % uncertainties

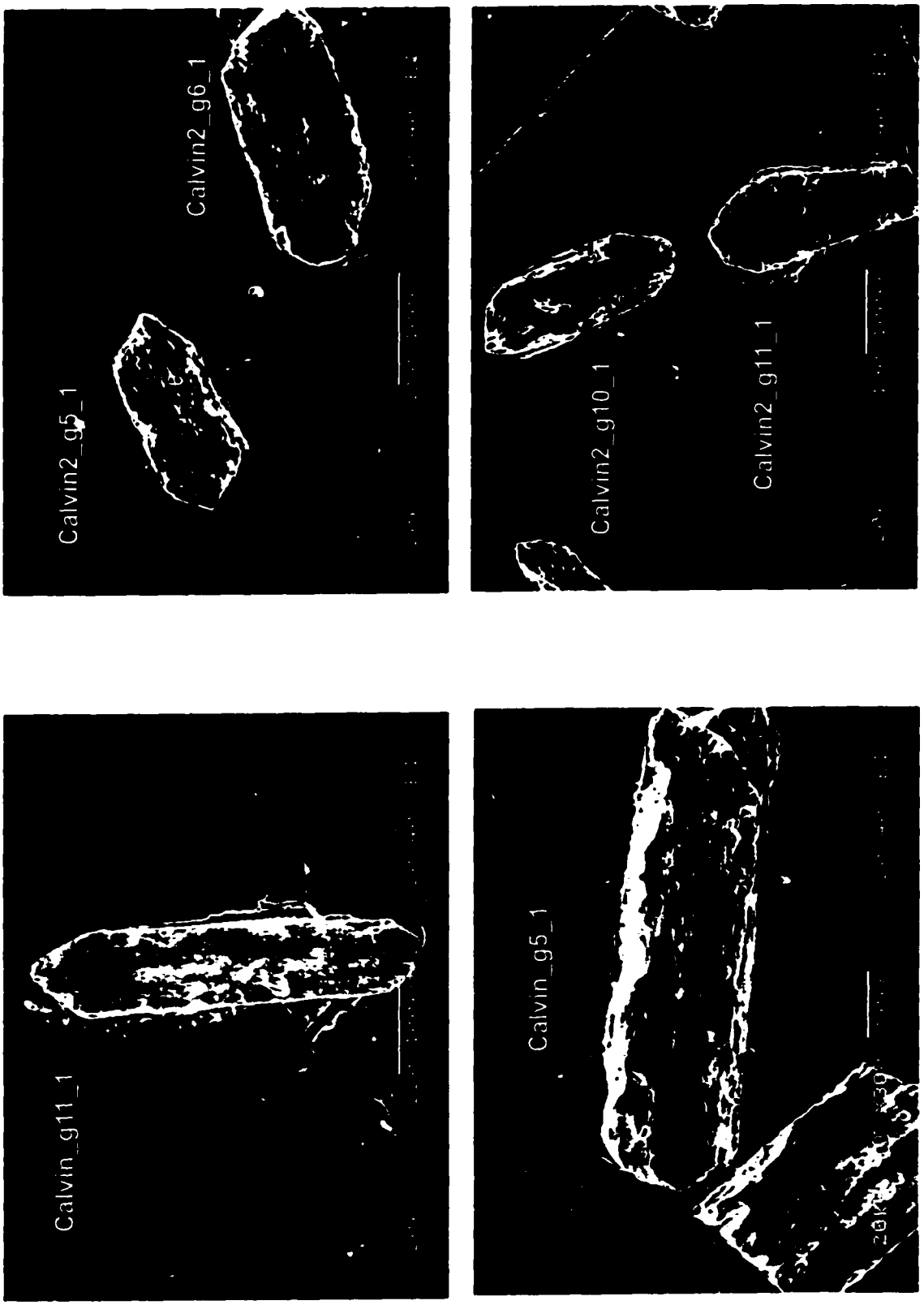

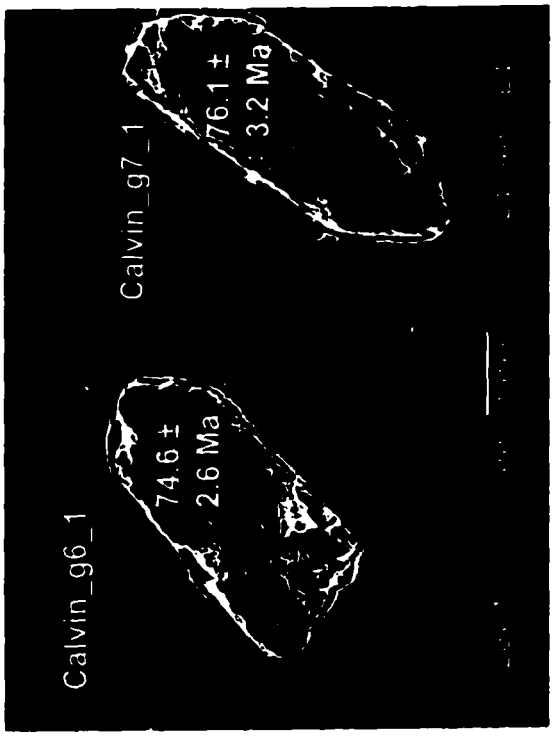

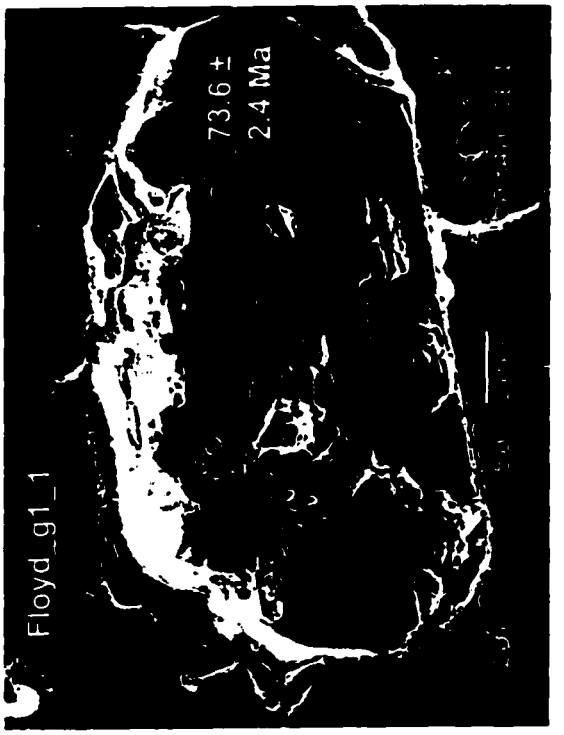

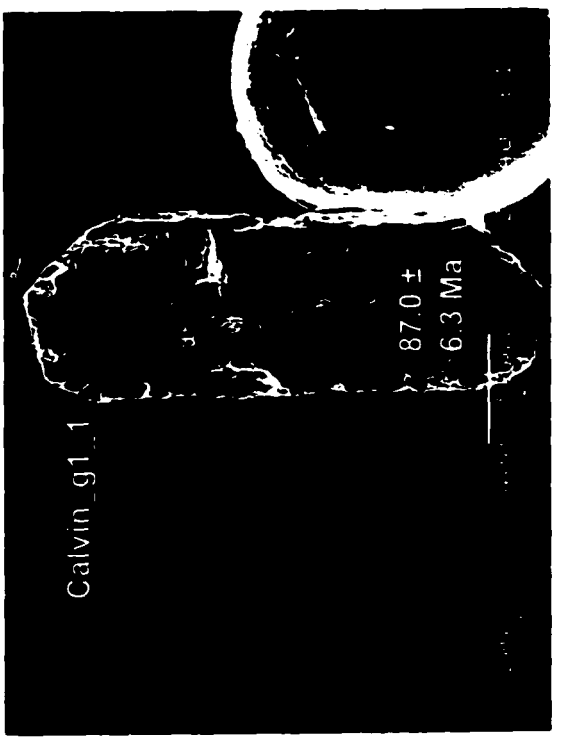

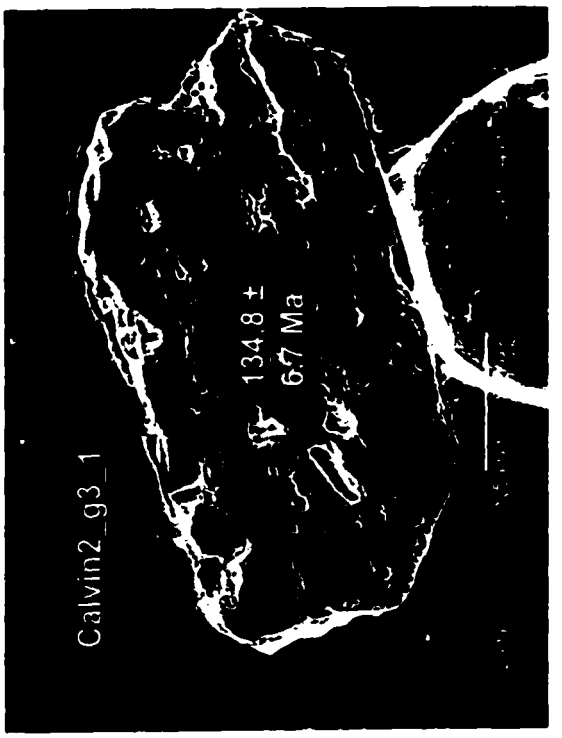

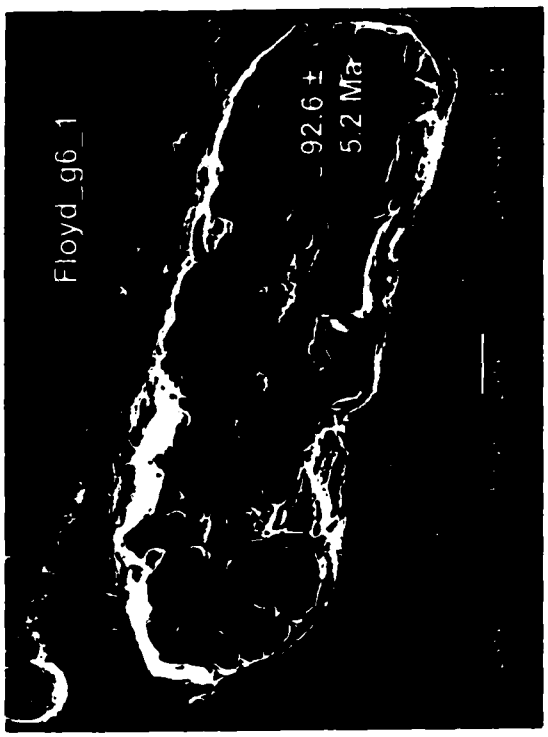

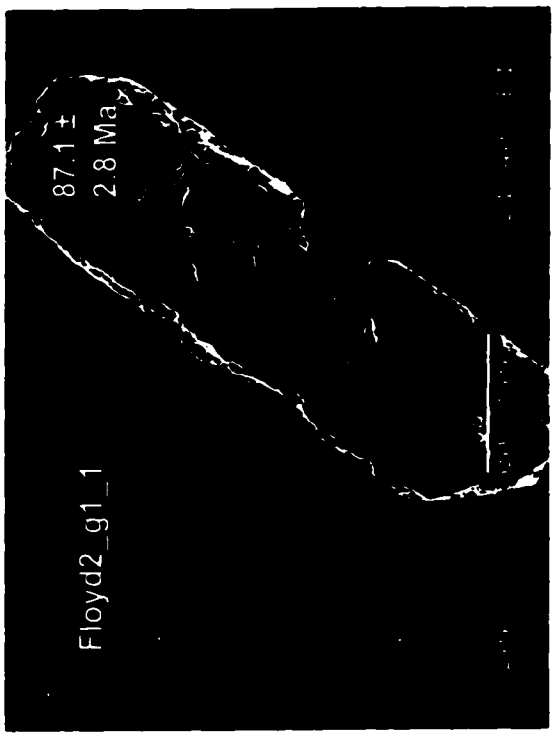

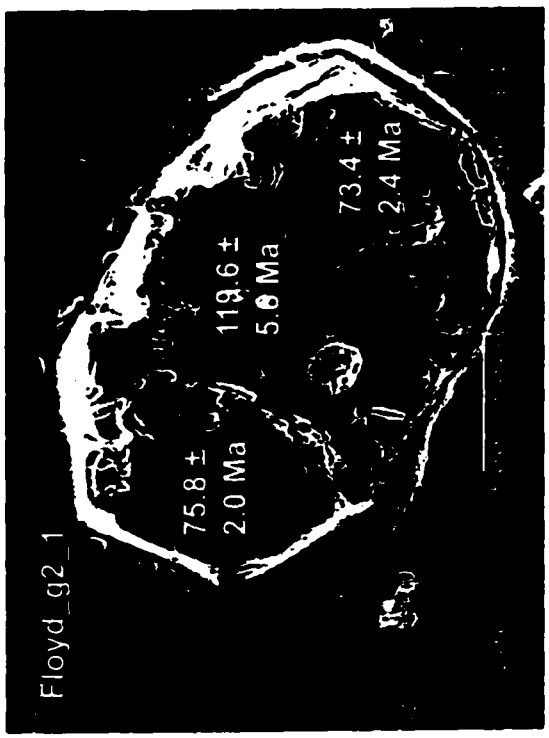

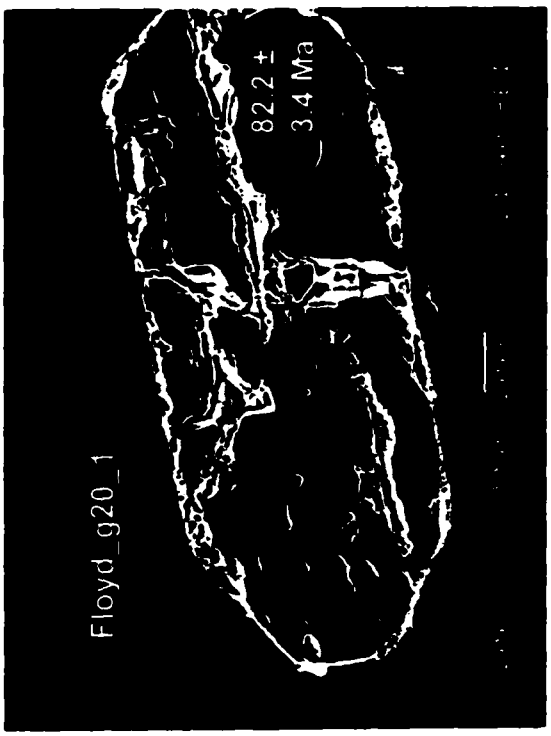

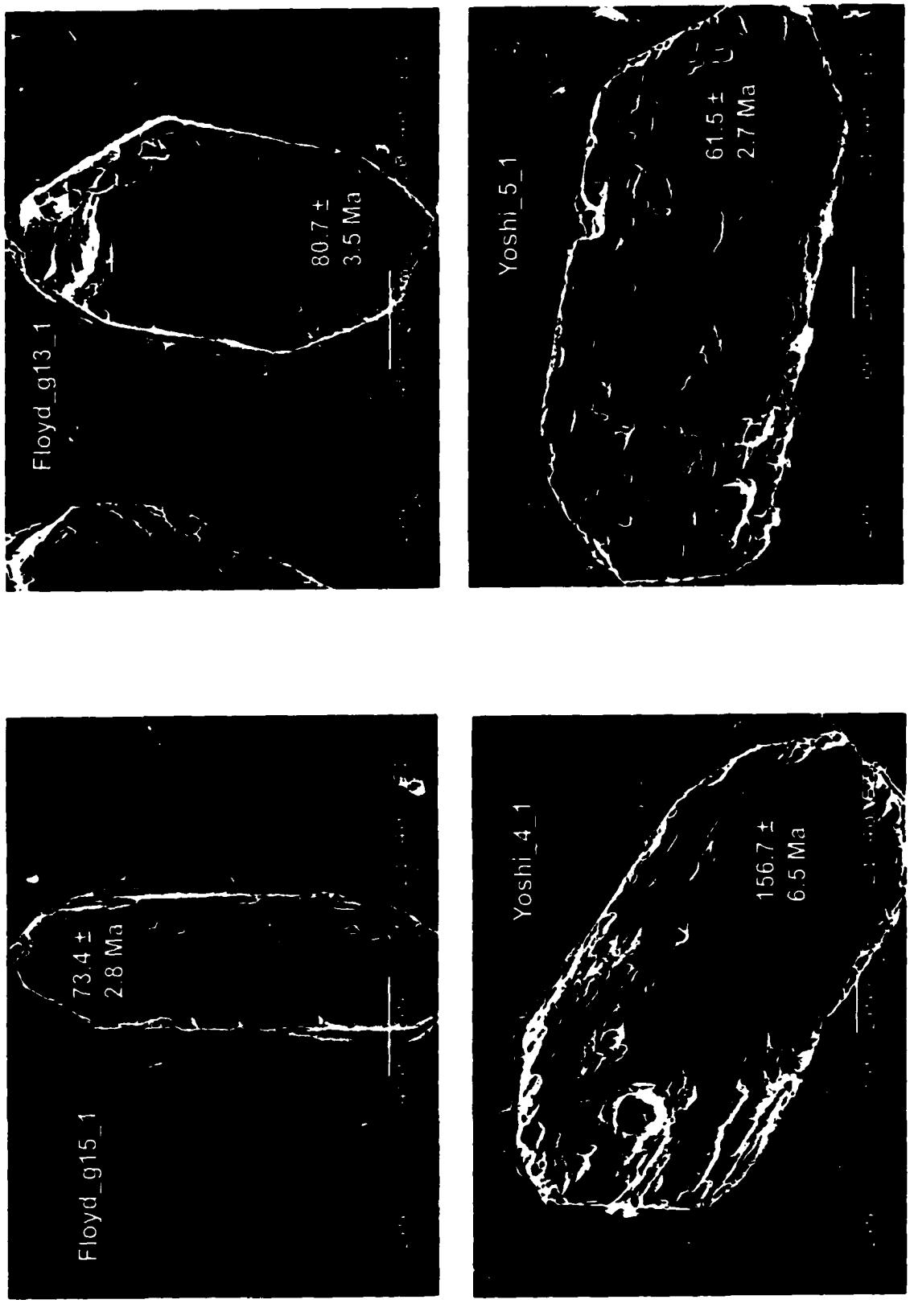

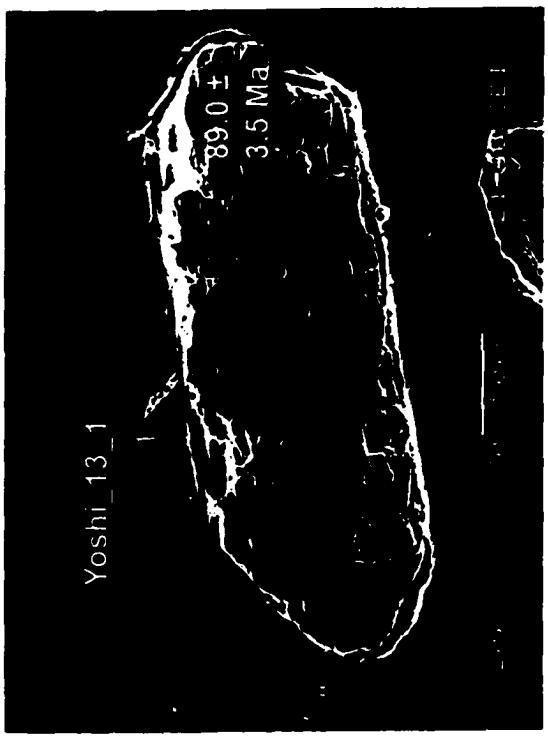

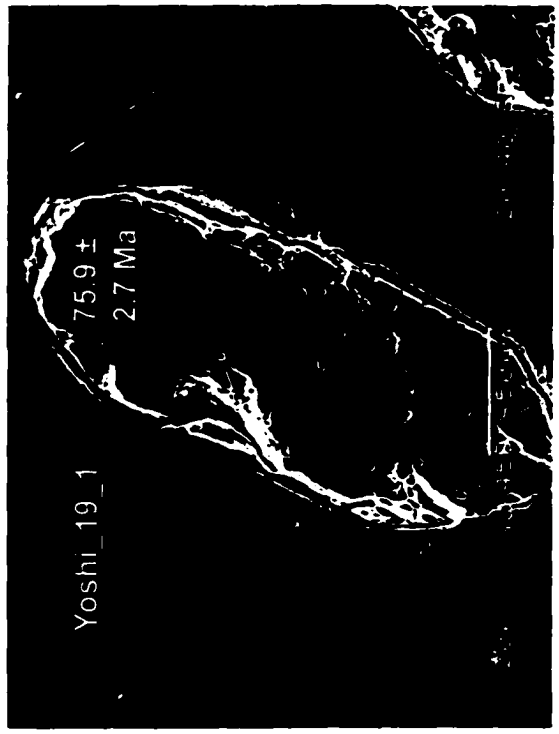

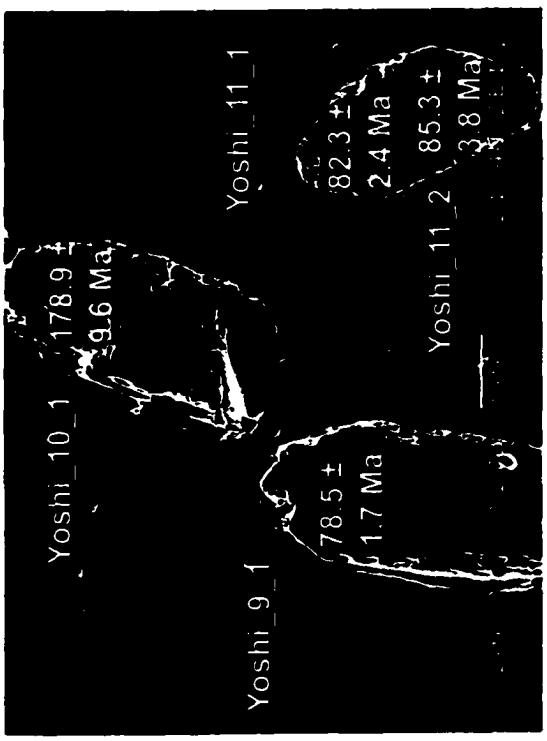

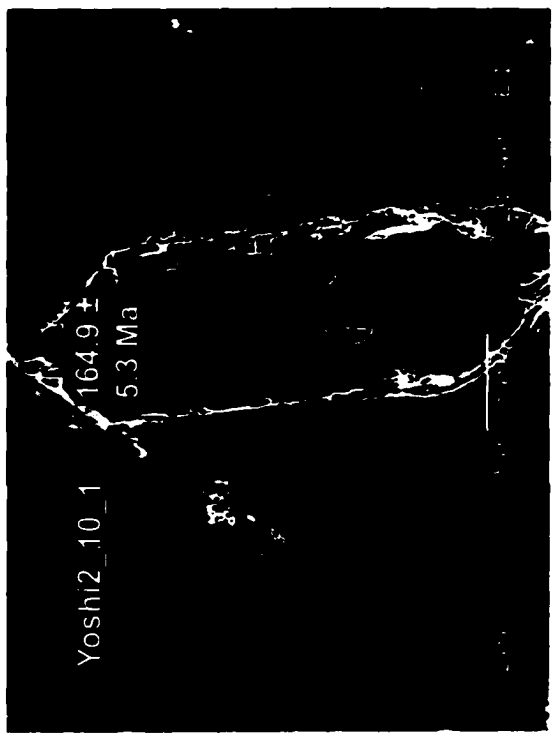

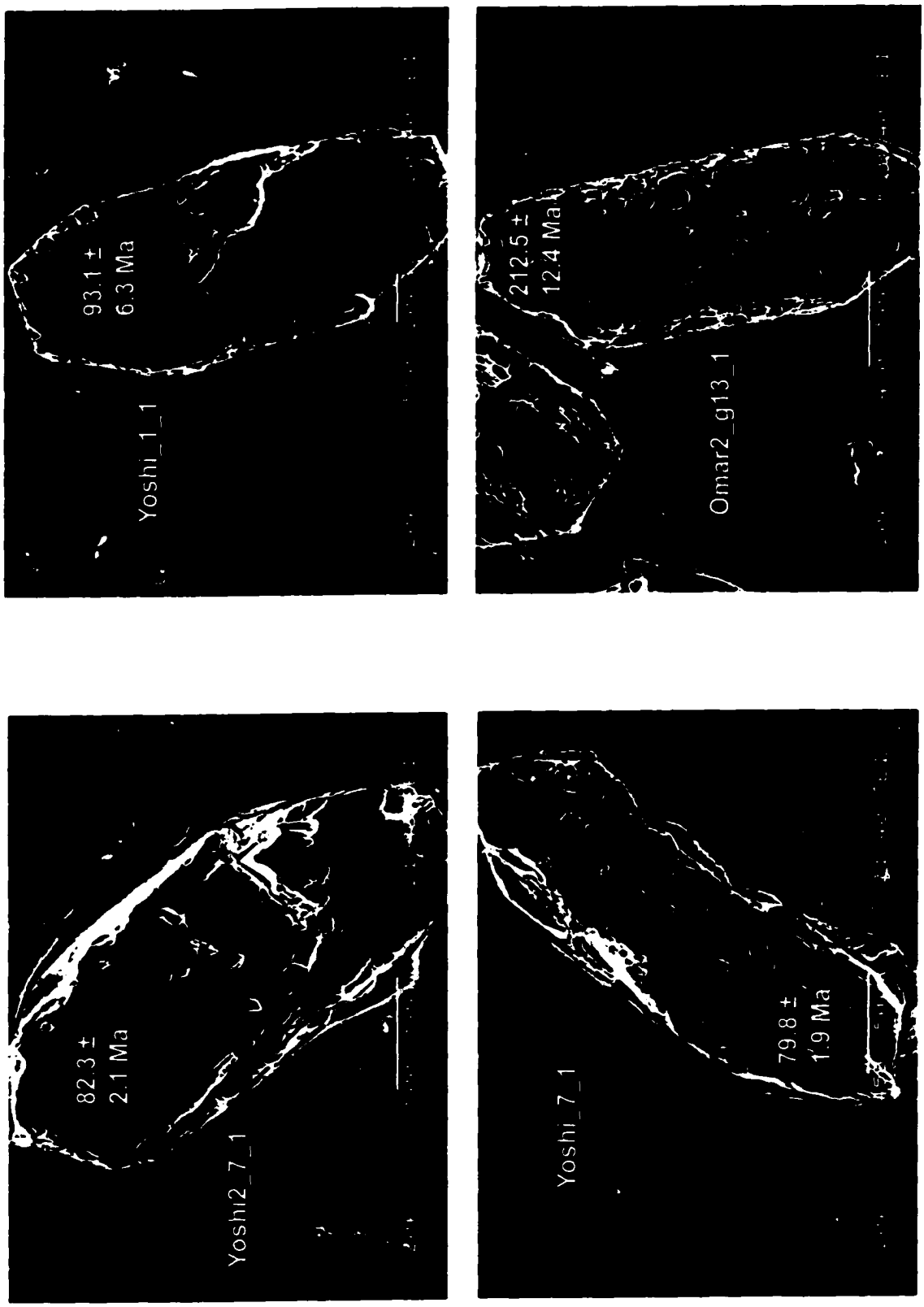

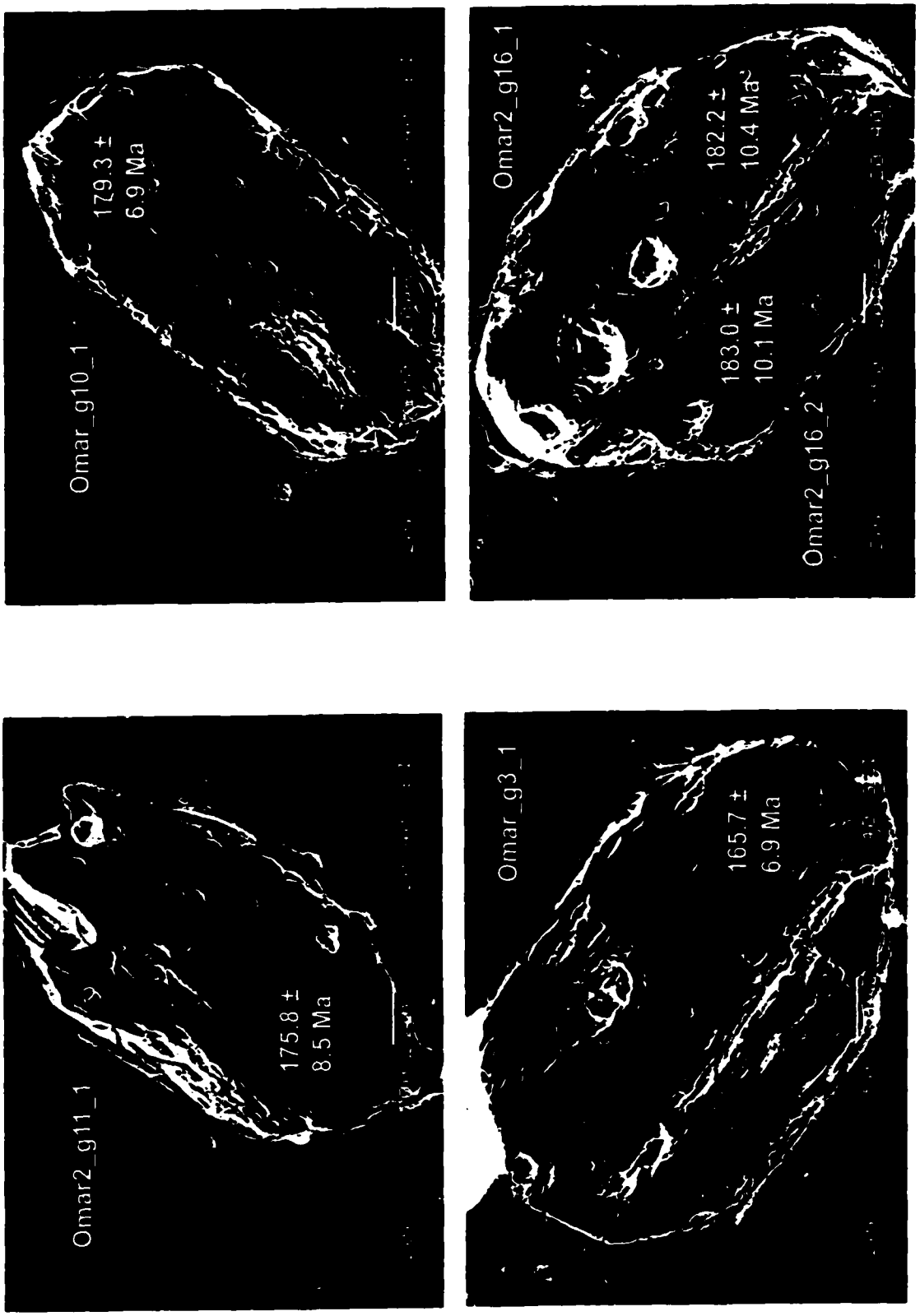

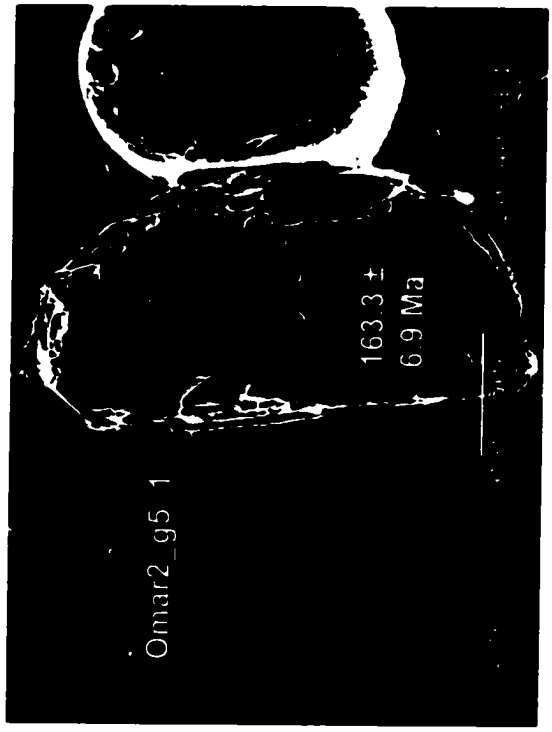

APPENDIX D

$^{40}Ar/^{39}Ar$ isotopic analyses

CALVIN, Hornblende, 15.88 mg, J = 0.001893 ± 0.5%

4 amu discrimination = 1.00398 ± 0.31%, 40/39K = 0.0132 ± 89.00%, 36/37Ca = 0.0002770 ± 2.28%, 39/37Ca = 0.0007435 ± 0.37%

step	T (C)	t (min.)	^{36}Ar	^{37}Ar	^{38}Ar	^{39}Ar	^{40}Ar	$\%^{40}Ar^*$	$\%^{39}Ar$ released	Ca/K	$^{40}Ar^*/^{39}ArK$	Age (Ma)	1s.d.
1	750	12	1.883	1.292	0.417	5.286	673.276	18.1	1.3	1.9325	22.7883	76.19	1.89
2	850	12	0.100	0.758	0.066	3.561	107.062	79.3	0.9	1.6829	22.1387	74.07	0.54
3	950	12	0.136	8.950	0.139	8.965	231.305	87.1	2.1	7.9076	21.7404	72.76	0.54
4	990	12	0.101	8.231	0.124	6.544	168.566	88.4	1.6	9.9689	21.7343	72.74	0.60
5	1010	12	0.084	10.843	0.118	7.705	187.670	92.8	1.8	11.1576	21.7017	72.63	0.54
6	1030	12	0.135	22.132	0.249	14.946	358.795	92.9	3.6	11.7426	21.8868	73.24	0.51
7	1050	12	0.265	76.060	0.718	48.882	1141.248	95.7	11.7	12.3411	22.2882	74.56	0.48
8	1060	12	0.152	55.876	0.559	36.776	844.944	97.5	8.8	12.0495	22.2879	74.55	0.47
9	1075	12	0.121	49.565	0.505	32.813	749.971	98.2	7.8	11.9793	22.2989	74.59	0.49
10	1090	12	0.074	25.915	0.261	16.930	392.470	98.5	4.0	12.1399	22.4500	75.09	0.49
11	1110	12	0.068	15.920	0.166	10.118	238.710	97.0	2.4	12.4800	22.1241	74.02	0.59
12	1135	12	0.166	62.701	0.587	38.881	900.736	97.4	9.3	12.7921	22.4491	75.08	0.49
13	1160	12	0.261	128.730	1.260	81.115	1850.260	98.2	19.4	12.5881	22.3966	74.91	0.48
14	1190	12	0.103	42.085	0.422	26.699	614.315	98.3	6.4	12.5026	22.3984	74.92	0.49
15	1220	12	0.095	39.248	0.389	25.063	576.900	98.5	6.0	12.4206	22.4234	75.00	0.49
16	1400	12	0.189	84.264	0.804	54.078	1237.556	98.3	12.9	12.3587	22.3963	74.91	0.48
								Cumulative $\%^{39}Ar$ rlsd =	100.0		Total gas age =	74.65	0.42
											plateau age =	74.80	0.42
											(steps 7-16)		

note: isotope beams in mV rlsd = released, error in age includes 0.5% J error, all errors 1 sigma

(Not corrected for decay)

FLOYD, Hornblende, 7.80 mg, J = 0.001895 ± 0.5%

4 amu discrimination = 1.01600 ± 0.53%, 40/39K = 0.0132 ± 89.00%, 36/37Ca = 0.0002770 ± 2.28%, 39/37Ca = 0.0007435 ± 0.37%

step	T (C)	t (min.)	^{36}Ar	^{37}Ar	^{38}Ar	^{39}Ar	^{40}Ar	$\%^{40}Ar^*$	$\%^{39}Ar$ released	Ca/K	$^{40}Ar^*/^{39}ArK$	Age (Ma)	1s.d.
1	750	12	0.882	0.312	0.208	2.353	353.383	27.7	1.2	1.7365	41.0324	135.09	4.16
2	850	12	0.125	0.202	0.048	1.167	65.115	47.6	0.6	2.2672	23.9843	80.19	1.13
3	950	12	0.109	2.626	0.077	3.781	118.655	77.9	2.0	9.1157	23.1938	77.60	0.74
4	990	12	0.070	1.849	0.040	2.320	72.485	78.8	1.2	10.4647	22.2751	74.59	0.96
5	1020	12	0.067	3.657	0.049	4.085	118.648	86.0	2.1	11.7593	23.5958	78.92	0.81
6	1050	12	0.344	47.960	0.772	47.686	1169.054	93.7	25.0	13.2168	23.0100	77.00	0.65
7	1070	12	0.140	33.237	0.553	34.113	796.034	97.5	17.9	12.8022	22.7008	75.99	0.63
8	1095	12	0.055	5.988	0.103	6.093	151.581	94.8	3.2	12.9136	22.5983	75.65	0.69
9	1130	12	0.062	8.622	0.133	8.290	202.585	97.2	4.4	13.6694	22.8830	76.58	0.68
10	1155	12	0.148	35.066	0.538	33.487	789.380	97.6	17.6	13.7632	22.9309	76.74	0.64
11	1200	12	0.081	15.126	0.239	15.140	359.770	97.7	8.0	13.1288	22.8155	76.36	0.64
12	1250	12	0.091	19.585	0.333	19.605	462.852	98.0	10.3	13.1275	22.8711	76.54	0.64
13	1400	12	0.065	12.277	0.198	12.288	293.951	98.4	6.5	13.1292	22.9214	76.71	0.65
									Cumulative $\%^{39}Ar$ rlsd =	100.0	Total gas age =	77.35	0.53
											plateau age =	76.46	0.53
											(steps 6-13)		

note: isotope beams in mV rlsd = released, error in age includes 0.5% J error, all errors 1 sigma

(Not corrected for decay)

YOSHI, Hornblende, 15.69 mg, J = 0.001890 ± 0.5%

4 amu discrimination = 1.00398 ± 0.31%, 40/39K = 0.0132 ± 89.00%, 36/37Ca = 0.0002770 ± 2.28%, 39/37Ca = 0.0007435 ± 0.37%

step	T (C)	t (min.)	^{36}Ar	^{37}Ar	^{38}Ar	^{39}Ar	^{40}Ar	$\%^{40}Ar^*$	% ^{39}Ar released	Ca/K	$^{40}Ar^*/^{39}ArK$	Age (Ma)	1s.d.
1	750	12	1.358	1.250	0.452	13.197	815.422	51.6	3.4	0.7562	31.6193	104.71	0.85
2	850	12	0.199	0.972	0.115	6.402	200.716	74.3	1.6	1.2124	22.4037	74.82	0.61
3	950	12	0.161	9.804	0.215	11.784	315.459	88.3	3.0	6.6544	23.0901	77.06	0.60
4	990	12	0.098	8.184	0.154	8.028	212.833	91.3	2.1	8.1574	23.3516	77.92	0.55
5	1010	12	0.113	13.075	0.201	9.658	260.368	91.7	2.5	10.8418	24.0539	80.21	0.55
6	1030	12	0.490	68.983	0.936	42.366	1129.095	89.6	10.8	13.0484	23.8270	79.47	0.52
7	1040	12	0.363	103.906	1.335	62.138	1513.342	95.4	15.9	13.4018	23.2230	77.50	0.50
8	1055	12	0.155	57.916	0.740	35.135	839.202	97.5	9.0	13.2103	23.1743	77.34	0.50
9	1075	12	0.075	24.262	0.309	15.099	361.914	98.2	3.9	12.8762	23.1054	77.11	0.52
10	1110	12	0.072	14.157	0.171	8.618	213.380	95.9	2.2	13.1648	22.8432	76.25	0.56
11	1140	12	0.187	62.432	0.735	34.743	836.237	96.5	8.9	14.4062	23.1002	77.09	0.49
12	1170	12	0.262	107.649	1.293	61.601	1478.828	97.4	15.7	14.0081	23.3568	77.93	0.50
13	1220	12	0.161	64.211	0.793	37.296	895.064	97.7	9.5	13.8000	23.3194	77.81	0.50
14	1400	12	0.199	77.939	0.965	45.404	1085.274	97.7	11.6	13.7590	23.2236	77.50	0.50
							Cumulative $\%^{39}Ar$ rlsd =		100.0		Total gas age =	78.65	0.43
											plateau age =	77.38	0.11

note: isotope beams in mV rlsd = released, error in age includes 0.5% J error, all errors 1 sigma

(Not corrected for decay)

(steps 7-14)

OMAR, Hornblende, 12.92 mg, J = 0.001889 ± 0.5%

4 amu discrimination = 1.01600 ± 0.53%, 40/39K = 0.0132 ± 89.00%, 36/37Ca = 0.0002770 ± 2.28%, 39/37Ca = 0.0007435 ± 0.37%

step	T (C)	t (min.)	^{36}Ar	^{37}Ar	^{38}Ar	^{39}Ar	^{40}Ar	$\%^{40}Ar^*$	$\%\ ^{39}Ar$ released	Ca/K	$^{40}Ar^*/^{39}ArK$	Age (Ma)	1s.d.
1	750	12	4.029	2.537	1.099	13.107	2764.750	57.8	10.2	2.5879	122.1119	374.45	3.90
2	850	12	0.469	1.972	0.260	8.965	598.641	78.1	7.0	2.9413	51.7750	168.34	1.54
3	950	12	1.745	29.879	0.816	19.197	2320.807	78.9	14.9	20.9244	96.0889	300.91	2.62
4	990	12	0.838	44.054	0.736	19.508	1738.383	87.4	15.1	30.4457	78.6381	249.86	2.10
5	1020	12	0.414	29.504	0.571	16.498	1133.393	91.0	12.8	24.0645	62.8482	202.39	1.67
6	1040	12	0.226	16.717	0.347	10.781	668.206	92.1	8.4	20.8453	57.0525	184.65	1.53
7	1060	12	0.157	9.913	0.195	7.023	426.463	91.6	5.4	18.9648	55.2091	178.97	1.49
8	1085	12	0.142	7.296	0.149	4.908	323.840	89.8	3.8	19.9791	58.5683	189.31	1.60
9	1130	12	0.233	13.776	0.232	7.261	543.214	90.2	5.6	25.5414	67.1047	215.31	1.81
10	1155	12	0.172	9.626	0.156	4.359	352.439	89.3	3.4	29.7663	71.2746	227.88	1.89
11	1200	12	0.193	15.372	0.162	3.527	410.372	90.0	2.7	59.2644	104.7411	325.70	3.11
12	1250	12	0.284	30.279	0.261	4.787	634.079	90.5	3.7	86.7072	121.8692	373.78	3.01
13	1400	12	1.072	202.749	0.856	9.041	2456.198	91.5	7.0	329.2724	275.5216	755.93	5.58
							Cumulative %39Ar rlsd =		100.0		Total gas age =	286.23	1.42

note: isotope beams in mV, rlsd = released, error in age includes 0.5% J error, all errors 1 sigma — no plateau

(Not corrected for decay)

CALVIN, K-feldspar, 15.93 mg, J = 0.001878 ± 0.5%

4 amu discrimination = 1.02246 ± 0.12%, 40/39K = 0.0132 ± 89.00%, 36/37Ca = 0.0002770 ± 2.28%, 39/37Ca = 0.0007435 ± 0.37%

step	T (C)	t (min.)	^{36}Ar	^{37}Ar	^{38}Ar	^{39}Ar	^{40}Ar	$\%^{40}Ar^*$	% ^{39}Ar released	Ca/K	$^{40}Ar^*/^{39}ArK$	Age (Ma)	1s.d.
1	448	18	6.877	0.069	1.387	7.098	2214.550	10.3	0.1	0.354684	32.2826	106.19	2.15
2	473	18	0.861	0.048	0.206	4.842	341.777	28.3	0.1	0.361698	19.4773	64.81	0.45
3	473	43	0.595	0.056	0.172	5.286	273.258	41.9	0.1	0.386539	19.2222	63.98	0.90
4	514	18	0.306	0.052	0.412	6.228	215.358	62.4	0.1	0.304633	20.6154	68.53	0.41
5	514	43	0.296	0.060	0.179	9.578	275.220	77.9	0.2	0.228554	19.8755	66.11	0.53
6	555	18	0.378	0.073	0.234	12.866	380.689	73.6	0.2	0.207009	21.2568	70.62	0.39
7	555	43	0.244	0.095	0.281	19.556	470.399	91.1	0.4	0.177235	20.5271	68.24	0.38
8	596	18	0.383	0.103	0.352	23.494	606.234	83.3	0.5	0.15995	21.1976	70.43	0.38
9	596	43	0.236	0.139	0.498	34.625	792.137	95.2	0.7	0.146462	20.9767	69.71	0.37
10	638	18	0.436	0.147	0.544	36.669	900.314	87.1	0.7	0.146258	21.2136	70.48	0.37
11	638	43	0.182	0.175	0.661	49.921	1094.120	98.0	1.0	0.127895	20.9362	69.57	0.37
12	679	19	0.324	0.174	0.648	49.262	1127.040	92.6	0.9	0.128865	21.0712	70.01	0.37
13	679	44	0.168	0.210	0.892	69.717	1501.860	98.8	1.3	0.109895	20.9208	69.52	0.36
14	720	19	0.319	0.192	0.865	66.302	1484.470	94.5	1.3	0.10565	21.0890	70.07	0.38
15	720	44	0.147	0.194	1.155	91.837	1962.970	99.4	1.8	0.077068	20.9877	69.74	0.38
16	761	19	0.177	0.165	0.971	76.128	1651.510	97.5	1.5	0.079074	21.1104	70.14	0.37
17	761	44	0.175	0.188	1.367	106.031	2261.630	99.1	2.0	0.064687	21.2344	70.55	0.40
18	802	19	0.201	0.139	1.042	84.077	1835.450	97.5	1.6	0.060315	21.2206	70.50	0.39
19	843	19	0.274	0.187	1.681	132.995	2871.070	97.7	2.6	0.051297	21.0724	70.02	0.37
20	884	19	0.302	0.205	2.238	180.818	3897.630	98.1	3.5	0.041362	21.1531	70.28	0.37
21	910	19	0.249	0.148	1.821	152.036	3279.350	98.2	2.9	0.035514	21.1761	70.36	0.37

CALVIN, K-feldspar (continued)									% ^{39}Ar				
step	T (C)	t (min.)	^{36}Ar	^{37}Ar	^{38}Ar	^{39}Ar	^{40}Ar	%^{40}Ar*	released	Ca/K	^{40}Ar*/^{39}ArK	Age (Ma)	1s.d.
22	935	19	0.298	0.138	1.906	152.060	3283.380	97.7	2.9	0.033109	21.1058	70.13	0.37
23	961	19	0.286	0.108	1.792	141.862	3081.610	97.7	2.7	0.027774	21.2197	70.50	0.37
24	976	19	0.222	0.089	1.473	116.033	2504.090	98.1	2.2	0.027983	21.0945	70.09	0.37
25	1002	19	0.304	0.097	1.496	116.223	2533.220	97.1	2.2	0.030448	21.1068	70.13	0.37
26	1018	19	0.316	0.099	1.387	107.313	2354.240	96.8	2.1	0.033657	21.1528	70.28	0.37
27	1033	19	0.377	0.099	1.302	100.666	2234.100	95.8	1.9	0.035879	21.1758	70.36	0.37
28	1048	19	0.433	0.104	1.292	98.532	2207.180	95.0	1.9	0.038507	21.1951	70.42	0.37
29	1064	19	0.551	0.131	1.343	99.269	2256.300	93.6	1.9	0.048144	21.1899	70.40	0.37
30	1074	19	0.520	0.134	1.233	92.215	2101.620	93.6	1.8	0.053014	21.2249	70.52	0.38
31	1084	19	0.548	0.141	1.200	89.703	2059.330	93.0	1.7	0.057346	21.2556	70.62	0.37
32	1089	19	0.606	0.168	1.364	99.404	2291.964	93.1	1.9	0.061659	21.3508	70.93	0.37
33	1089	24	0.584	0.163	1.266	94.991	2193.089	93.4	1.8	0.062603	21.3812	71.02	0.37
34	1089	39	0.690	0.188	1.397	104.151	2420.168	93.0	2.0	0.065854	21.3962	71.07	0.37
35	1089	59	0.864	0.221	1.712	125.838	2929.060	93.1	2.4	0.064072	21.3701	70.99	0.37
36	1089	74	0.954	0.221	1.714	125.224	2952.045	92.6	2.4	0.064387	21.4413	71.22	0.39
37	1089	74	0.781	0.187	1.423	101.459	2388.133	93.0	2.0	0.067242	21.3781	71.01	0.37
38	1089	74	0.700	0.161	1.199	86.213	2041.971	92.9	1.7	0.068131	21.4002	71.09	0.37
39	1089	74	0.632	0.159	1.021	75.236	1794.045	93.1	1.5	0.077102	21.4766	71.34	0.38
40	1089	89	0.689	0.149	1.083	78.729	1881.015	93.2	1.5	0.069047	21.4441	71.23	0.38
41	1089	119	0.804	0.160	1.286	91.153	2178.712	93.6	1.8	0.064038	21.4079	71.11	0.37
42	1089	149	0.896	0.174	1.385	97.294	2341.322	94.0	1.9	0.065246	21.4656	71.30	0.37
43	1141	19	0.545	0.118	0.797	54.927	1333.565	89.9	1.1	0.078377	21.5064	71.43	0.38
44	1200	15	1.364	0.239	2.092	150.429	3625.377	89.7	2.9	0.057964	21.5777	71.66	0.38

CALVIN, K-feldspar (continued)

step	T (C)	t (min.)	^{36}Ar	^{37}Ar	^{38}Ar	^{39}Ar	^{40}Ar	%^{40}Ar*	% ^{39}Ar released	Ca/K	^{40}Ar*/^{39}ArK	Age (Ma)	1s.d.
45	1230	15	2.162	0.348	3.687	267.872	6363.617	90.5	5.2	0.047396	21.5153	71.46	0.38
46	1300	15	4.127	0.468	9.853	734.625	17094.800	93.1	14.2	0.023242	21.7337	72.17	0.40
47	1350	15	2.954	0.293	5.774	433.725	10188.000	91.9	8.4	0.024646	21.6102	71.77	0.38
48	1400	15	0.670	0.069	1.015	75.094	1815.208	91.2	1.4	0.033522	21.7073	72.09	0.38
49	1500	15	0.616	0.089	0.804	57.505	1432.718	89.9	1.1	0.056464	21.9433	72.85	0.40
							Cumulative %^{39}Ar rlsd =		100.0		Total gas age =	71.01	0.35

note: isotope beams in mV, rlsd = released, error in age includes 0.5% J error, all errors 1 sigma

(Not corrected for decay)

FLOYD, K-feldspar, 13.62 mg, J = 0.001856 ± 0.5%

4 amu discrimination = 1.02246 ± 0.12%, 40/39K = 0.0132 ± 89.00%, 36/37Ca = 0.0002770 ± 2.28%, 39/37Ca = 0.0007435 ± 0.37%

step	T (C)	t (min.)	^{36}Ar	^{37}Ar	^{38}Ar	^{39}Ar	^{40}Ar	%^{40}Ar*	% ^{39}Ar released	Ca/K	^{40}Ar*/^{39}ArK	Age (Ma)	1s.d.
1	448	18	2.742	0.038	0.676	12.218	1156.330	31.8	0.2	0.127148	29.9911	97.73	0.65
2	473	18	0.291	0.040	0.205	11.627	315.328	76.1	0.2	0.140644	20.0491	65.91	0.37
3	473	43	0.210	0.033	0.199	14.199	338.119	90.5	0.3	0.095012	19.6070	64.49	0.36
4	514	18	0.131	0.039	0.223	17.054	382.175	92.9	0.3	0.093489	20.3227	66.80	0.38
5	514	43	0.144	0.043	0.314	23.267	509.337	97.9	0.4	0.075552	20.1758	66.32	0.35
6	555	18	0.108	0.045	0.363	28.290	618.666	96.7	0.5	0.065028	20.8784	68.59	0.36
7	555	43	0.112	0.039	0.506	39.958	852.365	99.9	0.7	0.0399	20.5971	67.68	0.35
8	596	18	0.101	0.060	0.510	40.477	865.983	97.9	0.7	0.060598	20.7642	68.22	0.36

FLOYD, K-feldspar (continued)

step	T (C)	t (min.)	^{36}Ar	^{37}Ar	^{38}Ar	^{39}Ar	^{40}Ar	$\%^{40}Ar^*$	% ^{39}Ar released	Ca/K	$^{40}Ar^*/^{39}ArK$	Age (Ma)	1s.d.
9	596	43	0.094	0.052	0.645	50.127	1060.250	99.8	0.9	0.042408	20.5608	67.56	0.36
10	638	18	0.091	0.047	0.629	50.721	1073.642	98.6	0.9	0.037881	20.7366	68.13	0.36
11	638	43	0.091	0.068	0.952	73.989	1564.500	99.9	1.4	0.037571	20.7825	68.28	0.37
12	679	19	0.090	0.378	0.878	67.142	1420.196	98.9	1.2	0.230164	20.8585	68.52	0.41
13	679	44	0.100	0.072	1.124	91.434	1930.490	99.9	1.7	0.032191	20.8381	68.46	0.36
14	720	19	0.088	0.085	0.971	78.508	1661.450	99.1	1.4	0.044261	20.9240	68.74	0.36
15	720	44	0.103	0.079	1.314	106.499	2242.850	99.9	1.9	0.030325	20.8263	68.42	0.36
16	761	19	0.064	0.070	1.020	82.490	1745.780	99.5	1.5	0.034691	21.0242	69.06	0.36
17	761	44	0.014	0.065	1.436	113.952	2413.760	99.9	2.1	0.023319	20.9668	68.87	0.36
18	802	19	0.074	0.059	1.060	84.524	1795.830	99.6	1.5	0.028536	21.0714	69.21	0.37
19	843	19	0.088	0.069	1.616	129.512	2743.940	99.5	2.4	0.02178	21.0686	69.20	0.36
20	884	19	0.104	0.076	1.976	160.823	3410.660	99.5	2.9	0.019319	21.0990	69.30	0.36
21	910	19	0.106	0.065	1.767	143.126	3047.210	99.4	2.6	0.018566	21.1549	69.48	0.37
22	935	19	0.121	0.060	1.572	128.829	2751.720	99.2	2.4	0.019039	21.1663	69.52	0.36
23	961	19	0.124	0.050	1.545	125.393	2693.620	99.2	2.3	0.016301	21.2626	69.83	0.36
24	976	19	0.115	0.042	1.343	108.429	2335.960	99.3	2.0	0.015835	21.3023	69.95	0.37
25	1002	19	0.157	0.048	1.460	116.769	2529.190	98.8	2.1	0.016805	21.3374	70.07	0.37
26	1018	19	0.155	0.053	1.331	108.309	2356.540	98.8	2.0	0.020004	21.4097	70.30	0.37
27	1033	19	0.178	0.055	1.352	104.722	2287.480	98.4	1.9	0.02147	21.4175	70.33	0.37
28	1048	19	0.201	0.049	1.328	105.548	2321.300	98.2	1.9	0.018978	21.5082	70.62	0.37
29	1064	19	0.206	0.055	1.371	108.457	2382.300	98.2	2.0	0.020731	21.4824	70.53	0.37
30	1074	19	0.191	0.058	1.285	102.177	2256.530	98.2	1.9	0.023205	21.6101	70.95	0.37
31	1084	19	0.198	0.043	1.275	99.432	2193.958	98.1	1.8	0.017679	21.5545	70.77	0.37

FLOYD, K-feldspar (continued)

step	T (C)	t (min.)	^{36}Ar	^{37}Ar	^{38}Ar	^{39}Ar	^{40}Ar	$\%^{40}Ar^*$	% ^{39}Ar released	Ca/K	$^{40}Ar^*/^{39}ArK$	Age (Ma)	1s.d.
32	1089	24	0.201	0.061	1.385	109.280	2412.900	98.4	2.0	0.022819	21.6026	70.92	0.40
33	1089	29	0.059	0.059	1.317	103.158	2283.080	100.0	1.9	0.023381	21.9519	72.05	0.38
34	1089	39	0.211	0.062	1.387	109.274	2427.860	98.8	2.0	0.023195	21.7306	71.33	0.37
35	1089	59	0.282	0.068	1.646	128.420	2836.090	98.9	2.3	0.021647	21.5237	70.67	0.39
36	1089	74	0.283	0.057	1.566	124.630	2783.083	99.3	2.3	0.018697	21.7393	71.36	0.47
37	1089	74	0.251	0.053	1.282	99.637	2236.660	99.5	1.8	0.021745	21.7812	71.50	0.38
38	1089	74	0.239	0.046	1.047	82.986	1869.570	99.6	1.5	0.02266	21.7533	71.41	0.38
39	1089	74	0.222	0.052	0.907	70.204	1591.480	99.9	1.3	0.03028	21.8086	71.58	0.37
40	1089	89	0.242	0.043	0.934	71.915	1639.800	99.9	1.3	0.024443	21.7859	71.51	0.38
41	1089	119	0.308	0.050	1.012	75.944	1738.160	100.0	1.4	0.026915	21.6082	70.94	0.37
42	1089	149	0.324	0.046	0.832	62.430	1452.920	99.9	1.1	0.030122	21.2616	69.82	0.37
43	1141	19	0.094	0.037	0.292	23.107	532.193	99.7	0.4	0.06546	21.9624	72.08	0.39
44	1200	15	0.203	0.047	0.847	64.781	1481.220	97.5	1.2	0.02966	22.0712	72.43	0.39
45	1230	15	0.310	0.061	1.487	116.492	2640.220	97.4	2.1	0.021407	21.9935	72.18	0.38
46	1255	15	0.429	0.070	2.300	182.490	4122.040	97.5	3.3	0.015681	22.0007	72.20	0.38
47	1300	15	1.096	0.173	6.046	473.033	10678.400	97.2	8.6	0.014951	21.9904	72.17	0.38
48	1350	15	1.749	0.199	10.019	798.279	17922.400	97.3	14.6	0.010191	21.9021	71.89	0.37
49	1400	15	0.757	0.085	2.877	225.637	5176.350	96.4	4.1	0.0154	22.0631	72.40	0.40
50	1500	15	0.257	0.046	0.371	27.385	683.157	94.3	0.5	0.06867	22.3987	73.48	0.38
									Cumulative $\%^{39}Ar$ rlsd =	100.00	Total gas age =	70.73	0.35

note: isotope beams in mV, rlsd = released, error in age includes 0.5% J error, all errors 1 sigma

(Not corrected for decay)

YOSHI, K-feldspar, 9.97 mg, J = 0.001864 ± 0.5%

4 amu discrimination = 1.02246 ± 0.12%, 40/39K = 0.0132 ± 89.00%, 36/37Ca = 0.0002770 ± 2.28%, 39/37Ca = 0.0007435 ± 0.37%

step	T (C)	t (min.)	^{36}Ar	^{37}Ar	^{38}Ar	^{39}Ar	^{40}Ar	$\%^{40}Ar^*$	$\%\ ^{39}Ar$ released	Ca/K	$^{40}Ar^*/^{39}ArK$	Age (Ma)	1s.d.
1	448	18	1.866	0.050	0.457	6.704	1007.260	47.0	0.2	0.293129	70.2891	222.12	1.37
2	473	18	0.276	0.046	0.098	4.353	171.470	57.5	0.1	0.415343	21.3757	70.49	0.43
3	473	43	0.244	0.043	0.111	5.273	174.845	72.8	0.1	0.320506	19.8527	65.56	0.49
4	514	18	0.136	0.046	0.109	6.447	171.102	82.6	0.2	0.280428	20.6760	68.22	0.42
5	514	43	0.143	0.048	0.133	8.404	209.236	94.6	0.2	0.224475	20.0525	66.20	0.39
6	555	18	0.105	0.050	0.144	10.306	241.910	91.8	0.3	0.190673	20.7038	68.31	0.40
7	555	43	0.106	0.056	0.198	14.329	322.542	99.9	0.4	0.153595	20.3651	67.22	0.40
8	596	18	0.141	0.069	0.224	16.301	378.741	92.0	0.4	0.166357	20.8481	68.78	0.37
9	596	43	0.108	0.089	0.316	23.426	512.730	99.5	0.6	0.149312	20.4923	67.63	0.36
10	638	18	0.116	0.091	0.308	24.054	529.157	95.7	0.6	0.148682	20.7094	68.33	0.39
11	638	43	0.112	0.112	0.523	39.900	853.795	99.9	1.0	0.110317	20.6557	68.16	0.36
12	679	19	0.121	0.110	0.487	37.963	814.164	97.0	1.0	0.113876	20.6195	68.04	0.36
13	679	44	0.109	0.105	0.743	56.513	1193.100	100.0	1.4	0.073019	20.6251	68.06	0.36
14	720	19	0.146	0.091	0.670	53.289	1149.860	97.3	1.4	0.067111	20.8756	68.87	0.37
15	720	44	0.098	0.084	0.975	76.571	1608.320	100.0	2.0	0.043113	20.6683	68.20	0.36
16	761	19	0.074	0.079	0.803	64.644	1363.540	99.2	1.7	0.048027	20.8493	68.78	0.36
17	761	44	0.102	0.082	1.220	95.943	2027.970	99.9	2.5	0.033588	20.8734	68.86	0.37
18	802	19	0.073	0.073	0.908	74.830	1579.590	99.5	1.9	0.038339	20.9052	68.97	0.36
19	843	19	0.116	0.084	1.482	118.770	2516.010	99.2	3.0	0.027795	20.9797	69.21	0.39
20	884	19	0.129	0.095	1.891	154.473	3287.630	99.2	4.0	0.024169	21.1203	69.66	0.37
21	910	19	0.138	0.075	1.751	139.330	2970.120	99.1	3.6	0.021155	21.1095	69.63	0.37

YOSHI, K-feldspar (continued)									% ^{39}Ar				
step	T (C)	t (min.)	^{36}Ar	^{37}Ar	^{38}Ar	^{39}Ar	^{40}Ar	%^{40}Ar*	released	Ca/K	^{40}Ar*/^{39}ArK	Age (Ma)	1s.d.
22	935	19	0.138	0.066	1.636	129.065	2751.920	99.0	3.3	0.020097	21.0913	69.57	0.37
23	961	19	0.152	0.063	1.509	121.461	2601.700	98.9	3.1	0.020384	21.1246	69.68	0.36
24	976	19	0.159	0.052	1.230	98.755	2134.590	98.6	2.5	0.020693	21.2137	69.96	0.37
25	1002	19	0.215	0.068	1.331	102.013	227.960	97.9	2.6	0.026196	21.2956	70.23	0.38
26	1018	19	0.234	0.062	1.143	89.052	1981.020	97.4	2.3	0.027361	21.5501	71.05	0.45
27	1033	19	0.250	0.060	1.041	80.014	1784.760	96.8	2.1	0.02947	21.4641	70.77	0.37
28	1048	19	0.294	0.071	0.997	75.784	1708.750	95.9	1.9	0.036819	21.4873	70.85	0.38
29	1064	19	0.308	0.074	0.974	72.306	1653.200	95.6	1.9	0.04022	21.6936	71.52	0.38
30	1074	19	0.283	0.073	0.845	64.732	1479.150	95.5	1.7	0.044319	21.6451	71.36	0.38
31	1084	19	0.274	0.080	0.751	58.928	1366.250	95.4	1.5	0.053353	21.8985	72.18	0.38
32	1089	24	0.279	0.086	0.860	92.679	1454.060	95.7	2.4	0.036467	21.9496	72.34	0.40
33	1089	29	0.266	0.078	0.759	58.264	1354.300	96.1	1.5	0.052612	21.9852	72.46	0.38
34	1089	39	0.286	0.076	0.784	60.488	1424.030	96.5	1.6	0.049378	22.2409	73.28	0.38
35	1089	59	0.378	0.077	0.943	70.467	1665.230	96.4	1.8	0.042943	22.1530	73.00	0.38
36	1089	74	0.398	0.075	0.901	67.948	1624.030	96.6	1.7	0.043378	22.2629	73.35	0.38
37	1089	74	0.348	0.063	0.750	54.477	1320.060	97.0	1.4	0.045448	22.4333	73.90	0.39
38	1089	74	0.316	0.057	0.651	46.277	1128.320	97.3	1.2	0.048406	22.4500	73.96	0.39
39	1089	74	0.305	0.057	0.563	40.135	986.730	97.3	1.0	0.055814	22.4240	73.87	0.39
40	1089	89	0.341	0.051	0.579	42.348	1044.390	97.8	1.1	0.047329	22.4122	73.84	0.40
41	1089	119	0.452	0.061	0.681	48.471	1215.610	97.3	1.2	0.049458	22.4134	73.84	0.39
42	1089	149	0.504	0.059	0.745	52.051	1312.270	98.4	1.3	0.044546	22.4559	73.98	0.40
43	1141	19	0.203	0.047	0.333	25.014	629.353	94.5	0.6	0.073843	22.9245	75.49	0.39
44	1200	15	0.512	0.066	0.849	60.754	1538.310	91.7	1.6	0.042693	23.0030	75.74	0.40

YOSHI, K-feldspar (continued)

step	T (C)	t (min.)	^{36}Ar	^{37}Ar	^{38}Ar	^{39}Ar	^{40}Ar	$\%^{40}Ar^*$	% ^{39}Ar released	Ca/K	$^{40}Ar^*/^{39}ArK$	Age (Ma)	1s.d.
45	1230	15	0.727	0.083	1.282	91.835	2307.840	91.8	2.4	0.035519	22.9497	75.57	0.40
46	1255	15	1.100	0.092	1.864	134.325	3372.250	91.1	3.4	0.026916	22.8383	75.21	0.40
47	1300	15	2.772	0.092	4.686	339.076	8500.180	90.8	8.7	0.010663	22.7962	75.08	0.39
48	1350	15	4.990	0.148	7.665	552.638	13912.700	89.8	14.2	0.010525	22.6533	74.61	0.39
49	1400	15	1.248	0.048	1.646	112.544	2905.240	88.7	2.9	0.016761	22.7131	74.81	0.43
50	1500	15	0.436	0.040	0.351	23.734	658.448	85.7	0.6	0.066234	22.6108	74.48	0.42
								Cumulative $\%^{39}Ar$ rlsd =	100.0		Total gas age =	72.32	0.36

note: isotope beams in mV, rlsd = released, error in age includes 0.5% J error, all errors 1 sigma

(Not corrected for decay)

OMAR, K-feldspar, 16.38 mg, J = 0.001883 ± 0.5%

4 amu discrimination = 1.02242 ± 0.14%, 40/39K = 0.0132 ± 89.00%, 36/37Ca = 0.0002770 ± 2.28%, 39/37Ca = 0.0007435 ± 0.37%

step	T (C)	t (min.)	^{36}Ar	^{37}Ar	^{38}Ar	^{39}Ar	^{40}Ar	$\%^{40}Ar^*$	% ^{39}Ar released	Ca/K	$^{40}Ar^*/^{39}ArK$	Age (Ma)	1s.d.
1	448	13	3.080	0.060	0.372	7.014	1546.790	42.8	0.1	0.298923	94.2133	294.63	1.81
2	473	13	0.431	0.052	0.155	5.315	301.540	61.2	0.1	0.341884	33.7482	111.15	0.67
3	473	43	0.410	0.055	0.165	7.363	300.398	69.3	0.1	0.261021	24.9789	82.92	0.49
4	514	13	0.248	0.053	0.148	7.865	520.675	88.2	0.1	0.235474	57.5448	185.60	0.97
5	514	43	0.260	0.066	0.211	12.456	376.318	88.9	0.2	0.18515	24.3803	80.98	0.49
6	555	13	0.379	0.078	0.291	15.793	1525.760	93.5	0.3	0.172579	90.1668	282.91	1.50
7	555	43	0.239	0.085	0.285	20.089	631.278	94.7	0.4	0.147848	28.1641	93.23	0.49
8	596	13	0.359	0.076	0.348	20.500	1626.540	94.4	0.4	0.129542	74.6283	237.22	1.21

OMAR, K-feldspar (continued)									% ^{39}Ar				
step	T (C)	t (min.)	^{36}Ar	^{37}Ar	^{38}Ar	^{39}Ar	^{40}Ar	%^{40}Ar*	released	Ca/K	^{40}Ar*/^{39}ArK	Age (Ma)	1s.d.
9	596	43	0.186	0.107	0.361	25.596	736.389	98.1	0.5	0.146071	26.7682	88.72	0.48
10	638	13	0.342	0.103	0.428	25.980	1603.320	94.7	0.5	0.138532	58.1716	187.52	0.96
11	638	43	0.165	0.111	0.418	33.268	860.469	99.1	0.6	0.116586	24.5210	81.43	0.45
12	679	14	0.174	0.097	0.357	25.661	926.131	96.0	0.5	0.132084	34.2801	112.85	0.59
13	679	44	0.148	0.102	0.502	39.289	949.534	99.7	0.7	0.090714	23.1631	77.02	0.42
14	720	14	0.154	0.089	0.387	29.038	891.621	96.5	0.5	0.107096	29.2961	96.87	0.52
15	720	44	0.125	0.104	0.587	45.462	1067.400	99.9	0.8	0.079934	22.6647	75.40	0.40
16	761	14	0.092	0.084	0.341	27.655	690.907	98.2	0.5	0.106134	24.1208	80.13	0.43
17	761	44	0.140	0.114	0.573	45.393	1054.700	99.5	0.8	0.087753	22.3222	74.28	0.40
18	802	14	0.089	0.089	0.387	29.181	698.700	98.3	0.5	0.106571	23.1569	77.00	0.41
19	843	14	0.154	0.145	0.685	53.019	1293.970	97.6	1.0	0.095562	23.6616	78.64	0.42
20	884	14	0.205	0.182	0.873	69.342	1708.640	97.3	1.3	0.091711	23.8821	79.36	0.42
21	910	14	0.193	0.169	0.845	66.093	1650.780	97.4	1.2	0.089346	24.2301	80.49	0.43
22	935	14	0.201	0.161	0.881	67.243	1795.500	97.5	1.2	0.083661	25.9426	86.04	0.46
23	961	14	0.268	0.174	1.032	76.625	2272.210	97.2	1.4	0.079346	28.7599	95.15	0.50
24	976	14	0.251	0.157	0.976	73.538	2313.050	97.6	1.3	0.074599	30.5738	100.98	0.53
25	1002	14	0.399	0.194	1.380	105.708	3736.140	97.3	1.9	0.064126	34.3807	113.17	0.60
26	1018	14	0.432	0.199	1.602	120.804	4438.120	97.5	2.2	0.057559	35.8400	117.82	0.62
27	1033	14	0.508	0.215	1.951	150.480	5771.320	97.7	2.7	0.049923	37.5215	123.16	0.66
28	1048	14	0.590	0.239	2.438	184.109	7149.110	97.8	3.4	0.045359	38.0528	124.85	0.65
29	1064	14	0.679	0.273	2.947	222.607	8747.400	97.9	4.1	0.042851	38.5650	126.47	0.66
30	1074	14	0.643	0.260	2.993	227.374	8897.680	98.1	4.1	0.039955	38.4659	126.16	0.66
31	1084	14	0.625	0.335	3.016	232.022	9104.980	98.2	4.2	0.050449	38.6127	126.62	0.66

OMAR, K-feldspar (continued)

step	T (C)	t (min.)	^{36}Ar	^{37}Ar	^{38}Ar	^{39}Ar	^{40}Ar	$\%^{40}Ar^*$	$\%\ ^{39}Ar$ released	Ca/K	$^{40}Ar^*/^{39}ArK$	Age (Ma)	1s.d.
32	1089	19	0.656	0.329	3.510	269.783	10562.000	98.4	4.9	0.042611	38.6026	126.59	0.66
33	1089	24	0.574	0.307	3.059	234.161	8908.460	98.4	4.3	0.04581	37.4796	123.03	0.64
34	1089	39	0.622	0.341	3.459	269.908	10138.000	98.6	4.9	0.044145	37.0499	121.67	0.64
35	1089	59	0.670	0.366	3.615	275.761	10318.000	98.6	5.0	0.046375	36.8682	121.09	0.63
36	1089	74	0.628	0.312	3.158	238.350	8991.780	98.7	4.3	0.045738	37.1097	121.86	0.64
37	1089	74	0.475	0.209	2.356	179.778	6807.200	99.0	3.3	0.040621	37.2445	122.28	0.64
38	1089	74	0.408	0.166	1.828	138.463	5275.640	99.0	2.5	0.04189	37.3910	122.75	0.64
39	1089	74	0.379	0.143	1.505	111.638	4292.740	99.0	2.0	0.044757	37.6097	123.44	0.65
40	1089	89	0.402	0.135	1.483	110.153	4256.330	99.2	2.0	0.042823	37.7355	123.84	0.65
41	1089	119	0.470	0.151	1.585	119.068	4629.850	99.4	2.2	0.044312	37.8916	124.34	0.65
42	1089	149	0.532	0.141	1.597	117.061	4593.150	99.6	2.1	0.042087	38.0641	124.88	0.65
43	1141	19	0.230	0.128	1.082	81.833	3397.950	98.9	1.5	0.054654	40.9159	133.90	0.70
44	1200	15	0.667	0.420	4.155	314.621	12895.600	98.7	5.7	0.046645	40.9159	133.90	0.70
45	1250	15	0.923	0.738	8.051	637.705	23425.600	98.9	11.6	0.040437	36.4695	119.82	0.62
46	1300	15	0.390	0.321	2.827	220.442	7999.920	98.9	4.0	0.050881	35.9396	118.14	0.63
47	1350	15	0.177	0.128	0.587	45.295	1698.690	99.3	0.8	0.098743	36.5818	120.18	0.63
48	1400	15	0.163	0.089	0.365	28.153	1118.520	99.4	0.5	0.110462	38.3065	125.65	0.68
49	1500	15	0.327	0.085	0.379	24.729	1017.680	94.5	0.5	0.120105	37.5902	123.38	0.69
									Cumulative $\%^{39}Ar$ rlsd =	100.0	Total gas age =	119.85	0.55

note: isotope beams in mV, rlsd = released, error in age includes 0.5% J error, all errors 1 sigma

(Not corrected for decay)

APPENDIX E

U-Th/He apatite chemical analyses

U/Th-He Apatite Data - California Institute of Technology

Sample	Raw Age (Ma)	Corrected Age (Ma)	U (ppm)	Th (ppm)	He (nmol/g)	Mass (μg)	Ft	radius (μm)	length (μm)	Age (Ma) ± 1σ	elevation (km)
Calvin(c):laser	16.14	23.00	19.20	60.33	2.93	1.95	0.70	51.43	137.14	23.59 ± 0.82	1.230
Calvin(d):laser	18.19	24.17	10.33	32.37	1.78	5.29	0.75	54.28	334.27		
Floyd(a):laser	33.12	42.50	11.44	39.01	3.72	7.09	0.78	62.85	334.27	40.19 ± 3.26	1.847
Floyd(b):laser	29.81	37.89	37.31	94.39	9.66	8.73	0.79	62.85	411.41		
Yoshi(a):laser	17.21	22.72	9.87	50.50	2.04	5.56	0.76	57.14	317.13	21.15 ± 2.22	1.217
Yoshi(b):laser	15.01	19.58	10.76	50.79	1.85	5.96	0.77	60.00	308.56		
Omar(a):laser	26.00	36.75	30.41	70.24	6.64	2.69	0.71	45.71	239.99	35.10 ± 2.33	1.369
Omar(b):laser	24.08	33.45	33.53	60.09	6.25	2.82	0.72	48.57	222.85		

VITA

Graduate College
University of Nevada, Las Vegas

Joseph Louis Kula

Local Address:
1551 Lorilyn Ave. #1
Las Vegas, NV 89119

Home Address:
123 Hawthorne Ave.
Nutley, NJ 07110

Degrees:
Bachelor of Science, Geoscience, 2000
Montclair State University, NJ

Master of Science, Geoscience, 2002
University of Nevada, Las Vegas

Special Honors and Awards:
UNLV Graduate Student Association Research Grant, Fall 2002
UNLV GREAT Scholarship, Summer 2002
UNLV Geoscience Department Research Grant, Spring 2002
Phi Kappa Phi Honors Society, 2001-2002
UNLV Graduate Student Association Research Grant, Fall 2001
UNLV Graduate Student Association Research Grant, Spring 2001
UNLV Geoscience Department Research Grant, Spring 2001
Arizona Nevada Academy of Science Research Grant, Spring 2001

Publications:
Kula, J.L., Spell, T.L., and Wells, M.L., 2002, Syntectonic intrusion and exhumation of a Mesozoic plutonic complex in the Late Cretaceous, Granite Mountains, southeastern California: Geological Society of America Abstracts with Programs, v. 34 p. 249.

Taylor, W.J., Criscione, J.J., Gilbert, J.J., Justet, L., Kula, J.L., Schiefelbein, I., Sheely, J.C., and Stickny, E., 2001, Geometry and neotectonics of the north California Wash Fault, Nevada: Geological Society of America Abstracts with Programs, v. 33, p. 58.

Kula, J.L. and Gorring, M.L., 2000, Tectonic setting and protolith for middle Proterozoic amphibolites within the Losee gneiss of the New Jersey Highlands: Geological Society of America Abstracts with Programs, v. 32 p. 455.

Thesis Titie: Thermochronology and Geobarometry of the Granite Mountains, southeast California; Exhumation of a Plutonic Complex During Collapse of the Sevier Orogen

Thesis Examination Committee:

Chairperson, Dr. Terry L. Spell, Ph.D.
Committee Member, Dr. Michael L. Wells, Ph.D.
Committee Member, Dr. Rodney V. Metcalf, Ph.D.
Graduate Faculty Representative, Dr. Barbara A. Luke, Ph.D.